EXPLORING RETINAL NEURON RESPONSES TO DEFOCUSED IMAGES IN THE MOUSE RETINA

SO CHUNG HIM

PhD

The Hong Kong Polytechnic University

2024

The Hong Kong Polytechnic University

School of Optometry

Exploring Retinal Neuron Responses to Defocused Images in the Mouse Retina

So Chung Him

A thesis submitted in partial fulfilment of the requirements for the degree of Doctor of Philosophy

July 2024

CERTIFICATE OF ORIGINALITY

I hereby declare that this thesis is my own work and that, to the best of my knowledge and belief, it reproduces no material previously published or written, nor material that has been accepted for the award of any other degree or diploma, except where due acknowledgement has been made in the text.

_____ (Signed)

So Chung Him
_____ (Name of student)

Abstract

Purpose

Although myopia, or nearsightedness, is a health problem worldwide, the mechanisms of its development remain unknown. It is hypothesized that refractive errors could result from the impact of defocused visual signals on various types of retinal neurons. This research study aimed to explore whether defocused images influence the signaling processes of individual types of retinal ganglion cells, specifically alpha retinal ganglion cells (αRGCs), as well as dopaminergic Amacrine Cells (Dopaminergic ACs), AII ACs, and Horizontal Cells (HCs). Additionally, the study examined the role of connexin 36 gap junctions (Cx36 GJs) in modulating these effects.

Methods

Several strains of mice, C57BL/6, KCNG-YFP, EGR-1, Fam81a, and Cx36-knockout, were used in this study. A custom-made device was used to project defocused images onto the retina under the microscope. Mightex 1000 generated light bars, annulus, and spots of varying sizes. Biophysical response of αRGCs, DACs, AII ACs, and HCs were recorded by patch clamp in flat-mounted retinas. Intracellular dye injection and confocal microscopy were then applied to confirm and study the morphology of neurons in the mouse retinas. The Generalized linear model (GLM) was used to predict RGC responses in normal and lens-induced myopic mice in order to study the myopic retina. Additionally, stretched soma and retinas were investigated to simulate myopic conditions. Gap junction blocker-Meclofenamic acid (MFA, 100μM), was applied to the retinas to study the impact of uncoupling AII ACs.

Study 1. This study investigated whether the biophysical characteristics of alpha retinal ganglion cells (αRGCs) differ between normal Cx36 knockout mice and those with lens-induced myopia (LIM) retinas. The study applied a generalized linear model (GLM) to predict the coding efficiency between focused and defocused images of RGCs in these mice.

Study 2. This study explored whether there are differences in the biophysical responses of alpha retinal ganglion cells (αRGCs) between focused and defocused image stimuli and to observe whether there is a difference in biophysical responses when the soma and retinas were stretched to mimic myopic conditions in both normal and Cx36 KO mice.

Study 3 This study investigated whether dopaminergic ACs and AII ACs demonstrated differences in their responses to focused versus defocused images. To uncouple the coupling between AII ACs, gap junction blocker was applied.

Study 4. The study investigated whether there are differences in the biophysical responses of horizontal cells (HCs) to focused and defocused images.

Summary

The neurons in the retina, such as αRGCs, HC, AII ACs, and dopaminergic ACs, can exhibit different responses to focused or defocused images. Gap junctions within retinal circuits might have a significant impact on the development of visually induced myopia.

Results

Study 1. The study revealed that the intact retinal circuitry, especially connexin 36 (Cx36), is essential in encoding the difference in visual signaling between focused and defocused images. The varied outcomes of the generalized linear model (GLM) with an offset in lens-induced myopia (LIM) retinas indicated the possibility for correction and adaptability within the retinal circuitry of myopic eyes.

Study 2. The biophysical response of a single RGC could accurately reflect the image projection of optical stimuli associated with myopic and astigmatic defocus. The process requires an intact retina circuit that includes Cx36.

Study 3. Dopaminergic ACs responded with distinctively different biophysical properties to focused and defocused images, thereby potentially influencing dopamine release in the retina and contributing to the development of myopia. Uncoupled AII ACs exhibited the capacity to detect both focused and defocused images, whereas AII ACs with robust coupling possessed the capability to eliminate noise related to defocused images.

Study 4. The biophysical properties of HCs allow these cells to reflect spot/annulus pattern stimuli and focused/defocused images.

Conclusions

This thesis helps to understand the role of Dopaminergic ACs, AII ACs, HCs and Cx36 GJs in decoding and modulating the focused and defocused images, which could be reflected by a single αRGCs. The research may elucidate the neurons in retinal circuit involved in refractive errors and provide potential targets for myopia control.

Publications and Presentation

Publications

1. Banerjee S, Wang Q, **So CH,** Pan F. Defocused Images Change Multineuronal Firing Patterns in the Mouse Retina. **Cells.** 2020 Feb 25;9(3):530.
2. Banerjee S, Wang Q, Tang G, **So C,** Shan SW, Li KK, Do CW, Pan F. Functional connexin35 increased in the myopic chicken retina. **Vis Neurosci.** 2021 May 14;38:E008.
3. Banerjee S, Wang Q, Zhao F, Tang G, **So C,** Tse D, To CH, Feng Y, Zhou X, Pan F. Increased Connexin36 Phosphorylation in AII Amacrine Cell Coupling of the Mouse Myopic Retina. **Front Cell Neurosci.** 2020 Jun 1;14:124.
4. **So C**, Zhang T, Wang Q, Qiu C, Elie LA, Pan F. The response of retinal ganglion cells to optical defocused visual stimuli in mouse retinas. **Exp Eye Re**s. 2024 Feb 19;241:109834.
5. Wang Q, Banerjee S, **So C,** Qiu C, Lam HC, Tse D, Völgyi B, Pan F. Unmasking inhibition prolongs neuronal function in retinal degeneration mouse model. **FASEB J.** 2020 Nov;34(11):15282-15299.
6. Wang Q, Banerjee S, **So C,** Qiu C, Sze Y, Lam TC, To CH, Pan F. The Effect of Low-Dose Atropine on Alpha Ganglion Cell Signaling in the Mouse Retina. **Front Cell Neurosci.** 2021 May 5;15:664491.
7. Wang Q, **So C,** Zuo B, Banerjee S, Qiu C, Ting Z, Cheong AM, Tse DY, Pan F. Retinal ganglion cells encode differently in the myopic mouse retina? **Exp Eye Res.** 2023 Sep;234:109616.

Conference Presentation

1. **So Chung Him**, Zhang Ting, Wang Qin, Tse Dennis Y, Feng PAN. Biophysical effects of focused and defocused image stimuli on dopaminergic amacrine cells and AII amacrine cells in the mouse retina. **The Association for Research in Vision and Ophthalmology (ARVO).** May 2024.
2. **So Chung Him**, Feng Pan. Exploration of the mechanism of refractive errors in the mouse retina. **The Association for Research in Vision and Ophthalmology (ARVO).** May 2023.
3. **So Chung Him**, Feng Pan. Exploration of the mechanism of refractive errors in the mouse retina. The 2023 **Mightex Research Excellence Award – Third place award**. November 2023.
4. **So Chung Him,** Pan Feng. Nearsightedness: Images treatment. **3 Minute Thesis (3MT)** competition in the Faculty of Health and Social Sciences. June 2023
5. **So Chung Him**, Zhang Ting, Pan Feng. Effect of acute intraocular pressure elevation on mouse alpha retinal ganglion cell. **PolyU Academy for Interdisciplinary Research (PAIR)**. May 2023

Acknowledgements

I would like to express my sincere appreciation and gratitude to the individuals who have played an instrumental role in shaping my research journey and supporting me throughout my PhD studies.

First and foremost, I am deeply grateful to Dr. Pan Feng, my chief supervisor, for providing me with the opportunity to embark on this remarkable research endeavor at PolyU. I vividly remember my first visit to his lab, which marked the beginning of a transformative experience. Despite accidentally breaking the experimental setup in the initial stages, Dr. Pan Feng remained supportive and encouraged my growth as a researcher. His unwavering guidance, patience, and belief in me have been invaluable. I am truly thankful for his mentorship and the numerous opportunities he bestowed upon me, including participation in competitions and conferences, which eventually led to me receiving the Mightex Excellent Research Prize.

I would also like to extend my heartfelt gratitude to my co-supervisor, Dr. Dennis Tse, for his generosity in allowing me to share my ideas and research in his lab meetings and for welcoming me into his team. Being part of Dr. Dennis's team has been an honor, and I deeply appreciate his patience, kindness, and the knowledge I gained through his guidance during my learning process.

I am indebted to Dr. Do Chi Wai and Dr. Pan Li for providing me with the invaluable opportunity to work under their guidance on a guided study subject. Their profound knowledge and innovative ideas in response to my inquiries and interests have been a constant source of inspiration and motivation throughout my research journey.

Furthermore, I am immensely grateful for the input and support I have received from Prof. Henry Chan and Dr. Samantha SHAN. Their guidance and assistance in both my research and career development have been instrumental in shaping my academic growth.

I would like to acknowledge the collective efforts and contributions of the entire research teams and collaborators at PolyU, without whom this work would not have been possible. I extend my heartfelt appreciation to my fellow labmates, Dr. Seema Banerjee, Dr. Qin Wang, Ms. Qiu Chunting, Ms. Zhang Ting, and Ms. Yang KangYi, for their support, camaraderie, and collaboration. Special thanks go to Dr. Qin Wang for her initial support and guidance, as well as to Ms. Zhang Ting for her generous assistance during my PhD studies.

I am also grateful to Mr. CATRAL Patrick, Mr. Mezbah Uddin, Mr. Jiajun Wang, Mr. Ayana, Mr. Anson Lau, Dr. Abokyi Samuel, Dr. Christie Lam, and Dr. Bing Zuo, who were part of Dennis's Lab. Working, learning, and sharing joyful moments with all of you will always hold a special place in my heart. I deeply appreciate the companionship, care, and support I received, particularly from Kirl Patrick, from the time I joined as a research assistant until now.

I would like to extend my thanks to Mr. KK Li, Mr. Daqian Lu, and Ms.Yuan Yuan for their support. Your presence and encouragement have been invaluable, and I am honored to have had you by my side throughout this challenging journey.

I am profoundly grateful to my family for being my pillar of emotional support during the ups and downs of my work. I want to express my heartfelt thanks to my loved ones, especially my sisters and brother, for taking care of our parents and providing unwavering emotional support, even when they may not have fully understood the intricacies of my work. Additionally, I would like to

express my gratitude to my friends, Mr. Wayne and Mr. Lawrence, for their constant companionship and support.

Lastly, I want to offer a special appreciation to my wife, Hailie, whose unwavering support and understanding have been the bedrock of my journey. Her presence, care, and understanding have been invaluable, and I am eternally grateful for her continuous support. With her by my side, I have never felt alone, and I could not have navigated the challenges of my PhD studies without her. Thank you, my dear wife, for being my rock.

To all the individuals mentioned above and to those who have supported me in ways beyond words, I extend my deepest gratitude. Your love, encouragement, and support have been pivotal in my academic and personal growth. Without each and every one of you, I would not have reached the point where I stand today. Thank you all for being an integral part of my journey and for making it a truly remarkable and fulfilling experience.

Sincerely,

So Chung Him

Table of Contents

List of Figures

Chapter 1

Chapter 2

Chapter 3

Chapter 4

Chapter 5

List of Abbreviation

Abbreviation	Explanation
AC	Amacrine cell
Ach	Acetylcholine
AIC	Akaike information criterion
AII AC	AII amacrine cell
AL	Axial length
BC	Bipolar cell
DA	Dopamine
DAC	Dopaminergic amacrine cell
EPSC	Excitatory postsynaptic current
GABA	Gamma-aminobutyric acid
GCL	Ganglion cell layer
GJ	Gap junction
GJD2	Gap junction protein delta 2
GLM	Generalized linear models
HC	Horizontal cell
INL	Inner nuclear layer
IPL	Inner plexiform layer
IpRGC	Intrinsic photosensitive retinal ganglion cell
IPSC	Inhibitory postsynaptic currents
LIM	Lens-induced myopic

LNP	Linear-Nonlinear-Poisson
MFA	Gap junction blocker
mGluR	Metabotropic glutamate receptor
OCT	Optical Coherence Tomography
OKR	Optokinetic reflex
OLED	Organic light-emitting display
RBC	Rod bipolar cell
RE	Refractive error
RF	Receptive field
RT	Retinal thickness
OCT	Spectral-domain–optical coherence tomography
SEM	Standard error of the mean
SNP	Nucleotide polymorphisms
VCD	Vitreous chamber depth
WT	Wild-type
αRGC	Alpha retinal ganglion cell

CHAPTER 1 Introduction

1. Retina

The retina, situated at the posterior segment of the eyeball, is a specialized layer important in the transformation of light signals into electrical signals. These signals are subsequently transmitted to the brain, facilitating the perception of visual images. This intricate process involves the orchestrated functionality of various cells, including photoreceptors, bipolar cells, and retinal ganglion cells. The retina also encompasses two lateral inhibitory pathways, comprising a singular type of horizontal cell as the primary inhibitory network and at least 60 subtypes of amacrine cells as the secondary inhibitory network[1].

1.1 Photoreceptors

Photoreceptors, situated on the retina's outermost layer, are categorized into two main types in both human and mouse retinas: rod and cone photoreceptors. These cells structurally consist of four main regions: cell body, synaptic terminal, the outer and inner segments. The key functional molecule, opsin, situated within the outer segment discs, plays a crucial role in process of phototransduction. This process involves the absorption of light by photoreceptors, initiating electrical responses that transform light information into a format interpretable by the inner retina[2]. In the darkness, photoreceptors undergo depolarization, increasing the release of glutamate due to enhanced sodium and calcium ion channel conductance. Conversely, exposure to light causes photoreceptors to hyperpolarize.

Rod photoreceptors are uniquely sensitive and capable of detecting a single photon under scotopic (low-light) conditions, thereby influencing the postsynaptic signaling of downstream cells. In comparison, cone photoreceptors require a significantly higher photon count to elicit a response. This sensitivity differential is crucial in low-light environments, where rods predominate to maximize photon capture. Rods constitute 95% of the photoreceptors in the human retina, with cones accounting for the remaining 5%. This ratio is similarly skewed in mice, with approximately 97% rods and 3% cones[3]. To enhance light response acquisition in electrophysiological studies, mouse retinas are subjected to dark adaptation, optimizing rod cell sensitivity[4].

The spatial arrangement of rod and cone photoreceptors within the retina is both intermingled and mosaic. The area of the receptive field is controlled by the retinal ganglion cells that span the photoreceptor area, except in the fovea region, where each cone is directly linked to a single bipolar cell and one retinal ganglion cell, facilitating a densely packed cone arrangement. This structural organization in the human fovea sets the resolution limit, determined by the minimal spacing between cones. Conversely, the mouse retina lacks a foveal structure, rendering its entire retinal composition akin to the peripheral retina observed in primates.

1.2 Bipolar cells

Within the inner nuclear layer (INL), bipolar cells (BCs) serve as critical interneurons and are differentiated into 15 distinct subtypes of cone bipolar cells (CBCs), alongside a singular type of rod bipolar cell (RBC) in murine retinas[5]. The dendritic processes of these cells form connections with photoreceptors at ribbon synapses, while their axonal terminations synapse in specific sublaminae, establishing synaptic contacts with the dendrites of specific retinal ganglion cell types.

This architecture enables the efficient relay of visual information from the photoreceptors to the terminal neurons.

BCs play an essential role in the segregation of ON and OFF visual pathways, which is attributed to their divergent responses to the neurotransmitter glutamate. Upon illumination, photoreceptors reduce glutamate release, leading to depolarization of ON-bipolar cells and hyperpolarization of OFF-bipolar cells, attributed to the differential expression of ionotropic and metabotropic glutamate receptors, respectively [6].

In the retinal circuitry of mice, RBCs play a role in disseminating signals from rod photoreceptors to both ON and OFF cone bipolar cells via the primary rod pathway. Additionally, a supplementary circuit, known as the tertiary rod pathway, exists, providing a direct interface between rods and OFF cone bipolar cells, and bypassing the involvement of rod bipolar cells [7].

1.3 Horizontal cells

Horizontal cells (HCs) are interneurons that contact photoreceptors and BCs via lateral inhibition. Their cell bodies are situated in the outermost inner nuclear layer (INL) of the retinas. In low-light conditions, photoreceptors release glutamate, which depolarizes HCs and stimulates the release of more glutamate. This, in turn, hyperpolarizes nearby photoreceptor cells, enhancing contrast perception. In contrast, bright light triggers less glutamate release from photoreceptors, causing HCs to hyperpolarize [8]. This feedback mechanism enables the retina to enhance contrast perception during visual processing. Horizontal cells have much larger receptive fields than cones and rods, allowing modulation and processing of visual information over a broad range of areas. These functions may contribute to the retina's ability to adapt to different light intensity ranges[9].

1.4 Amacrine cells

Amacrine cells (ACs), which are the most diverse interneurons in the inner nuclear layer of mouse retinas, connect with BCs and retinal ganglion cells (RGCs) through inhibitory neurotransmitters Gamma-aminobutyric acid (GABA) and glycine. ACs contribute to the inhibitory postsynaptic signal of ganglion cells, termed feedforward inhibition. In addition, ACs provide feedback inhibition to bipolar cells. For example, the A17 amacrine cell releases GABA to its connecting rod bipolar cell (RBC), which affects RBC depolarization[10]. Both feedback and feedforward inhibition aid ACs to make an important contribution to the RGC receptive field.

1.4.1 AII Amacrine cells

Bistratified glycinergic neurons known as AII amacrine cells (AII ACs) are situated in the innermost stratum of the inner nuclear layer (INL) and exhibit a non-random mosaic distribution. They have a unique morphology, consisting of lobular appendages and arboreal dendrites in sublamina a and b of the inner plexiform layer (IPL), respectively. Prox1 immunostaining has revealed that AII ACs constitute approximately 10% of the amacrine cell population in the murine retina[11].

AII ACs play a fundamental role in the primary rod pathway by distributing rod signals to ON and OFF-ganglion cells via different pathways. They establish sign-converting chemical connections with OFF-cone bipolar cells via glycine. In contrast, AII ACs enable sign-conserving electrical connections with ON-cone bipolar cells through gap junctions. The process of depolarizing electrical stimulation from ON cone bipolar cells to AIIs triggers the release of inhibitory glycine

onto OFF cone bipolar cells, causing hyperpolarization, which is commonly referred to as crossover inhibition[12].

AII ACs are vital in collecting scotopic signals from RBCs and transmitting these to ON and OFF pathways. In addition, All ACs in the mouse retina are interconnected through homologous connexin36 gap junctions (Cx36 GJs), which are the prominent subunit of gap junctions (GJs) in the area. These GJs help signal averaging and synchronization during visual processing[13]. Recent studies suggest that Cx36 may influence eye growth and the retinal circuitry, which is accountable for coding images that are either in focus or out of focus[14].

1.4.1.1 Input of AII Amacrine Cells

In the retina of rabbits, the On-center receptive fields of AII ACs receive glutamatergic inputs in sublamina b with rod bipolar cells. This input accounts for approximately 30% of the total input in mouse retinas. Conversely, the surrounding responses of AII ACs are inhibited by GABAergic, spiking amacrine cells[15]. Additionally, other amacrine cells, such as dopaminergic amacrine cells, also act as presynaptic to AII ACs, making up approximately 40% of the synaptic inputs[16]. AII ACs also make glycinergic connections with OFF-CBC that is situated at the lobular appendages in sublamina a of the inner plexiform layer.

AII amacrine cells receive electrical signals through gap junctions. Specifically, AII ACs are connected to ON-cone BCs through either heterogeneous or homogenous gap junctions, whilst connecting to other AII ACs relies on homogenous Cx36 GJs. These GJs allow for direct electrical communication between retinal neurons. The signal propagation in gap junctions is two-way in photopic conditions, AII ACs receive signals from cone-cone to BCs-AII circuits through gap

junctions. However, under dim light conditions, AII ACs rely mainly on synapses from the primary rod pathway [17].

1.4.2 Dopaminergic Amacrine Cells

Dopaminergic amacrine cells (DACs) are positioned in the innermost of the inner nuclear layer (INL) and serve as the sole source of retinal dopamine. Although they make up less than 0.01% of all neurons, they play a vital role in modulating key visual processes in murine retinas, such as light adaptation and circadian rhythm. DACs have two to three primary dendrites and one to two thin axons extending from their somata, forming an irregular dendritic field[18]. They spread their dendrites and axons to the outermost stratum of the IPL and co-stratify with photosensitive RGCs. Additionally, the dendrites of DACs encircle the surface of AII amacrine cell bodies, creating ring-like structures around the origin of its primary dendrite or cell body.

1.4.1.2 Input of Dopaminergic Amacrine Cells

The DACs are a unique type of neuron that receive glycine and GABA as inhibitory inputs at light on and light off, respectively. The glycinergic input comes from the RBC-glycinergic AC circuits, whereas the GABAergic signal emanates from the OFF CBC-GABAergic AC circuits. The release of dopamine has been shown to be primarily linked to rod signals[19] [20], while DACs receive glutamatergic signals from intrinsically photosensitive ganglion cells (ipRGCs) in addition to from ON cone bipolar cells, both of which utilize ionotropic glutamatergic synapses. In summary, DACs

receive both excitatory and inhibitory signals through the ON pathway and inhibitory signals through the OFF pathway[21].

1.5 Retinal ganglion cells

Retinal ganglion cells (RGCs) are situated in ganglion cell layer (GCL) and represent the sole neurons in the retina that communicate with the brain. RGCs receive postsynaptic signals from Amacrine cells (ACs) and BCs and convey these signal via the optic nerve, lateral geniculate, and finally to the visual cortex.

RGCs can be categorized into at least 40 subtypes according to their morphology, physiological function, gene expression, and molecular characterization. Although more than half of RGC types have been identified, the precise function of many RGCs in image formation is not fully understood[22].

1.5.1 Alpha (α) Retinal ganglion cells

Alpha retinal ganglion cells (αRGCs) possess the largest somata (>15um) of RGCs, stout axons and mono-stratified dendritic fields in GCL, comprising approximately 5% of the total RGC population. In mouse retinas, αRGCs have high neurofilament (SMI-32) and osteopontin (Opn) protein levels. All αRGCs express voltage-gated K+ channel subfamily G member 4 (Kcng4). The retina of a KCNG4-cre; thy1-stop-YFP1 mouse stained with antibodies for GFP is shown to be primarily made up of αRGCs[23] [24].

In the mammalian retina, the basic subtypes of αRGCs are classified as ON centre and OFF centre. Four alpha RGCs are defined by their light response: ON-sustained, ON-transient, OFF-sustained, and OFF-transient. Alpha RGCs display specialized physiological properties, including short response latency and rapid axonal conduction, allowing them to be the primary conduits for transmitting signals to the brain[25].

1.5.1.1 Inputs of αRGCs

Electrical synapses that allow direct electrical communication between neighboring neurons, are usually referred to as gap junction channels. Researchers have utilized neurobiotin to trace down the gap junction coupling pattern of αRGCs. OFF αRGC couples with amacrine cells and other αRGCs to form gap junctions, while the ON αRGC only connects to amacrine cells in the INL[26].

Postsynaptic currents (PSCs) also refer to chemical synapses, where the presynaptic neurons, such as BCs and ACs, release neurotransmitters and bind to receptors of postsynaptic neurons. This binding leads to the voltage change in the postsynaptic neuron membrane. The PSCs of αRGCs have been intensively studied and can be categorized into excitatory postsynaptic currents (EPSCs) and inhibitory postsynaptic currents (IPSCs) depending on the type of neurotransmitter binding. RGCss express $GABA_A$, $GABA_B$, and glycine receptors. Pharmacological experiments have revealed that the glycinergic and GABAergic ACs play a role in inhibitory input of αRGCs. Specifically, glycinergic ACs receive input from BC and then feed forward the inhibition to αRGCs. In contrast, wide-field GABAergic ACs receive input from their corresponding BCs and influence Glycinergic ACs. It is noteworthy that certain subtypes of ACs contain voltage-gated

sodium channels enabling them to generate action potentials, which propagate transient and sustained inhibition to αRGCs[27].

1.5.1.2 Outputs of αRGCs

αRGCs are the terminal neurons that summate and process ON and OFF visual information in the inner retina. They are highly enriched with voltage-gate ion channels, enabling them to initiate action potential and convey these in the form of spikes or bursts of activity to brain nuclei. The frequency and timing of the spikes carry crucial information about the visual stimuli, such as visual contrast. αRGCs, which receive postsynaptic input from multiple neurons that are activated by light stimuli, integrate postsynaptic signals from these cells and produce their own spikes in advance of reaching the threshold. This process is referred to as the light-evoked response. Four types of light-evoked responses of αRGCs have been described[23], including Off-sustained/transient and On-sustained/transient.

2. Synapses

Communication between neurons occurs at specialized junctions known as synapses, which can be categorized into two main types: chemical synapses and electrical synapses. Chemical synapses function through the release and reception of chemical neurotransmitters, which are used to transmit signals between neurons. In contrast, electrical synapses facilitate straightforward electrical communication between neurons, allowing for fast and synchronized signaling within neural networks.

2.1 Chemical synapses

Chemical synapses function through the release of chemical neurotransmitters to facilitate signal transmission between neurons. Neurotransmitters, including glutamate and dopamine, traverse the synaptic cleft and bind to particular receptors on the postsynaptic membrane of target cells, eliciting either excitatory or inhibitory impacts on the neurons or cells. These chemical synapses are pivotal in the transmission and processing of information in retinas, facilitating precise and adaptable communication between cells and supporting intricate visual computations.

2.1.1 Dopamine

Dopamine (DA) serves as the primary catecholamine in the retina and its release, which appears to follow a circadian rhythm, aids in transmitting signals throughout the retinal circuitry. Dopamine affects both postsynaptic and presynaptic receptors and diffuses to extrasynaptic receptors via a process called volume transmission[28]. Dopamine regulates voltage-gated ion

channels on target cells through five subtypes of G-protein coupled receptors, including D1-like (D1 and D5) and D2-like (D2, D3, and D4) receptors, present across the entire retina[29]. These receptors are presented in various types of retinal neurons: D1-like receptors are primarily expressed by horizontal cells and some BCs, ACs, and RGCs, while D2-like receptors are found in dopaminergic ACs and photoreceptors[30].

The activation of dopamine receptors influences the activity and signaling of retinal neurons; for example, the existence of D1 and D4 dopamine receptors in photoreceptors and inner retinal neurons significantly contributes to the decreased sensitivity of ganglion cells. Dopamine also influences the gap junctions between Horizontal cells, AII amacrine cells, and RGCs.[31].

2.1.2 Glutamate

Glutamate serves as the primary excitatory neurotransmitter in retinas, being released by photoreceptor cells (rods and cones) in response to light offset to initiate the processing of visual information. It activates receptors on bipolar cells, thereby enabling the transmission of visual information throughout the retinas. Glutamate receptors are categorized into ionotropic glutamate receptors (iGluRs) and metabotropic glutamate receptors (mGluRs). iGluRs act as ligand-gated ion channels that mediate excitatory neurotransmission, while mGluRs, a family of G-protein-coupled receptors, can be further subdivided into NMDA (N-methyl-D-aspartate), AMPA (α-amino-3-hydroxy-5-methyl-4-isoxazolepropionic acid), and kainate receptors[32, 33]. iGluRs response excitatorily to glutamate, causing neurons to hyperpolarize in response to light, and are located on OFF-BCs. Conversely, mGluR6 response inhibitorily to glutamate, resulting in neurons depolarizing in response to light, and are located on ON-BCs[34].

2.1.3 Gamma-aminobutyric acid (GABA)

GABA serves as the primary inhibitory neurotransmitter in retinas, being released by amacrine cells and horizontal cells to establish lateral connections. The signaling of GABA is pivotal in shaping center-surround receptive fields[35], direction selection, and the light sensitivity of RGC[7]. Its physiological effects are controlled by three subtypes of neuronal receptors: ionotropic GABAA and ionotropic GABAC receptors, which modulate chloride channels, and metabotropic GABAB receptors, which are G-protein coupled receptors[36]. GABA receptors are expressed on various retinal neurons, such as cones, HCs, BCs, ACs, and RGC[37, 38]. It facilitates lateral inhibition and regulates the dynamic range of retinal processing.

2.1.4 Glycine

Glycine, an inhibitory neurotransmitter, plays a role in inhibitory signaling in retinas. It is discharged by glycinergic ACs and influences receptors on BCs and RGCs, thus contributing to the regulation of excitatory-inhibitory balance. Glycine receptors act as ligand-gated chloride channels, which are present on all neurons that receive signals from these glycinergic (small-field) amacrine cells. As a result, receptors can be found on specific bipolar cell axons, as well as on the dendrites of many ACs and RGCs. The impact of glycinergic synapses on retinal signals involves the inhibition of inner retinal function while simultaneously exciting the outer retina.

2.1.5 Acetylcholine

Acetylcholine (Ach) is produced and discharged by starburst amacrine cells and influences visual processing by interacting with various cholinergic receptors found on various types of neurons,

including BCs, ACs, and RGCs[39]. ACh receptors consist of ionotropic nicotinic acetylcholine receptors (nAChRs) and metabotropic muscarinic acetylcholine receptors (mAChRs). The nAChRs function as ligand-gated ion channels. Within the retinas, ACh is pivotal in adjusting visual signaling, including aspects of brightness, contrast sensitivity, and motion detection[40, 41].

2.2 Electrical synapses

Electrical synapses enable direct passage of ions and signaling molecules between neurons, forming a type of synaptic connection. Unlike chemical synapses, which depend on neurotransmitters for interneuronal communication, electrical synapses allow for rapid and bidirectional signaling via gap junctions. The key structural component of electrical synapses is the GJ, which is created by the alignment of two connexons (or hemichannels), each from one of the adjacent cells. These connexons, which are composed of six connexin proteins, form a channel that bridges the intercellular gap between the two neurons[42].

2.2.1 Gap junction

Gap junctions, also known as intercellular channels, have a crucial role in transmitting electric signals between nearby cells. In the retinas of mice, these gap junctions are widespread and serve to average signals, reduce noise, and synchronize neurons[43]. A gap junction's structure comprises two connexons, with one located in each of the neighboring cells. Connexons are made up of connexin proteins and form hexameric protein complexes. Each connexon lines up with its counterpart in the neighboring cell, creating a narrow channel or pore between neurons. These gap junction channels permit the passage of ions, small molecules, and electrical signals, facilitating cell communication and coordination of their functions.

2.2.1.1 Connexin36 gap junction

The gene of gap junction protein delta 2 (GJD2), has exhibited a strong association with refractive error. GJD2 encodes Connecin36, a protein that forms GJs in retinas[44, 45]. Gap junctions are electrical synapses that allow direct communication with neighboring neurons. They consist of two hemichannels called connexons and connect with the cytoplasm of two neighboring cells via gap junction channels. These channels are found in five types of neurons in the retinas and assist in transmitting and processing visual signals.

Gap junction channels can consist of two same homomeric hemichannels, such as Connexin36 mediated GJs, which consist of specific connexin proteins that form intracellular pathways between two adjacent neurons. These GJs are highly expressed in mouse retinas, including connecting RGCs to ACs[46].

In the retina, Cx36 modifies signal-to-noise signals, averages noise, and synchronizes signals. The conductance of the Cx36 is regulated by neurotransmitters, including dopamine and nitric oxide[47]. This regulatory mechanism suggests that cell-to-cell communication through the Cx36 may significantly contribute to myopia development. This is supported by studies that have shown that the Cx36 phosphorylation in the animal retinas is affected by myopia[48, 49]. To date, limited studies have demonstrated the impact of Cx36 gap junctions in myopia and their relationship remains elusive.

3. Myopia

Myopia, characterized by abnormal axial length, results in the focal point of light stimuli falling in front of the retina. This condition causes distant objects to appear blurry while nearby objects remain clear. Recent studies have drawn attention to the significant increase in the prevalence of myopia, creating a global concern. In the late 1940s, studies estimated that the prevalence of myopia among East and Southeast Asian school children ranged from 20% to 40%. [50]. This percentage has now increased to 80%-90%[51]. Projections indicate that by 2050, approximately half of the world's population will be affected by myopia, with 9.8% suffering from high myopia. High myopia carries the potential risk of severe sight-threatening complications, such as retinal detachment, which can lead to blindness due to associated complications[52].

3.1 Myopia etiology

Multiple factors, including genetics and environment, contribute to myopia progression. Visually guided emmetropisation is commonly used to interpret the development of myopia. This theory suggests that sharp images regulate the growth of the sclera. If the sharp image falls behind or in front of the retina, this will lead to the development of either myopia or hyperopia in an attempt to align the axial length to the refractive power of the lens and cornea. Animal studies conducted on chicks[53], mice[54], and guinea pigs[55], have provided promising evidence to support this theory.

However, as vertebrate retinas are complicated and little is known how the communication between each class of neurons is processed. Studies in tree shrews and chicks, which have shown that their eyes can be induced into myopia even after the input from RGCs to optic nerve is

blocked[56, 57]. These findings suggest that retina-to-scleral communication could be a possible pathway in stimulating axial elongation. From light stimulations to RGCs and scleral, multiple cell types and neuronal pathways are believed to be involved, and the exact cells, neurons, and/or pathways are challenging to determine.

3.2 AII amacrine cells in myopia

The pathway from the retina to the sclera is believed to play a significant role in the development of myopia. This pathway involves visual signals being fed forward to RGCs, which generate spikes and feedback from other ACs. In photopic light conditions, AII ACs primarily receive excitatory signaling from CBCs[58]. As AII ACs are connected to most CBCs, with approximately half connected through Cx36 gap junctions, changes to the receptive field of AII ACs could impact the likelihood of RGCs firing. In myopic mouse retinas, there is increased phosphorylation of Cx36 and coupling, indicating that defocused vision could alter the RF of AII ACs and RGC firing[14].

AII ACs appear to have strong coupling between each other with homologous Cx36 gap junctions. Cx36 gap junction channels connect the AII AC and CBC network, and their conductivity is greatly influenced by dopamine and adenosine. Dopamine is known to inhibit myopia development, with D1 receptors playing a crucial role in this process[59]. The strength of coupling between AII ACs is modulated by the presence of D1 receptors in Cx36 GJs[60]. In light conditions, dopamine decreases the coupling between AII ACs, potentially striking a balance between receptive field moderation and signal-to-noise ratio to the next-order neurons[29].

3.3 Dopaminergic amacrine cells in myopia

Various molecules have been reported to the axial length of the eyeball. Of these, dopamine has been suggested as the link between DACs and myopia and is also proposed as the stop signal that regulates axial growth. Both animal and human research have shown that the amount of time spent in sunlight is directly correlated to a decrease in myopia development. This is because bright light tends to stimulate the release of dopamine in the retinas, which then slows or stops axial growth in school-aged children. Dopamine also contributes to modulating the phosphorylation or dephosphorylation of GJs. This modulation could lead to a change in signal-to-noise ratio or enhance sharp vision detection. However, the exact mechanism by which dopamine regulates axial growth remains unclear.

Dopamine is primarily created and released by dopaminergic ACs within retinas, which bind to two kinds of receptors, namely D_1-like and D_2-like G-protein-coupled receptors. Dopamine production increases when the retina is exposed to light. When D_1-like receptors are activated, they decrease the conductance of GJs between HC to HC, AII to AII, AC to AC, and between AC-GC. In contrast, D_2-like receptor activation results in increased gap junction conductance between rod and cone (R-C), between RGCs (GC-GC), and between ganglion cells and amacrine cell (GC-AC)[47]. In the retinas of both mice and chickens with myopia induction, it has been observed that there are functional increments present in the gap junctions between AII and AII, which is due to a decrease in D_1-like receptor activation. These findings highlight the vital role played by the pathway between dopamine and gap junctions in regulating the development of myopia.

3.4 Alpha RGCs in Myopia

Alpha retinal ganglion cells (αRGCs) serve a fundamental role as their ON and OFF visual functions are correlated with contrast sensitivity perception. Mice without ON alpha RGCs exhibit behavior deficits in contrast sensitivity[61]. Many studies have suggested that contrast sensitivity is closely associated with myopia[62, 63]. In addition, previous studies have suggested that defocused images, which differ from focused images in shape and contrast, alter the signaling of some alpha RGCs[49, 64].

Retinal ganglion cells (RGCs) play a role in the development of myopia by synthesizing visual information into electrical signals and transmitting these to the visual cortex and/or modulating scleral development through a feedback loop[65]. This visually-guided theory and the retina-to-scleral pathway provide a possible explanation for the mechanism of myopia. However, before defining this pathway, it is essential to ascertain whether the retina is capable of detecting defocus and defocus-induced changes. Among the various types of RGCs, the alpha RGCs have demonstrated sensitivity to contrast, suggesting that they may serve as primary actors in modulating myopia development.

3.5 Dopaminergic AC, AII AC and RGC in Myopia

Animal model studies have indicated that blur signals trigger a signaling pathway from photoreceptors, leading to cellular and biochemical changes in retinas that result an increase in axial length. The rod pathway plays an essential role in regulating retinal dopamine levels and the myopia development [66-68]. In the photoreceptor layer, up to 97% of photoreceptors are rods, with gap junction coupling between rods and cones responsible for almost all electrical

connections[69]. Researchers have demonstrated that rod-dominant peripheral vision contributes to emmtropization[70]. Within rod pathway, AII ACs, key interneurons in primary rod pathways (the most sensitive for scotopic vision), separating rod signals to ON and OFF-CBCs, also contribute to cone-mediated (photopic) vision by enabling ON signals to cross-inhibit OFF ganglion cells. In addition, connexin36, a homologous gap junction present between AII-AII, has been found to increase phosphorylation in the myopic retina[14, 71].

Light is believed to impact AII-AII gap junction coupling by regulating the release of dopamine from DACs. DACs establish synapses on AII ACs, linking them tightly to rod pathway that carries scotopic light signals to RGCs. The scotopic signal between rod and cone photoreceptor inputs to the RGCs is controlled by AII AC, and this process is also regulated by DACs[72]. Studies have suggested that DACs interact with rods, cone photoreceptors, and ipRGCs. However, only rods are directly linked to the release of dopamine at high light intensities, possibly through connexin-36-dependent rod pathways[20].

Dopamine can alter the conductance of gap junctions, as detailed in the previous section. AII ACs play an essential role in establishing connections between the neurons of the rod and cone pathways, forming links with both similar and dissimilar Cx36-containing gap junctions. The interaction between AII amacrine cells and dopaminergic ACs is strong, where dopamine affects the coupling of gap junctions by enhancing their phosphorylation. Another possible pathway that influences dopamine release is the rod/cone-driven ipRCG-DACs route, which is also associated with refractive development[73].

However, the exact dopamine downstream mechanism remains uncertain. In mammalian retinas, all the retinal neurons express dopamine receptors, with the dopamine D2 receptors(D2Rs) being the compound most studied in the modulation of myopia development. Pharmacological and

genetic research has demonstrated that dopamine receptors can inhibit form-deprivation myopia (FDM). Although reports suggesting the presence of D2Rs in the sclera are controversial, they have been found in many terminal sites, such as corneal endothelial, epithelial, and retinal ganglion cells. This receptor distribution indicates dopamine may have various downstream effects on myopia[74]. Dopamine D1 receptors (D1Rs) are widely distributed in bipolar, amacrine, and ganglion cells, indicating dopamine can change the signaling of RGCs in myopic retinas, such as via AII-RGC coupling and its upstream pathway[75].

Dopamine act on the receptors in particular visual pathways, leading to changes in the visual signal or altering of DA concentration may affect visual pathway activity. Both of these possible underlying mechanisms indicate that RGCs are able to reflect the alteration: Activation of D2 receptors can increase RGC excitability, potentially affecting visual information processing in retinas, while the D1-type seems to have the opposite effect[76].

In brief, the Dopaminergic ACs, AII AC and RGCs could be the determining neuron for transferring myopic signals and regulating axial length growth.

4. Light stimuli

Mightex (Toronto, Ontario, Canada) designs a range of spots and annuli with varying diameters to examine the receptive field characteristics of amacrine cells. Typically, these receptive fields exhibit a center-surround arrangement, whereby the center can be activated by light (on-center), while the surrounding area is inhibited (off-surround), or vice versa. Based on this premise, in this study, spots of different sizes were presented to activate the center region and annuli around the spot to activate the surrounding region. Both the spots and annuli were positioned at the midpoint of the identified receptive field[77].

The responses to spot and annulus stimuli offer insights into how neurons process contrast and edges, which are essential for visual perception. Spots can be applied to investigate the center receptive field with the strongest light response[78], while the surrounding can adjust sensitivity to the fine spatial structure by influencing how the center integrates visual signals across space[79]. This method can yield information about the polarity, size, and kinetic of neurons, but it is based on the assumption of circular symmetry.

5. Research questions

5.1 Do the biophysical properties of αRGC response differ for focused/defocused images?

Based on the theory of visually-guided ocular growth, the retina plays a pivotal role in regulating axial elongation by processing optical stimuli. A previous research conducted by this group revealed that a population of RGCs exhibited distinct firing patterns when presented with focused and defocused images, indicating the presence of a specific RGC pathway that can recognize these signals. To determine whether the individual visual pathways that originate from the retina can react to focus and defocus, a single αRGC biophysical response that integrates all visual information within its receptive field was employed.

5.2 Does the myopic retina encode visual information differently from the normal retina?

The biophysical response of αRGCs serves as a valuable tool for assessing the condition of retinal circuitry. However, it is important to recognize that defocus adaptation could potentially impact the synaptic connections between neurons within a myopic retina. It is crucial to determine whether RGCs in myopic retinas can accurately convey these signals, as this would aid in unraveling the underlying mechanisms of myopia development. Additionally, determining whether RGCs in myopic retinas encode visual information differently from those in normal retinas could offer insights into the potential for retinal plasticity and amendment of myopic retinas.

5.3 Do defocused images have an effect on the signaling of dopaminergic ACs and AII ACs in the mouse retina?

The secondary lateral inhibitory networks consist of over 60 distinct types of amacrine cells, which are responsible for complex visual functions, including directional-selective, motion, and light adaption. Although challenging, it is essential to identify the specific types of neurons involved in regulating focus/defocus in order to fully comprehend the cellular pathway of myopia development. In particular, Dopaminergic ACs, as the sole source of dopamine release, and AII ACs, as key interneurons in scotopic vision, were investigated in the current study.

5.4 Do horizontal cells contribute to modulating focused/defocused signals?

The RGC signal, integrated from the glutamatergic pathway, may be shaped by lateral inhibitory networks. The first inhibitory networks are comprised of horizontal cells that generate center-surround receptive fields and contrast enhancement effects in bipolar cells and RGCs. The current study aimed to determine whether horizontal cells have a role in regulating focus and defocus in the retinas, which is crucial to comprehending the cellular pathway of myopia development.

5.5 Does the absence of Cx36 GJs play a role in encoding focused/defocused images?

Cx36 GJs are primarily present in mouse retinas, particularly connecting between cone/cone AII/AII ACs, AII ACs/CBC, and RGCs/ACs in the inner and outer retina. Previous studies of this

group have shown that their phosphorylation level increased in myopic mice and chick retinas. The current study aimed to investigate how these gap junctions affect the focused/defocused image coding of RGCs.

6. Objectives and hypothesis

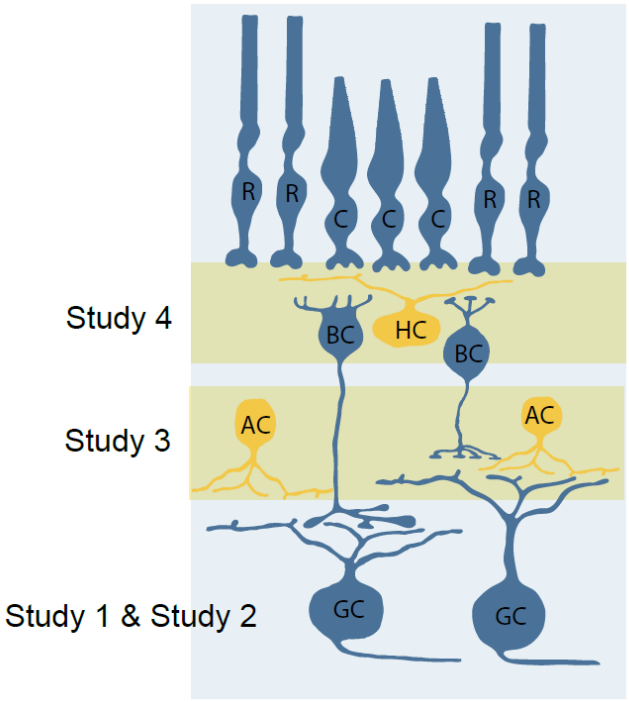

Figure 1 Study on retinal neurons

The focus of studies 1 and 2 are the retinal ganglion cells (RGCs), specifically αRGCs, which are indicative of the vertical signal flow, whilst study 3 is centered on amacrine cells, encompassing Dopaminergic ACs and AII ACs, Study 4 involves the horizontal cells. As such, studies 3 and 4 represent the secondary and first inhibitory networks, respectively.

Aim 1: To investigate the biophysical responses of αRGCs in decoding focused/defocused images.

Hypothesis: Given the distinctive firing patterns of a population of RGCs and the spike responses of individual RGCs to projected focused and defocused images, it may be postulated that the biophysical response of a single αRGCs can reflect focused and defocused images.

Aim 2. To investigate whether the myopic retina computes visual information differently from the normal retina via GLM prediction.

Hypothesis: It is possible for the retinal structure to undergo changes during the development of myopia. The distinct performances of GLM model application on αRGCs suggest possible amendment and plasticity of the retinal circuit in myopic retinas.

Aim 3. To determine the specific types of amacrine cells involved in regulating focused/defocused signals.

Hypothesis: As dopamine release is solely mediated by dopaminergic amacrine cells, it is suggested that the biophysical response of DACs reflects the focused/defocused signals. Furthermore, it is also postulated that AII amacrine cells, which are closely associated with Cx36 gap junctions and dopaminergic amacrine cells, may also reflect these signals when uncoupled.

Aim 4. To determine the role of horizontal cells in regulating focused/defocused signals.

Hypothesis: Horizontal cells receive direct inputs from rods and cones, which are able to regulate signals to bipolar cells, which ultimately affect RGCs. It is proposed that horizontal cells may have the ability to reflect the projection of focused and defocused images.

Aim 5. To investigate the role of Cx36 GJs in decoding focused/defocused signals.

Hypothesis: The phosphorylation of Cx36 GJs is suggested to be linked to the development of myopia. The absence of Cx36 GJs in mouse retinas could potentially impact the decoding of myopic defocus and astigmatic blur signals for RGCs and ACs.

CHAPTER 2 Retinal ganglion cells encode differently in the myopic mouse retina

(Note: This chapter is published in "experimental eye research Sep 2023; doi: doi.org/10.1016/j.exer.2024.109834". Permission to include the published material has been granted by the corresponding author, who is also the supervisor of the candidature.)

1. Introduction

Refractive errors are vision problems that arise when the eye cannot focus light properly onto the retina, leading to blurred or distorted vision. The primary types are myopia, hyperopia, and astigmatism[80]. It has been estimated that by 2050, approximately half of the world's population will be affected by myopia, with 9.8% experiencing high myopia and a potential risk of severe sight-threatening issues, such as retinal detachment. These complications can ultimately lead to blindness[81, 82]. However, the underlying cellular mechanisms responsible for the development of these conditions are not fully understood. This study aimed to investigate the cellular-level aspects of myopia.

The process that aligns vision and axial length, known as emmetropisation, is regulated by defocus. In a myopic eye, the eyeball grows excessively, causing distant objects to project in front of the photoreceptors. This defocus adaptation may affect synaptic connections between neurons within the myopic retina. Previous research has indicated that visual signaling from RGCs to the optic nerve can be altered in the myopic retina[49]. In addition, defocused images differ in varying light intensity and blurry edges from focused images can modify the firing patterns of RGCs, as

they are projected in front of the retina[64]. Retinal ganglion cells (RGCs) process all visual information from the inner retina, including signals from bipolar and amacrine cells. Consequently, they can be used to analyze the status of retinal circuitry, including disrupted gap junctions and altered signaling cascades. Thus, the coding of RGCs could be used to test the circuitry of the myopic retina with a computational model and compare this to that in the normal retina.

Generalized linear models (GLMs) can establish a linear connection between the response of retinal ganglion cells and stimuli by applying a series of linear filters and point nonlinearity. This model can be used to fit and examine spike trains from electrophysiological recordings of RGCs[83]. Compared to photoreceptors, focused/defocused image decoding from RGCs may require more computational effort. This is because the encoding process in the retina may require the downstream visual area to first decode the RGC signals using an internal retinal model[84, 85]. Alternatively, it is possible that RGCs themselves are capable of computing the focused image without heavy reliance on the internal dynamics of the retina [86, 87]. Despite extensive research in this area, the mechanism by which images are processed by RGCs in myopic retinas is not yet fully understood. To simulate and compare normal and myopic conditions, the expected response of RGCs in both normal and myopic retinas when encoding focused and defocused images were integrated into a GLM model for analysis.

This study focused on alpha retinal ganglion cells (αRGCs), which serve fundamental ON and OFF visual functions, playing an important role in contrast perception. They are easily identified by their largest soma, stout axon, and mono-stratification of their dendritic fields[23].

The GJD2 gene plays an important role in myopia development. It is believed that variations in the GJD2 gene may result in alterations in the expression of Connexin (Cx)36 gap junction. This gap junction is found in large numbers in the inner plexiform layer and may act as a key component

in the intact retinal circuits. Cx36 gap junctions are potential modulators of myopia development with their function of noise reduction, signal averaging, and synchronization in the retina[13]. Additionally, previous research by this team suggested there was increased phosphorylation of Cx36 of AII amacrine cells in the myopic retina[14]. Therefore, Cx36 knockout mice were used to investigate the importance of intact retinal circuits.

The study emphasized the crucial significance of a fully operational neural circuit within the retina and proposed that the processing of visual information in a myopic retina may deviate from that of a normal retina.

2. Methods

2.1 Animals

Mice as models for myopia research have several advantages. 1. The contrast sensitivity of mice is similar to human peripheral vision. 2. The mouse genome shares 85% similarity to the human genome and can be readily manipulated. 3 Myopia in mice is correlated with elongation vitreous chamber of the eye, similar to that in humans[88]. Thus, mice were used in this study.

Adult wild-type (WT) mice of both genders C57BL/6J (RRID: IMSR_JAX:000664), weighing between 15 to 20 grams, postnatal age 16-56 days (n = 56) were used in the study. Additionally, Kcng4-YFP (n = 11) mice[89] of both genders, weighing between 15 to 25 grams and aged between 6 to 8 weeks were used to label ON and OFF alpha RGCs (αRGCs). These mice were cross-bred from Ai32 mice (B6;129S-Gt(ROSA)26Sortm32(CAG-COP4*H134R/EYFP) Hze/J, RRID: IMSR_JAX: 012569) and KCNG4cre mice (B6.129(SJL) KCNG4tm1.1(cre)Jrs/J, RRID:IMSR_JAX:029414). The KCNG4cre mice have Cre recombinase inserted into the locus encoding potassium channel modulator, and Ai32 mice express a channelrhodopsin-2/EYFP fusion protein following exposure to Cre recombinase. The cross-bred mice from KCNG4cre and Ai32 mice have YFP labeled αRGCs[89], including ON and OFF αRGCs[23].

Homozygous Cx36-knockout(KO) mice (RRID: MGI:3810172) were also used in the study, which were bred in the laboratory of David Paul, Harvard Medical School (Cambridge, MA), and kindly provided by Samuel M. Wu, Baylor College of Medicine (n = 6, aged 6–8 weeks, weight between 15–25 grams). The Cx36-knockout mice were checked by genotyping to select homozygous genetic knockout mice.

The mice were raised in a 12-hour light/dark cycle and treated humanely throughout the study. Prior to enucleation, the mice were anesthetized with an intraperitoneal injection of ketamine and xylazine (Alfassan International, Woerden, Zuid-Holland, The Netherlands) [100 mg/kg and 20 mg/kg, respectively], and lidocaine hydrochloride (20mg/ml) was dripped onto eyelids. The anesthetized animals were killed by cervical dislocation immediately after enucleation. All animal procedures were conducted in accordance with the Animal Subjects Ethics Sub-Committee of the Hong Kong Polytechnic University.

2.2 Animal Preparation

Following administration of anesthesthesia, the eyes of mice were enucleated under red dim light conditions. The dorsal section of the midperipheral retina in the nasotemporal plane was then used for patch-clamp recordings, before being flattened and attached to a modified translucent Millicell filter ring (Millipore, Bedford, MA, USA). The retinas were then bathed in oxygenated Ringer's solution[90] and continuously bubbled with 95% O2–5% CO2 mixture while being maintained at a temperature of around 32 °C[7, 91].

2.3 Patterned light stimulation

A green OLED display produced by Yunnan OLiGHTEK Opto-Electronic Technology Co, Yunnan, China, was used for retinal stimulation, with a resolution of 800 × 600 pixels and a refresh rate of 85Hz. The OLED display was controlled by an Intel (Santa Clara, CA, USA) Core Duo computer running Windows 7 system. A Nikon (Tokyo, Japan) 40x water-immersion objective

(CFI Apo 40XW NIR, NA = 0.8) was employed allowing 250 μm in diameter of the retina to receive light stimuli. Under the 40x objective, each pixel presented as 0.25um on the retina, with a diameter of 15um. Spatial frequency stimuli were generated by PsychoPy from the University of Nottingham and were projected onto the outer segment of photoreceptors. The background light intensity was ~700 isomerizations Rh*/rod/s while the highest stimulus was ~1.816 × 105 Rh*/rod/s. The rod pathway is saturated at this background illumination level, only the cone pathways can mediate the light response[92]. All images were produced by a 1-second stimulation followed by a 5-second interval. Focused/defocused 125 μm diameter images with 0.0067 cycles/degree were applied as shown in Figs 2.1, 2.5, 2.6, 2.7 and 2.8. The system used to generate defocused images was custom-made, using a physical movable lens for image projection on the photoreceptor outer segment, rather than digital blurring. According to the Schaeffel, 2008 calculation, an axial elongation of 5um would induce 1 Diopter (D) refractive error in the mouse retina. Thus, 100 μm away from the photoreceptor's outer segment can induced either plus or minus 20 diopters refractive error under microscopy, depending on the direction of lens defocus (Fig 2.1).

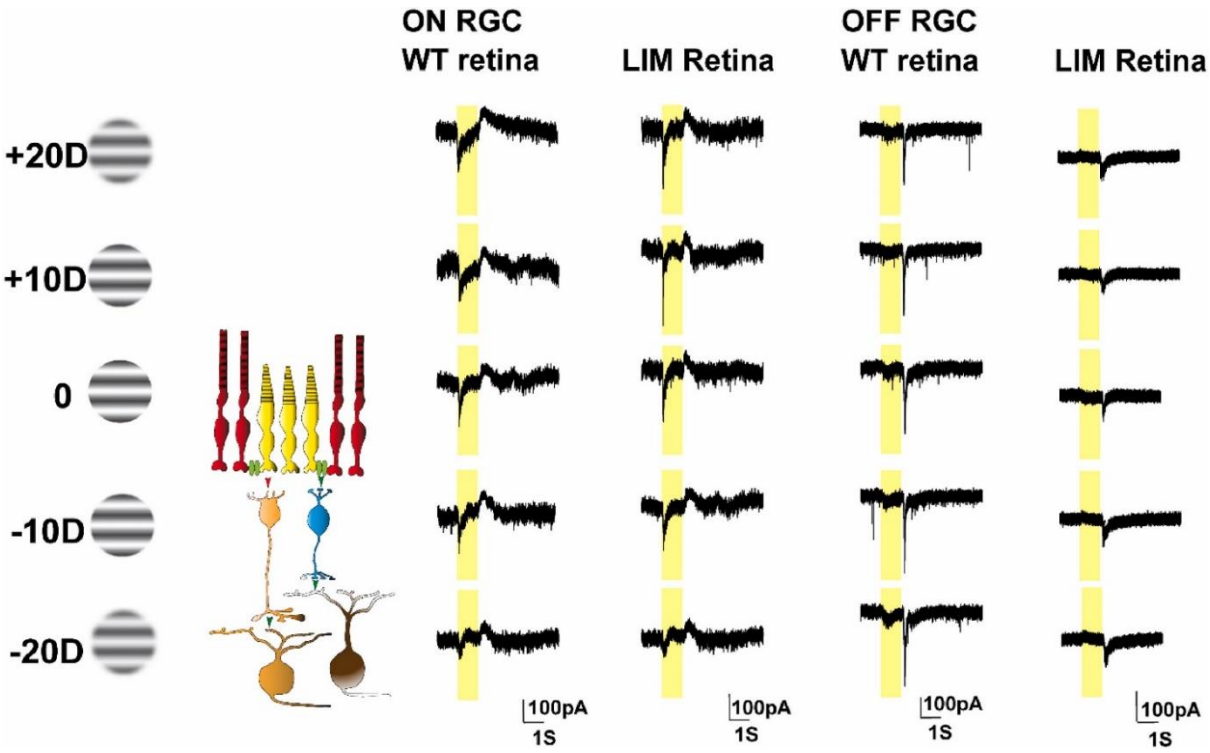

Figure 2. 1 Schematic representation of the responses of ON and OFF αRGCs to focused and defocused image stimuli.

An image with a focused 125 µm diameter and 0.0067 cycles/degree was projected onto the outer segment of the photoreceptors. This focused image is considered to be at 0 diopters. Afterward, defocused images at ±10 and ±20 diopters were projected onto different retinal layers using a microscope. This was determined based on the calculation that a 5 µm defocus could cause a refractive error of plus or minus 1 diopter [93]. The light intensities varied between 3.74 x 10^4 Rh*/rod/sec and 3.85 x 10^4 Rh*/rod/sec. Whole-cell light responses of ON and OFF αRGCs were recorded and examined from LIM and normal (Wild-Type, WT) retinas.

The grayscale nature scene images (Fig 2.11) sourced from Google were transformed using Adobe Photoshop 7 (Adobe Inc, San Jose, CA, USA) and subsequently used to examine the responses of retinal ganglion cells (RGC) to images containing diverse subjects, including landscapes, people, and animals.

2.4 Electrophysiology

Recording of extracellular and whole-cell RGCs was e conducted using an Axopatch 700B amplifier (Axon Enterprises, Scottsdale, AZ, USA) connected to a Digidata 1550B interface (Axon Enterprises) and pCLAMP 10 software from Molecular Devices (San Jose, CA., USA). Visualization of cells was achieved using near-infrared light at 40 × magnification with a Nuvicon tube camera (Dage-MTI, Michigan City, IN) and differential interference optics on a fixed-stage microscope (Eclipse FN1; Nikon, Tokyo, Japan). The retinas were bathed with Ringer's solution (120 mM NaCl, 2.5 mM KCl, 25 mM NaHCO3, 0.8 mM Na2HPO4, 0.1 mM NaH2PO4, 1 mM MgCl2, 2 mM CaCl2, and 5 mM D-glucose) at a speed of 1-1.5 ml per minute. The bath solution was continuously bubbled with 95% O2–5% CO2 at approximately 32 °C. Electrodes pulled to 5−7 MΩ resistance were used with an internal solution (120 mM potassium gluconate, 12 mM KCl, 1 mM MgCl2, 5 mM EGTA, 0.5 mM CaCl2, and 10 mM HEPES) (adjusted to pH 7.4 with KOH) was used in experiments to avoid lockage of spiking. The whole-cell excitatory postsynaptic potentials (EPSPs) were recorded with an internal solution containing cesium to improve the space clamp and block spiking. The chloride equilibrium potential (ECl) with these internal solutions was approximately −63 mV.

The recordings were digitally sampled at a speed of 10 kHz using Axoscope Molecular Devices software and sorted using an Offline Sorter (Plexon, Dallas, TX) and NeuroExplorer (Nex Technologies, Littleton, MA, USA) software. For the whole-cell recording, the kinetics of excitatory postsynaptic currents (EPSCs) were measured and compared, with focus on the area bounded by the trace and the baseline, time, and slope of Maximal rise (decay) (the slope from within the region bounded by the start of the search region and the peak) of EPSPs. For comparison

purposes, the spike frequencies were normalized. Cells were dye-injected with Neurobiotin and Lucifer Yellow-CH using pipette tips[94].

2.5 Immunohistochemistry staining

The ON and OFF αRGCs were confirmed by Neurobiotin injection after RGCs recording (Fig 2.2). The attached retinas were removed from the filter paper and immersed in a solution of 2% N-(3-dimethylaminopropyl)-N′-ethylcarbodiimide hydrochloride ("carbodiimide"; Sigma-Aldrich, Burlington, MA, USA) in 0.1 M PBS at pH 7.5 for fixation. After 30 min at room temperature, the retinas were washed with 0.1 M PBS at pH 7.4, and then blocked with a solution of 3% donkey serum in 0.1 M PBS containing 0.5% Triton-X 100 and 0.1% NaN3 overnight. The retinal tissues were incubated with diluted primary antibodies (in a solution of 0.1 M PB with 0.5% Triton-X 100 and 0.1% NaN3, mixed with 1% donkey serum) for 3-5 days at 4 °C. Finally, the retinal tissues were mounted in Vectashield (Vector Laboratories, Newark, CA, USA) for confocal scanning.

To verify ON and OFF αRGCs, the retina tissues were fixed in a 4% paraformaldehyde solution for 15 min. Subsequently, the tissues were incubated with choline acetyltransferase antibody (ChAT, goat anti-ChAT, Millipore- Sigma, Billerica, MA, USA; Cat# AB144P, RRID: AB_2079751) at a concentration of 1:500 for 7 days at 4 °C. Following incubation, the tissues were washed with 0.1 M phosphate-buffered saline (PBS) and then mounted for image capture in a Zeiss LSM 800 with an Airyscan confocal microscope (ZEISS, Thornwood, NY, USA) using a 43 × objective (NA 1.3).

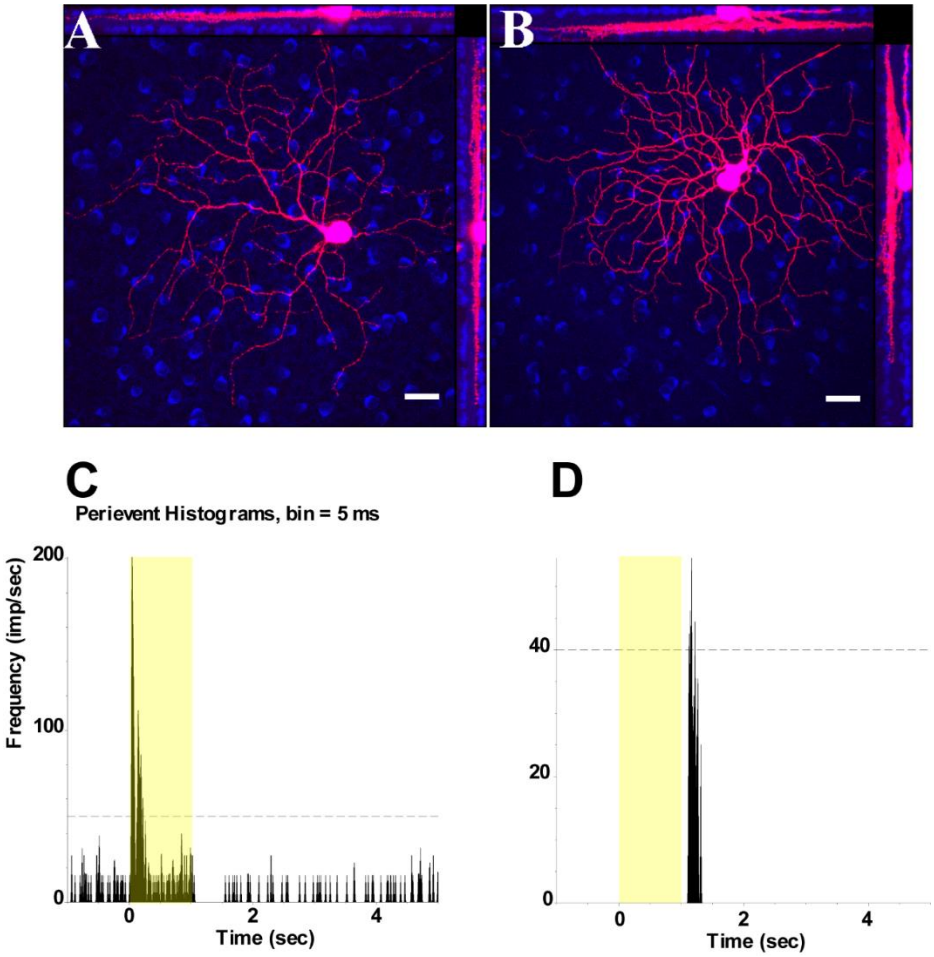

Figure 2. 2 ON and OFF αRGCs in the retinas of Wild-Type mice.

Representative images depicting ON (A) and OFF (B) αRGCs in the mouse retina were identified following patch recording procedures. The top and right side images illustrate the stratification of double-labeled ON and OFF αRGCs with anti-ChAT antibodies (in blue) in the WT mouse retina. Scale bar: 20μm. Peristimulus time histograms (PSTHs) displaying light-evoked responses of ON αRGCs (C) and OFF αRGCs (D) were generated. The presentation involved a 525-nm full-field light stimulation with an intensity of 131 Rh* per rod s−1, indicated by the yellow bar. The dotted line represents the 99% confidence limits, above which correlations exceed chance levels.

2.6 Data acquisition and analysis

Origin software (Origin-Lab, Northampton, MA, USA) was used to perform the statistical analyses. The significance = ($p<0.05$) was determined by the Student t-test, used to compare each specific defocus and focus. Unless indicated otherwise, the data is presented in terms of mean values ± standard error of the mean (SEM).

2.7 Generalized linear model

Generalized linear models (GLMs) are a type of mathematical model that has been frequently used to study how neurons in the visual system process visual information. A specific GLM used to study spike representation is the Linear-Nonlinear-Poisson (LNP) model (Fig 2.3)[85, 95]. This model comprises linear filters, a nonlinear function, noise from an exponential family distribution, and statistical properties for fitting the model to data. The weight vector k is essential to GLM filtering the stimulus. It helps determine how strongly different visual features influence the neurons' spiking activity. The input of each neuron is described by a set of filters, including a stimulus filter and a post-spike filter that capture dependencies on the neurons' spike history. The responses from these filters are summed and then exponentiated to obtain the neuron's instantaneous spike rate.

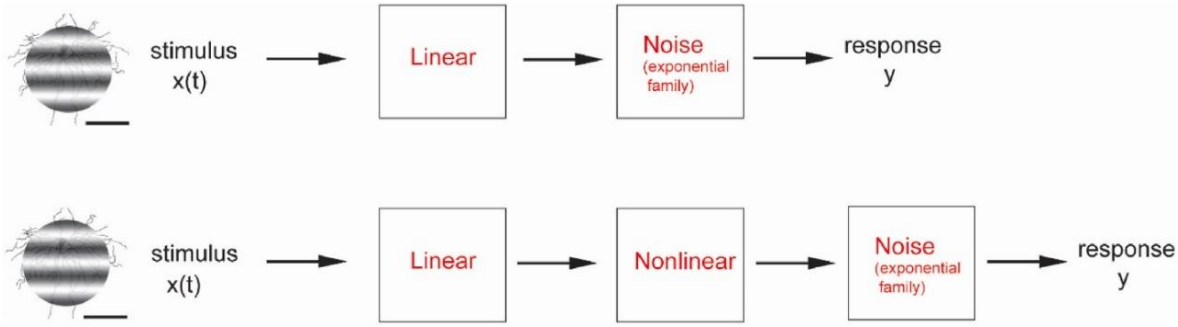

Figure 2. 3 Schematic of generalized linear encoding model (GLM).

The upper figure shows a linear model. The lower figure shows a linear-nonlinear-Poisson (LNP) model. The model comprises a linear filter to describe how the neuron integrates the stimulus over time and space; a point nonlinearity to transform filter output into the neuron's response range; and exponential-family noise to capture stochasticity in the responses.

This study focused on the activity of the ON / OFF αRGCs in mouse retinas and how they responded to different powers of defocused and focused images. GLM models were able to predict various aspects of neuron activity, including spike count, spike rate, spike time, and spike trains, when projecting focused /defocused images to the neuron receptive field. The GLM models included two main components: a linear filter k and a nonlinear function. The linear filter k determines how well the stimulus s(t) matched the filter. The baseline offset (y-intercept) was set in linear regression, which accounts for any constant bias in the cell's response, such as spontaneous firing. The nonlinear step was based on the output of the receptive field ks(t) of the linear filter, accounting for spike threshold and response saturation. To improve the accuracy of the model predictions, the model incorporated the exponential-family noise to capture stochasticity in the neuron responses[96, 97].

2.8 Evaluating model performance

Pseudo- R^2 scores were applied to evaluate the GLM predictive performance Pseudo- R^2 also can be applied to capture the explained variability in various types of regression models, for example the Poisson function, instead of trial-averaged firing rates as required by the standard R2 measure of explained variance[98].

In contrast, the Akaike information criterion (AIC), is a method for model comparison by comparing the fitness or goodness-of-fit of different models. In this study, the AIC was used to compare the performance of two GLM models: an exponential nonlinearity GLM model (exp-GLM) and a nonparametric estimate of the nonlinearity GLM model (np-GLM). The np- GLM assumes a GLM with an exponential nonlinearity but makes a "nonparametric" estimate of the nonlinearity.

2.9 Lens-induced myopic (LIM) mouse models

The myopic mouse model was induced by wearing head-mounted eyeglasses[99]. The right eyes of mice were implemented with customized minus 30 diopter lenses (poly methyl methacrylate, (PMMA), while the left eye served as a control (Fig 2.4). The spectacles lens was fitted when mice reached postnatal day 21. Refractive error and axial length were measured after five weeks of wear.

2.10 Refraction measurements in mouse model

Refractive error (RE) was measured by an infrared photorefractor (Steinbeis Transfer Center, Stuttgart, Germany). To ensure mydriasis and cycloplegia, the mouse eyes were treated with tropicamide, phenylephrine hydrochloride solution (Mydrin-P ophthalmic solution; Santen Pharmaceutical Co., Ltd., Osaka, Japan) 10 min prior to measurement. Mice were then lightly anesthetized with an intraperitoneal injection of ketamine (Vedno, St. Joseph, MO, United States) and xylazine (Akorn, Decatur, IL, United States) [10 and 1 mg (kg body weight) $^{-1}$, respectively] before obtaining RE measurements. Averages of twenty measurements were taken for each eye. The axial length (AL) of LIM models was also measured using spectral-domain–optical coherence

tomography (SD-OCT, Bioptigen Spectral Domain Ophthalmic Imaging System, Envisu R4410 SD-OCT Leica Microsystems, Wetzlar, Germany). The mice were positioned in a cylindrical holder attached to an X-Y-Z movable stage in front of the SD-OCT light source, and streak retinoscopy was then used to confirm refractive error measurements. RE with >5D variance between these two methods was excluded. Finally, to ensure the normality of the corneal condition, corneal curvature was measured by an infrared photorefractor to avoid corneal damage of models.

3. Results

3.1 Lens-induced myopic (LIM) mouse models

Based on retinoscopy measurements, the myopia-induced eyes demonstrated refractive errors of −3.7 ± 0.7 D, while the contralateral eyes were +7.4 ± 0.5 D (mean ± SEM, $P < 0.05$, $n = 8$)(Figure C). The axial length was defined as the length from the corneal surface to the retinal pigment epithelium (RPE). The axial length in LIM eyes was 3.65 ± 0.12 (mean ± SEM) mm, which was significantly greater than the contralateral control eyes, 3.36 ± 0.03 mm ($p < 0.05$, $n = 8$) (Figure D). An average increment of 0.29 ± 0.03 mm in AL was observed in LIM eyes.

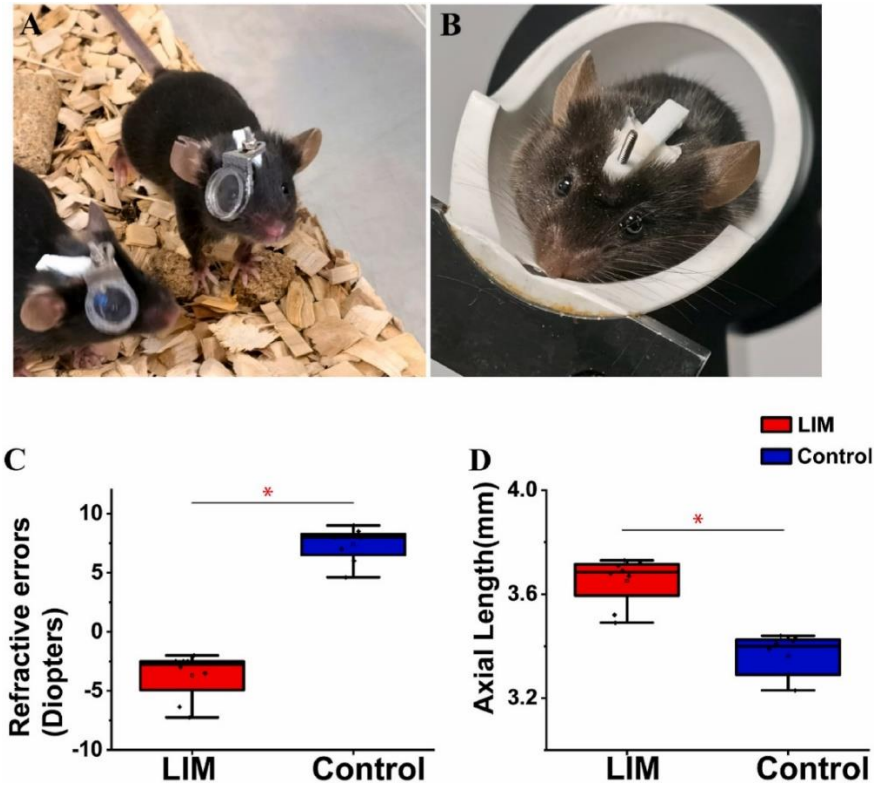

Figure 2. 4 Lens-Induced Myopia (LIM) mouse and Optical Coherence Tomography (OCT) measurement.

A: The image shows a LIM mouse wearing skull-mounted eyeglasses. B: Refraction measurements were taken of the LIM mouse eye while the mouse was under light anesthesia to ensure stable results. Refraction errors were determined while mice were awake. C: Photorefraction was used to measure refractive errors (RE) of the mice. The red star indicates a significant difference between the eyes of LIM mice and control (untreated) eyes. D: Optical Coherence Tomography (OCT) was used to measure the axial length of the mouse eye, from the corneal surface to the retinal pigment epithelium layer.

3.2 The biophysical properties of RGCs in normal and myopic retinas

The first experiment involved the examination of the whole-cell response of ON and OFF alpha RGCs recorded in the retinas of normal and LIM mice receiving a projection of focused and defocused image stimuli. A clear image with a spatial frequency of 0.0067 cycles/degree was projected at 0 diopter (focused image) on the outer segment of the photoreceptors. Based on Schaeffel's calculation, roughly every 5μm away from the outer segment of the photoreceptors creates a refractive error equal to either plus or minus 1 diopter. Defocused images of ±10 and ±20 diopters, with the light intensities varying from 3.74 x104 Rh*/rod/sec to 3.85 x104 Rh*/rod/sec, were projected onto the various layers of the retinas via the microscope. The defocused images altered the light intensities and image size of the receptive field of RGCs compared to the focused image. Thus, the EPSC of ON and OFF αRGCs were recorded in the retinas of normal and LIM mice and compared with those of Cx36 KO mice retinas, representing intact and deficit retinal circuits, respectively.

To compare the biophysical properties of light-evoked EPSCs in normal and LIM retinas, several murine parameters were measured from the responses of ON and OFF αRGCs: area, time to

maximum rise (decay), maximum rise (decay) slope, and 80%–20% rise (decay) time and slope. The murine response properties were chosen for their ability to reflect the physical characteristics of the neurons and their processing distinction of focused/defocused images. The kinetics of the response properties of RGCs were analyzed in normal and LIM retinas under the focused image, ±10 D and ±20 D defocused images (Fig 2.5). It is hypothesized that the response to a focused image will be either maximal or minimal in contrast to defocus, due to their superior signal-to-noise ratio in intact retinas[64].

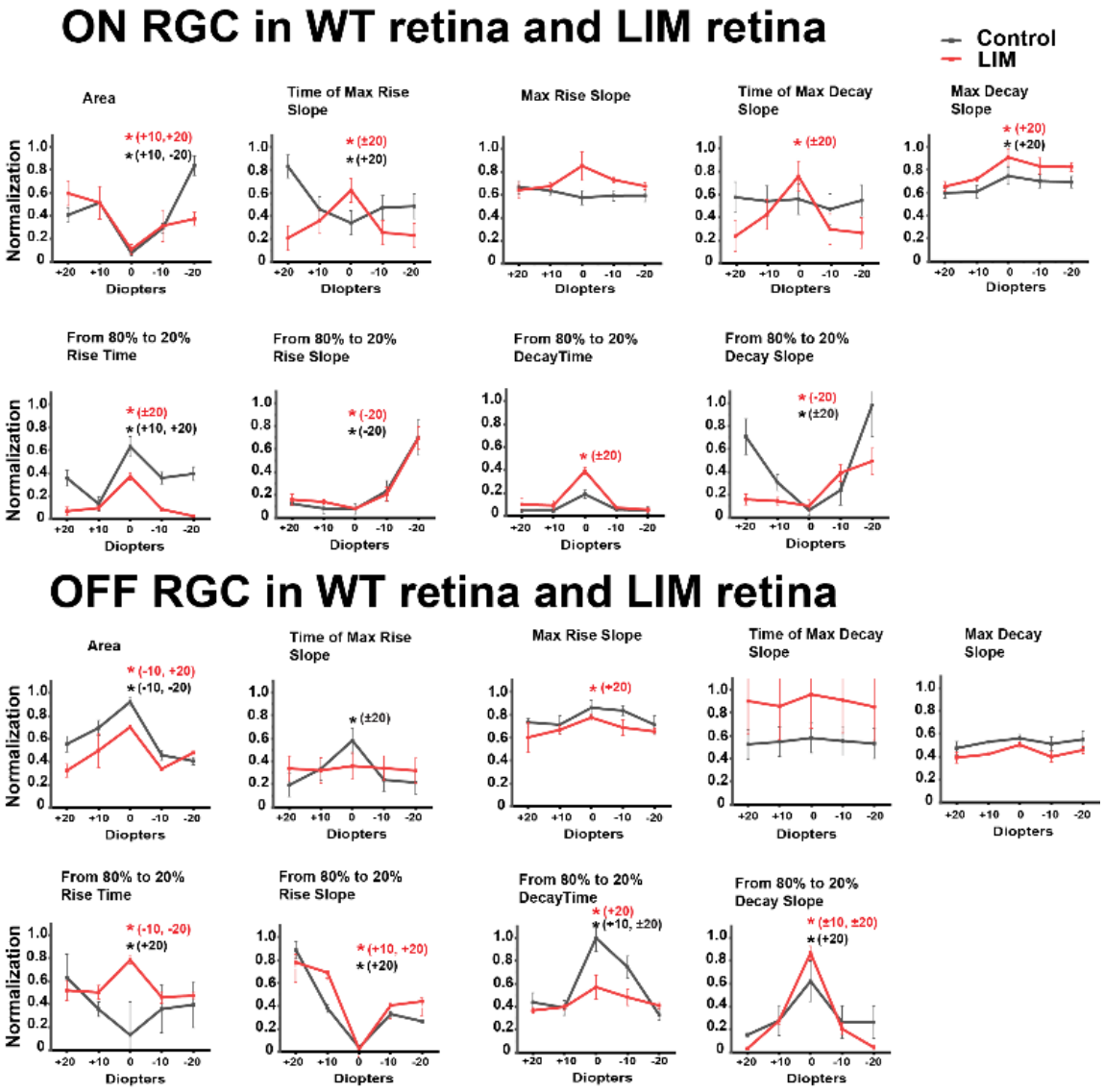

Figure 2. 5 Biophysical properties of whole-cell response in ON and OFF αRGCs in normal (WT) and LIM retinas.

Whole-cell recordings were taken from ON and OFF αRGCs in normal (WT) and LIM retinas and then normalized. The area, time of maximal rise(decay) slope, maximal rise(decay) slope. From 80% to 20% rise(decay), time and slope were compared in normal and LIM retinas after normalization. Under the focused image, the ON and OFF αRGCs in both normal and LIM retinas had maximal or minimal responses in these biophysical measurements. A star indicates a significant difference (t-test, $p<0.05$). The numbers demonstrate that the focused image (0D) significantly differed from the defocused images. Eight of the nine (89%) measurements in the ON and OFF αRGCs resulted in a maximal or minimal response in the normal retina. All measurements yielded maximal or minimal responses in both ON αRGCs and OFF αRGCs in the LIM retina.

In both the normal and LIM retinas, the EPSC of ON/OFF αRGCs with either maximal or minimal amplitude in the murine response parameter measurement was obtained under focused image stimulation. Among these response properties, 89% of ON/OFF αRGCs in normal retinas had either maximal or minimal response. However, a similar finding was not observed in the response parameters of the time of max decay slope for ON αRGCs and the max decay slope for OFF αRGCs. Six of the eight response property measurements in ON/OFF αRGCs in the normal retina showed a significant difference between focused and at least one of the defocused images (t-test, $p < 0.05$). Compared with LIM retinas, all nine response properties of the NO/OFF αRGCs showed either maximal or minimal response for both focused and defocused images. Six of the nine measurements had a significant difference between focused and other defocused images (t-test, $p < 0.05$).

From the analysis of 12 ON and OFF αRGCs in the normal retinas, two-thirds of measurements showed either maximal or minimal responses, respectively. A similar response pattern was observed in 39 ON αRGCs in the LIM retinas, although a slightly lower (56%) response rate was found in 57 OFF αRGCs. The analysis of EPSC kinetics revealed that a single RGC could reflect the focused/defocused images both in the normal and myopic (LIM) retinas. It is noteworthy that these response parameters to focused/defocused images were not significantly different between the two types of retinas.

Cx36 gap junctions connect αRGCs and amacrine cells. In Cx36 KO mice retinas, the lack of Cx36 could result in problems in the functioning of the retinal circuitry and may affect their ability to focus/defocus[100]. The analysis of the response amplitude of EPSCs in αRGCs of Cx36 KO mouse retinas revealed that two of nine (22%) of ON αRGCs and one t of nine (11%) of the OFF αRGCs recorded maximal or minimal response (Fig 2.6). Further analysis of the nine response properties suggests that there were no differences between focused and defocused image projection. In addition, 16.7% of 10 ON αRGCs and 8.6% of 9 OFF αRGCs showed a maximal or minimal response in Cx36 KO mice retinas, which was significantly different from the results of normal and LIM retinas.

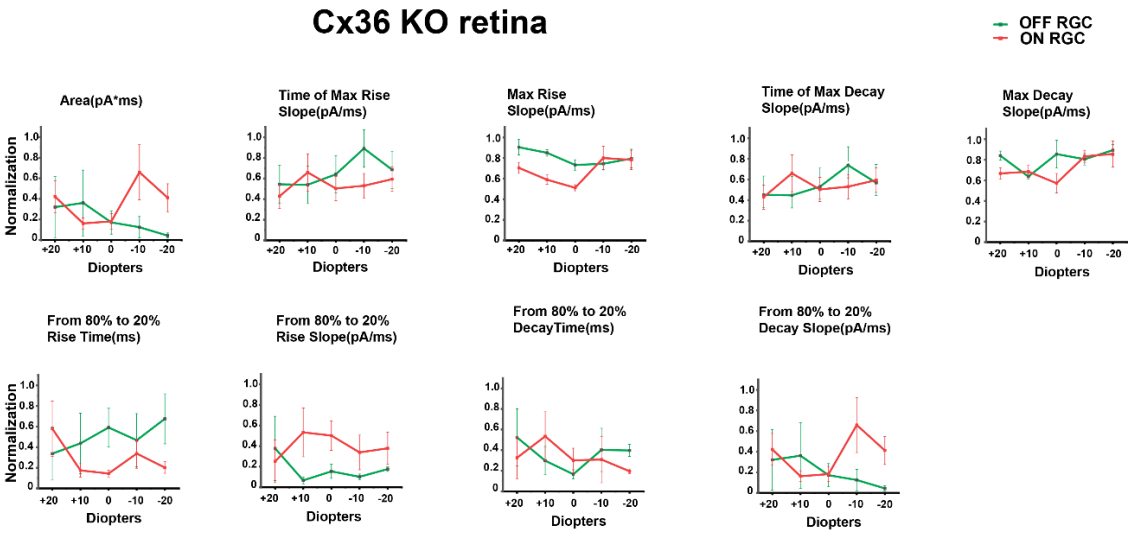

Figure 2. 6 Biophysical properties of whole-cell response in ON and OFF αRGCs in Cx36 KO retinas.

Whole-cell recording of ON and OFF αRGCs in Cx36 KO retinas showed that most maximal or minimal responses disappeared in the area, time of maximal rise(decay) slope, maximal rise(decay) slope, and from 80% to 20% of rise (decay) time and slope measurements. Only two of nine (22%) measurements in the ON αRGCs had a maximal or minimal response, compared to one of nine (11%) OFF αRGCs.

Together, the differences between Cx36 KO retinas, LIM, and normal retinas indicate that intact retinal circuits and amacrine cells coupled with RGCs may play an important role in processing focused and defocused images.

3.3 Computation of the GLM model for encoding focus/defocused images to RGCs in normal and myopic retinas

In subsequent experiments, Poisson GLMs were used to analyze the response of single neurons in both normal and LIM retinas. To improve the accuracy of the model's prediction, various filters were applied, including the stimulus filter, which analyzed the spatial-temporal integration of light; the post-spike filter, which mimics voltage-activated currents; the coupling filter, which represents synaptic interaction; and exponential nonlinearity, which implements a threshold for generating spikes. These filters and nonlinearity functions allow one neuron's activity to influence the activity of other neurons in the population. This leads to shared variability in the model's response. αRGCs have different subtypes, each with distinct physiological and morphological features. These subtypes also exhibit different response dynamics, such as sustained and transient responses.

To access how well the GLM models decode differences across αRGCs, the spike count of each ON and OFF αRGC in normal retinas was recorded and predicted using a linear Gaussian GLM (Fig 2.7). The stimulus was normalized and the model's performance compared with and without offset by using pseudo-R^2.

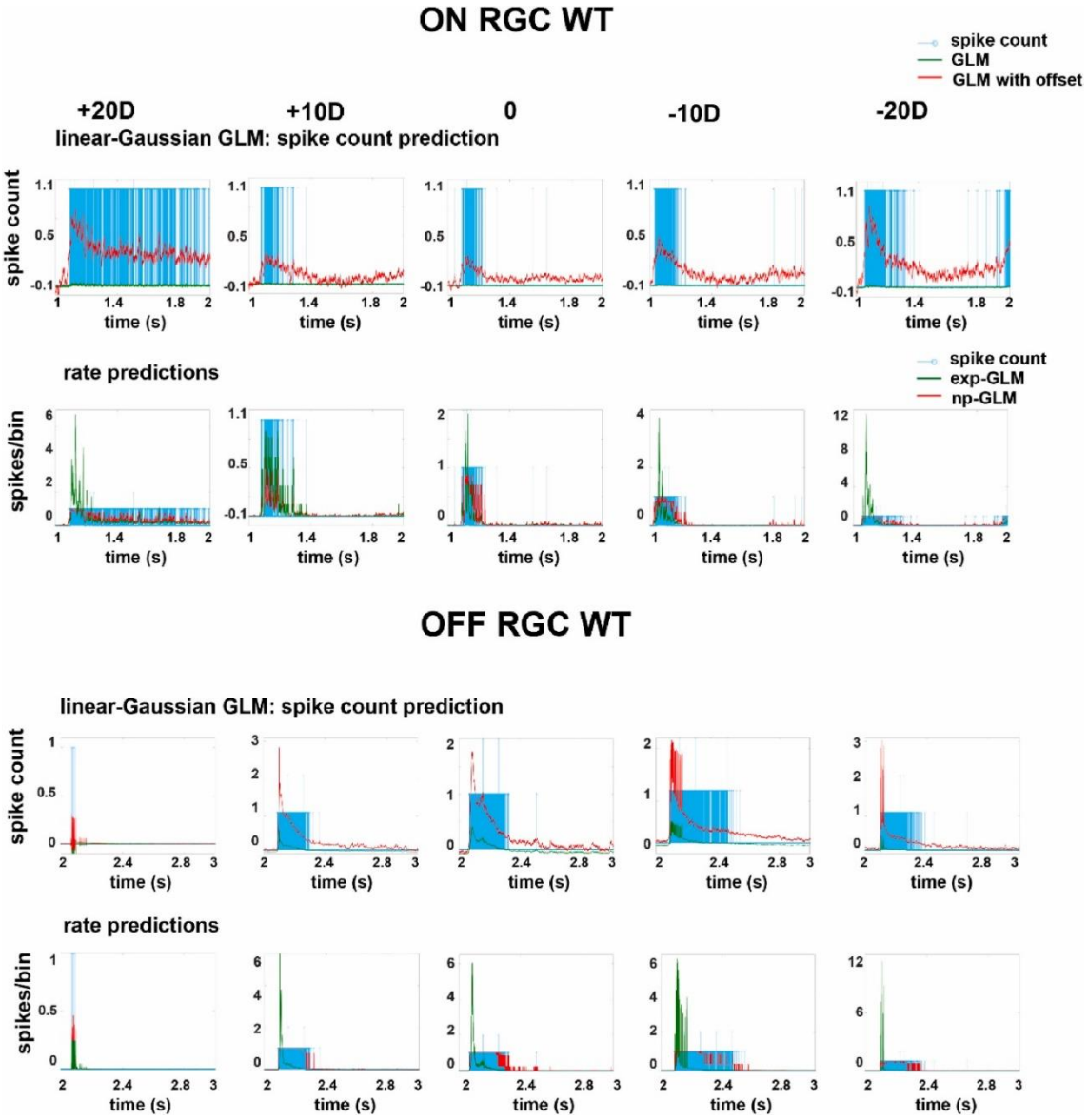

Figure 2. 7 GLM models applied in ON and OFF αRGCs analyses in normal (WT) retinas.

GLM models were applied to predict the spike count (upper row) and rate (lower row) under focused and defocused image projections of different powers. X axis: time in seconds; y axis: spike count in spike count prediction and spikes per bin in rate predications.

The results showed that the spike counts were better fitted when an offset was included in the model, with pseudo-R^2 being 0.1 for the focused image and ranging from 0.035 to 0.02 for defocused images (±10D and ±20D) projection in ON αRGCs. In contrast, the pseudo-R^2 was 0 without offset, and this was the case for both normal and LIM retinas (Fig 2.8). For OFF αRGCs, the pseudo-R^2 was 0.58 with offset in the focused image and ranged from 0.47 to 0.06 for defocused images, while the pseudo-R^2 was 0 for the model without offset. For LIM retinas, the pseudo-R^2 with offset was 0.1 in the focused image but ranged from 0.028 ± 0.08 (mean ± SEM) with defocused images in ON αRGCs, while compared to 0 without offset., while the OFF pseudo-R^2 was 0.05, and ranged from 0.02 ± 0.01, respectively. As a result, the linear Gaussian GLM models with offset were a better fit for the spike count prediction of ON and OFF αRGCs in normal and LIM retinas.

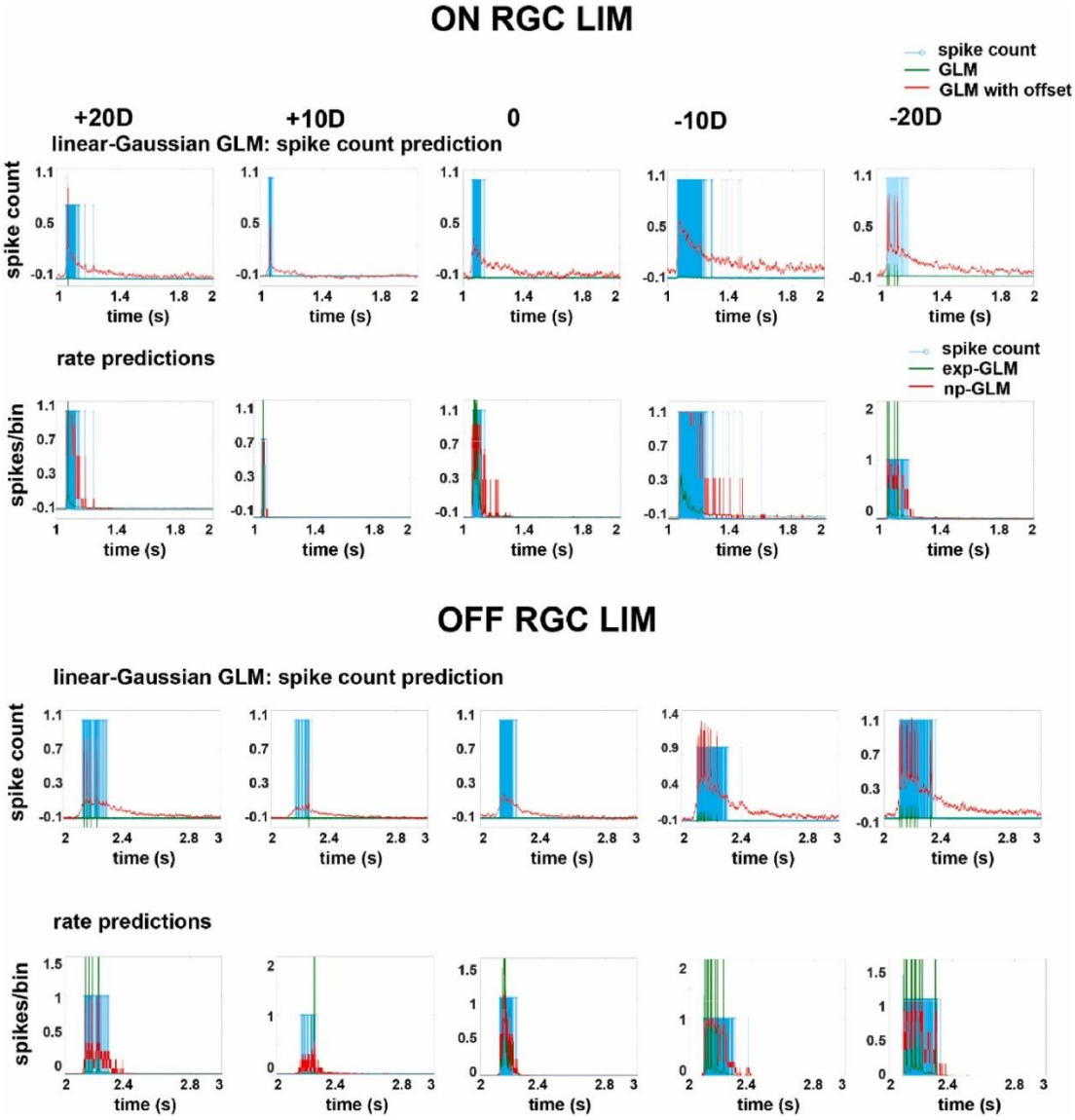

Figure 2. 8 GLM models applied in ON and OFF αRGCs analyses in LIM retinas.

GLM models were applied to predict the spike count (upper row) and rate (lower row) under focus and defocused image projections at different powers. X axis: time in seconds; y axis: spike count in spike count prediction and spikes per bin in rate predications.

To compare the spike rate prediction of the exponential nonlinearity GLM model (exp-GLM) and the nonparametric estimate of the nonlinearity GLM model (np-GLM), AIC (Akaike Information Criterion) was applied. The results showed that the np-GLM model better predicted the spike rate

for focused and defocused image projection. For the focused image, the AIC difference between exp-GLM and np-GLM was 201 (ON-αRGCs) and 1764 (OFF-αRGCs), indicating better fitting with np-GLM. Similarly, for defocused images (±10D and ±20D), the np-GLM fitting was superior in both ON and OFF αRGCs. In normal retinas, of the 15 ON and OFF αRGCs, the rate prediction was better fitted with np-GLM in 13 (87%), with only 2 (13%) showing a better fit with exp-GLM under +20D defocused images. Among the focused (0D) and defocused images (±10D and ±20D), +20D defocus projected the blurriest image on the retina. The assumption is that different subtypes of αRGCs recruit different amacrine cells to decode visual information, resulting in inconsistent fitting results of both models.

In LIM retinas, the np-GLM model provided a better fit for the rate prediction in focused/defocused images compared to the exp-GLM model, with a lower AIC value supporting the former. The AIC difference between the exp-GLM and np-GLM was 323 for the ON αRGCs and 426 for the OFF αRGCs under focused image projection. Further analysis revealed that 10/15 (66.7%) ON and OFF αRGCs in LIM retinas had a better fit with the np-GLM model, while the remaining five (33.3%) had a better fit with the exp-GLM model under defocused images (±10D and ±20D). The results indicated that αRGCs showed different performances with such focus/defocus projection in LIM retinas.

overall, the Linear-Gaussian-GLM model with offset was a better fit for the spike count of ON and OFF αRGCs by in both normal and LIM retinas. In terms of spike rate prediction, 87% of αRGCs had a better fit with np-GLM in normal retinas, but only e 67% in LIM retinas.

Using the GLM model, the raster plot was predicted to visualize the spiking activity of αRGCs over time in response to stimulus. In normal retinas, both ON and OFF αRGCs displayed clearer responses (11/15 ON and OFF αRGCs, with 4 uncertain cases) of spike trains under the focused

image projection. This response was compared to defocused images, especially ±20D. The raster plot (Fig 2.9**)** revealed that αRGCs may exhibit different spiking activities under focused/defocused images in normal retinas. In LIM retinas, the raster plot predicted by GLM showed that the OFF αRGCs response was relatively clear (8/12 OFF αRGCs, with 4 uncertain cases) under focused image projection, compared to OFF αRGCs under ±20D stimulus. In contrast, ON αRGCs responses were relatively clear under focus in normal retinas but not when under ±20D defocus in LIM retinas (8/15 15 αRGCs, with 7 uncertain). This suggested that the myopic retinal circuit may need to adapt to function similarly to normal retinas. Further investigation is needed to confirm these findings.

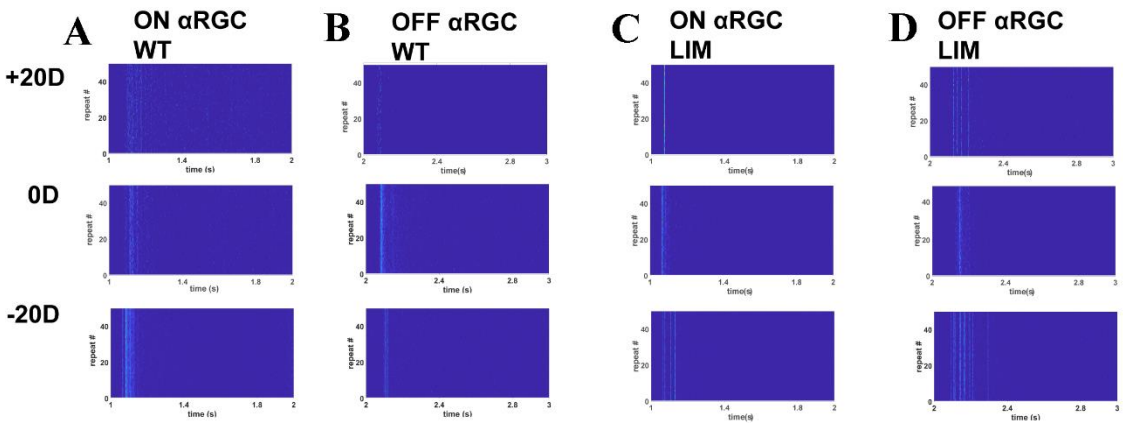

Figure 2. 9 Spike train prediction with the GLM model.

The raster plot of the spike train of ON and OFF αRGCs of normal and LIM retinas is shown. Focus(0D) and ±20D defocused images were compared. The raster plot showed that the spike trains were clearer under focused images than under ±20D defocused images (A, B and D). However, this was not the case under +20D stimulus in αRGC in the LIM retina (C).

The normalized pseudo-R^2 in the Linear Gaussian-GLM model with offset was used to compare how well the focused and defocused images could be predicted by retinas. In normal retinas, for only 4/15 (26.7%) pseudo-R^2 predicted the spike count well under focused image projection, while 2/15 (13.3%) under +10D, 1/15 (6.6%) under +20D, 4/15 (26.7%) under -10D and 4/15 (26.7%) under -20D defocused images (Fig 2.10A shows the normalized pseudo-R2). The results showed there is no significant difference in the ability to predict the spike count between focused and defocused images in normal retinas. However, in the LIM retinas with possible amendment retinal circuits, the linear-Gasussian GLM model with offset was better at predicting the spike count, with 9/15 (60%) under the focused image, while 4/15 (26.7%) under -10D, 2/15 (13.3%) under -20D (Fig 2.10B shows the normalized results with pseudo-R2). These results suggest that focused images were better encoded using the Linear-Gaussian-GLM model in LIM retinas. The differences in prediction accuracy between normal and LIM retinas indicate the changes in visual processing or retinal circuit plasticity in LIM retinas.

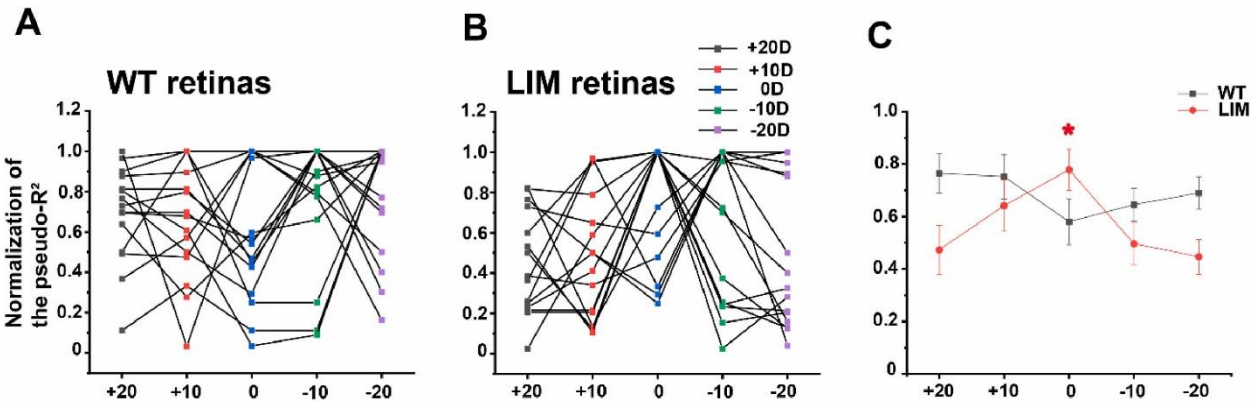

Figure 2. 10 Pseudo-R2 in linear-Gaussian-GLM model with offset to predict the spike count.

A: In normal (WT) retina, 26.7% (4 /5) pseudo-R2 the linear-Gaussian-GLM model with offset predicted the spike count well under a focused image, compared to 13.3% (2/15) under a +10 D

defocused image; 6.6% (1/15) under a +20 D defocused image; 26.7% (4 /15) under a −10 D defocused image; 26.7% (4/15) under a −20 D defocused image. There was no significant difference between focused and defocused images. B: In LIM retinas, 60% (9/15) pseudo-R2 in linear-Gaussian-GLM model with offset predicted the spike count under a focused image, compared to 26.7% (4/15) under −10 D defocused image; 13.3% (2/15) under a −20 D defocused image. C: Summary of normalized pseudo-R2 in normal and LIM retinas. Star indicates a significant difference (t-test, $p < 0.05$). X axis: Diopters; Y axis: Normalization of the pseudo-R2.

3.4 RGC responses to natural scene stimuli in the normal retina

To understand how a single retinal ganglion cell in normal retinas responds to different natural scenes like a forest, the sea, a rabbit, a human face, and a mouse, which could be distinguished by their differences in shape, contrast, and brightness. To test whether this model could accurately identify the coding of single RGCs, the pseudo-R^2 of the Linear-Gaussian GLM model with offset in normal retinas was measured.

The pseudo-R^2 of a Linear-Gaussian GLM model with an offset, which was used to predict spike count, varied for different scenes, with 0.01 for the forest, 0.14 for the sea, 0.04 for the rabbit, 0.1 for the human face, and 0.01 for the mouse. When predicting spike rate, AIC was compared and indicated that np-GLM was better than exp-GLM. Additionally, the true spike time and spike trains differed when natural images were projected.

Taking the forest image (Fig 2.11) as an example, the pseudo-R^2 value was 0.01 of this model with offset. However, the pseudo-R2 value could not be calculated for defocused forest images, which were induced to ±1 D and ±2 D from focus. The images were too similar when the defocused

natural scenes were more than ±3 D. The np-GLM model performed better at predicting spike rates for the focused forest image, while the exp-GLM model was more suitable for predicting the defocused forest images. The raster plots of the predicted spike trains by the GLM models also indicated a distinct response for the focused forest image.

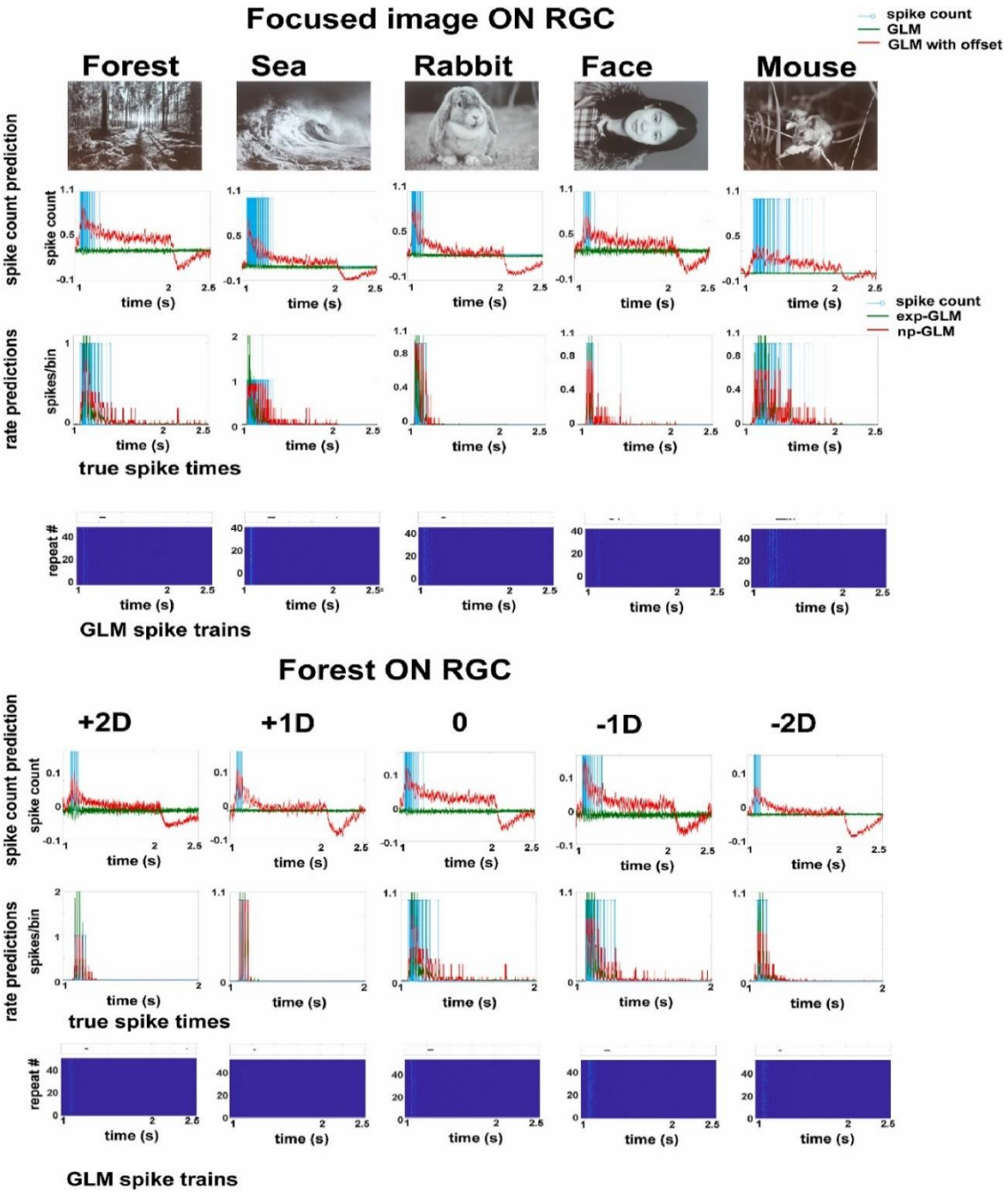

Figure 2. 11 GLM models predict natural scene stimulus on ON RGC in normal retinas.

The figures show GLM models applied to predict the spike count (upper row), rate (middle row), true spike times and spike trains (lower row) under different focused natural scene projections. The natural scenes are forest, sea, rabbit, face, and mouse from left to right. GLM models predict the spike count (upper row), rate (middle row), true spike times and spike trains (lower row) of the forest image well under focused, ±1 diopter, and ±2 diopter defocused projection.

4. Discussion

Myopia prevalence is continuing to increase worldwide. However, there are no effective methods to prevent or reverse myopia progression, partly due to a lack of understanding of how it develops. One major question is whether retinal circuits in myopic eyes process visual information differently in myopic than in normal eyes. To answer this question, the coding performance of RGCs in LIM and normal retinas was predicted and compared using the GLM model.

Understanding how RGCs encode the features of visual stimuli can provide insight into how retinas transmit visual information[101, 102]. More than 40 RGC subtypes exist in the mouse retina, each extracting specific features and exhibiting unique temporal response properties to the stimulus. The output of RGCs is determined by their retinal circuits, particularly between photoreceptor-to-bipolar cell synapses and coupled amacrine cells[103]. When retinas are exposed to defocused images with blurry edges and different contrast compared to focused images, the output to RGCs may be different[64]. Although RGCs may not directly sense the focused or defocused plane in the retina, the coding performance of αRGCs was investigated between normal and myopic retinas in this study.

Previous studies have shown that the αRGCs response varies between focused and defocused image projection, as well as their firing patterns[49]. This study used a model-based approach to explore further how myopic retinas affect the encoding of visual stimuli. The GLM model was employed to describe how stimuli are encoded in the spike trains of αRGCs, whose components can be compared to biophysical mechanisms[85]. The pseudo-R^2 values assessed by GLM were able to predict the difference in encoding performance between the ON and OFF subtypes of RGCs. The variation in coupling patterns between ON and OFF RGCs may explain this difference:

ON RGCs are only coupled with amacrine cells, while OFF RGCs are coupled with other OFF RGCs and amacrine cells[104]. These different coupling patterns may impact the encoding performance of RGCs.

Neural computation in the retinas is essential for visual processing and requires complex interconnections between cells. This study also raised a concern about whether the GLM model can be applied to analyze different subtypes of αRGCs similarly. However, according to former studies, the GLM model can effectively predict the responses of different subtypes of αRGCs under normal and intact circuit retinas[84, 105, 106]. If the retina is affected by myopia, there may be differences in how visual information is encoded by RGCs. Therefore, the predictions by the GLM model were applied to compare the differences between normal and myopic retinas. The difference was expected to be small. ON and OFF αRGCs were first recorded under focused and defocused image projection to test the differences. This recording was then fitted to the GLM model. The GLM model contains several filters adjusted to maximize the model's likelihood. The GLM model was then used to predict the spike counts, rate, true spike time, and spike trains of αRGCs in response to natural scenes. It was found that natural scenes induced different patterns of spike trains in the αRGCs. When predicting spike counts, the Linear-Gaussian GLM model was the best fit for predicting in both the normal and myopic retinas. There was no significant difference between focused and defocused image projection in predicting spike counts when comparing pseudo-R2 values, the pseudo-R2 was better at predicting spike counts for focused images than defocused image projection in myopic retinas. This variation indicates the circuit amendment exit in LIM retinas compared to normal retinas. With respect to spike rate prediction, AIC indicated that the np-GLM correctly predicted focused and defocused images in normal and LIM retinas. However, when a particularly blurry defocused image, +20D, was projected on the retinas, the

exp-GLM model provided a better fit in some subtype αRGCs in normal retinas. These αRGCs may recruit different subtypes or numbers of amacrine cells to encode visual information. There was also a difference in predicting the spike rate by np-GLM between normal and LIM retinas. It was observed that around 33% of αRGCs were a better fit in LIM retinas by exp-GLM under -10D and -20D defocused images, compared to 13% in normal retinas. The plasticity of the retinal circuit raises the likelihood that the LIM retina circuit modification could result from prolonged defocused status. Previous studies of this team have revealed that phosphorylation of Cx36 increases in myopic retinas, which may also suggest that the retinal circuits have acclimated to the myopic status[14, 71].

Although customized spatial frequency image stimuli revealed how RGCs encode visual information in normal and myopic retinas, this type of stimulus lacks realistic characteristics. To increase the complexity and diversity, natural scenes as stimuli are a better fit for studying RGC responses in the retina. These natural scenes contain a wide range of spatial frequencies and contrast levels, without color variations, which demonstrates single RGCs can accurately encode these different natural scenes in the normal retina. Both the focused and defocused status of natural scenes were projected onto the retina. The responses of RGCs were similar to those recorded using customized spatial frequency as stimuli.

More than two-thirds of αRGCs exhibited distinct response properties, in terms of the analysis in area, time of maximal rise (decay) slope, maximal rise(decay) slope, 80%–20% rise (decay) time, the EPSCs recorded from αRGCs revealed either maximal or minimal in response to focused images in normal and myopic retinas. These findings indicate that single RGC in both types of retinas exhibit similar biophysical responses to focused and defocused images.

In Cx36 KO mice, the inner and outer retinas were affected, with the loss of the primary rod pathway and secondary rod pathway in the outer retina and the disruption of Amacrine cell couplings with RGCs in the inner retina[47]. αRGCs in Cx36 KO retinas lost the maximal or minimal response in decoding the focused images, with more than 78% affected compared with normal and myopic retinas. Compared with focused, defocused images characterized by blurry edges, different focused planes, and contrast. These differences may require a filter function in the retina. ACs transfer signals to RGCs, leading to noise reduction, signal averaging, feedback inhibition, surround inhibition, and adaptation[107]. ACs may also participate in encoding the focused/defocused images in the normal and myopic retina. However, this process is disrupted by most ACs coupling RGCs in Cx36 KO mice. Overall, Cx36 KO mice lose the filters in their inner and outer retinas. Furthermore, human studies have suggested that the GJD2 gene (encoding Cx36 protein) may play a significant role in myopia development. Both humans and animals could be modulated by the Cx36 gap junction in myopia development[108, 109]. Further studies are needed to create LIM Cx36 KO mice and investigate the role of Cx36 role in this processing.

Retinal circuits could be altered if the defocused image stimulation remained. These changed entities of the retina could potentially serve as a therapeutic method for controlling myopia. However, long-term defocused status may trigger a series of irreversible cascades, leading to elongation of the length of the eye, . This may explain why myopia continues to progressing despite correcting ametropia.

5. Conclusion

The GLM model was used to compare the differences between normal and myopic retinas in decoding the focused/defocused image by ON and OFF αRGCs. Cx36 gap junction was found to play a critical role in computing this visual process. The diverse outcome of the GLM model with offset in LIM indicated the possible modification and plasticity of the retinal circuit in myopic retinas.

6. Limitation

Other animal models, such as marmosets or monkeys, may be more appropriate than the mouse model as they possess a retinal macular or fovea-like structure. For the purposes of this study, the LIM mouse model was observed and recorded at a single time point following three weeks of lens treatment in an 8-week-old mouse. Further investigation is required to evaluate the long-term efficacy of LIM models, as it is possible that adaptations in the retinal circuit could require a more prolonged timeframe to manifest.

CHAPTER 3 The response of retinal ganglion cells to optical defocused visual stimuli in mouse retinas

(Note: This chapter is published in "experimental eye research Feb 2024; doi: doi.org/10.1016/j.exer.2024.109834". Permission to include the published material has been granted by the corresponding author, who is also the supervisor of the candidature.)

1. Introduction

Animal studies have shown that myopia can be induced through compensatory responses of the eye, such as changes in anterior chamber depth, choroidal thickness, cornea, and primarily elongation of the vitreous chamber, resulting in the retina being exposed to blurred[110-112] or astigmatically defocused images[113]. Studies have suggested that retinal neurons can detect and respond to image focus, thereby regulating eye growth during refractive development[114]. Experiments involving goggle-wearing animals using chicks[115], tree shrews[116], mice[99], monkeys[117], and marmosets[111] have demonstrated the role of visual feedback in controlling eye growth. An important question is how the retinal neurons detect defocused images to initiate ocular compensation. The retina's ability to detect defocused images may occur at various stages of the neuronal visual pathways. Studies on monkeys[118] and chicks[57] have shown that myopia could still develop even after optic nerve sectioning to separate the eye from the brain. Thus, it appears that the dominant mechanism for detecting compensatory responses lies within the retinal circuitry rather than the brain. Furthermore, inhibiting retinal processing, but not post-retinal neural pathways, has been found to reduce compensation to cross-cylinder lenses in chick eyes,

suggesting the potential involvement of the retina in the presence of astigmatism[119]. These studies have demonstrated that exposure of the retina to defocused images leads to alter eye growth and refraction. However, despite the apparent key role of the retina, it remains unknown to what extent the retinal neurons can sense the complex spatial blur patterns caused by refractive errors.

The retina's role in the detection of astigmatism also remains to be determined. There has been some debate about the existence of “retinal astigmatism” [120]. Astigmatism can produce a specific pattern of optical aberrations in the retina, which may detect the distinct retinal defocused pattern caused by astigmatism originating from the eye or imposed optically. However, evidence from animal studies is controversial, as some animals have supported the theory that astigmatism induced by the lens in chicks is mediated by local signaling within the retina[121]. Using optical manipulation methods, more than half of the chick models fail to induce astigmatism[119]. Therefore, there is strong justification to explore the response characteristics of retinal neurons in relation to astigmatism and its effect on the retina. This study utilized custom-made astigmatic defocused stimuli to show the distinct responses exhibited by neurons in the retina to determine these response characteristics.

Retinal ganglion cells (RGCs), the final output neurons, may detect and encode various aspects of visual information, transmitting it to the brain[122], as they are capable of responding to focused or defocused images, potentially playing an important role in regulating growth, refraction, and myopia development in the retina[49, 64]. RGCs in the retina are particularly well-suited for mechano-sensing roles during myopia development. Over 40 types of RGCs have been identified in the retina and twice the number of amacrine cells (ACs)[123]. It has been suggested that RGCs may code differently in the myopic retina[124]. Recent studies have reported the involvement of certain types of RGCs, such as ON-delayed RGCs[125] and ipRGCs[63], in myopia development.

In this study, αRGCs were chosen as a representative as they are known to play a crucial role in visual processing and encode focused and defocused images differently in both normal and myopic retinas[122]. Additionally, αRGCs are characterized by having the largest somas, broader dendritic fields, and an evenly distributed mosaic-like pattern within the retina[23, 126]. The elongated axial length of the myopic retina could also significantly impact the properties of αRGCs, which are considered to reflect the characteristics of all RGCs in the retina.

Gap junctions are channels that enable direct cell-to-cell communication. One essential element of neuronal gap junctions, which are found in most retinal cell types[127], including RGCs, is Connexin 36 (Cx36), which is predominantly present in the inner retina. International genome-wide meta-analyses on myopia have shown that single nucleotide polymorphisms (SNPs) in the genome are associated with high expression of GJD2, the gene for the Cx36 protein. These findings suggest that Cx36 may be linked to refractive errors. Additionally, studies have demonstrated changes in the phosphorylation of Cx36 in murine retinas impacted by myopia[14]. Thus, Cx36 is a plausible modulator of myopia development[108, 109]. It has also been reported that the intact retinal circuit involving Cx36 is crucial for computing the disparity in visual signaling between focused and defocused images. ON and OFF αRGCs lose their coupling to amacrine cells, and OFF αRGCs fail to couple in Cx36 knockout (KO) mice[128]. In this study, genetically modified Cx36 KO mice were used as a control to investigate the impact of Cx36 deficiency on the retinal circuit.

In vitro, retinal stretching mimics some aspects of the myopic status. Spherically and astigmatically defocused images were optically projected onto the retina, and the biophysical responses of αRGCs were used to explore their dynamics. This study aimed to determine whether individual αRGCs have the ability to perceive the distinctive retinal blur patterns caused by

spherically defocused and astigmatically defocused images. The study also examined the biophysical properties of αRGCs when subjected to in vitro stretching as a simulation of myopia and how this may affect their response to focused or defocused images. The major aim was to determine whether αRGCs can accurately transmit visual information related to refractive errors onto the retina. If this does occur, it could lead to the development of novel early treatment strategies to prevent the onset of common visual conditions, including nearsightedness and astigmatism.

2. Methodology

2.1 Animals

All procedures on animals were approved by the Animal Subjects Ethics Sub-Committee of the Hong Kong Polytechnic University (Approval number: 20–21/128-SO-R-GRF). The study complied with the Guide for the Care and Use of Laboratory Animals published by the National Institutes of Health.

A mouse model was used in this study, as its eye has a scleral structure and fibroblasts similar to humans[110]. In addition, the mouse is particularly advantageous with its well-known retinal circuit and the availability of genetic lines to label specific cells such as ON and OFF αRGCs. Adult wild-type (WT) mice of either sex (postnatal day 16–56) C57BL/6J (RRID: IMSR_JAX:000664), weighing (15–20 g), were used in the study (n = 34). Kcng4-YFP (6–8 weeks, n = 11) mice[89], of either sex (weighing 15–25 g), were used for ON and OFF αRGC labeling as previously described[129]. Homozygous Cx36KO mice (Cx36−/−) (RRID: MGI:3,810,172), first generated in the laboratory of David Paul, Harvard Medical School (Cambridge, MA), were a kind gift from Samuel M. Wu, Baylor College of Medicine (n = 6, 6–8 weeks, weight 15–25 g). All animals were maintained in a 12-h light/12-h dark cycle. The mice were deeply anesthetized with an intraperitoneal injection of ketamine and xylazine [80 mg/kg and 10 mg/kg (body weight), respectively], and lidocaine hydrochloride (20 mg/ml) was applied locally to the eyelids and surrounding tissues before enucleation. For consistency, all mouse retinas were collected around 10 a.m. after overnight dark adaptation.

2.2 Retina preparation

Eyes were removed under dim red illumination. The retinas were dissected into four equal quadrants for patch-clamp recordings and attached to a modified translucent Millicell filter ring (Millipore, Bedford, MA, USA). The flattened retinas were superfused with oxygenated mammalian Ringer's solution composed of (mM): 120 NaCl, 2.5 KCl, 25 NaHCO3, 0.8 NaHPO4, 0.1 NaH2PO4, 1 MgCl2, 2 CaCl2 and 5 D-glucose[90]. The bath solution was continuously bubbled with 95% O2–5% CO2 and maintained at approximately 32 °C as described previously[7]. Anesthetized animals were killed by cervical dislocation immediately after enucleation.

2.3 Patterned light stimulation

A green (525 nm) organic light-emitting display (OLED) (OLEDXL, Olightek, Kunming, Yunnan, China; 800 × 600-pixel resolution, 85 Hz refresh rate) was controlled by an Intel Core Duo computer with a Windows 7 operating system. In this setup, using a Nikon 40× water-immersion objective (CFI Apo 40XW NIR, NA = 0.8), the area of the retina that received light stimuli was 250 μm in diameter. Under the 40× objective, the 15 μm diameter pixels of the OLED presented 0.25 μm/pixel on the retina. Grating images with a controllable spatial frequency were generated by PsychoPy (University of Notttingham, UK) were projected onto the photoreceptor layer. The background light intensity was ∼700 photoisomerizations per rod per second (Rh*/rod/s) (ILT5000 Research Radiometer, International Light Technologies, Inc., Peabody, MA, USA), and the highest stimulus was ∼1.816 × 105 Rh*/rod/s. Light intensities were calculated assuming an average rod density of 437,000 rods mm−2 and quantum efficiency of 0.67[130]. The rod pathway was saturated at this background illumination level, leaving the cone pathway to mediate the light

response in WT and Cx36KO mice[92]. All images were produced by a 1-s stimulation followed by a 5-s interval. A focused/defocused 125 μm diameter of 0.0067 cycles per degree (cpd) image was applied as shown in Fig 3.2, Fig 3.3, Fig 3.4, Fig 3.5, Fig 3.6, Fig 3.7.

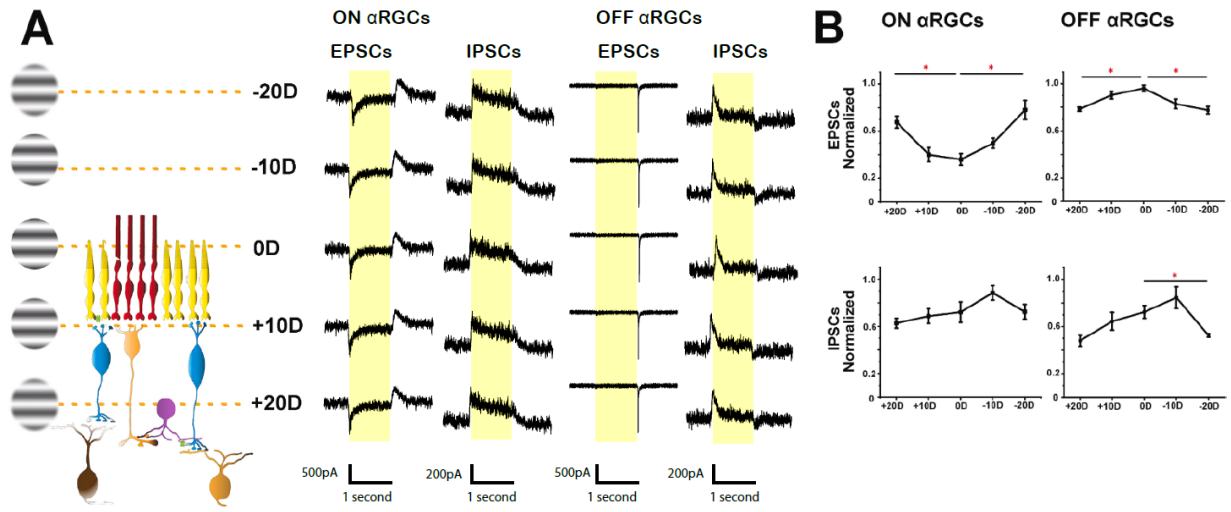

Figure 3. 1 Schematic of αRGCs responses to optically focused and defocused images

A: The schematic illustrates a focused image with a 125 μm diameter and a frequency of 0.0067 cpd projected onto the photoreceptors' outer segment. The focused image was determined at the position where the image was projected at the outer segment. This focused image was designed as having 0 D. By shifting the focus across the retinal layers, optically defocused images of ±10 and ± 20 D were created and projected onto the different retinal layers. The calculation for defocusing was based on a 5 μm defocus inducing ±1 D refractive error change[93], and the light intensities varied from 3.74 × 104 to 3.85 × 104 Rh*/rod/s. Excitatory postsynaptic currents (EPSCs) and inhibitory postsynaptic currents (IPSCs) of ON and OFF αRGCs were recorded in Wild-type retinas.

B: The normalized EPSCs and IPSCs responses of illustrated ON and OFF αRGCs are displayed. EPSCs of ON and OFF αRGCs showed significant differences between the focused image and ±20 D defocused image ($p < 0.05$, t-test, respectively). There was no significant difference in IPSCs of the ON αRGC between optically focused and defocused images, while IPSCs of the OFF αRGC differed significantly between the focused image and the −20D defocused image. An asterisk (*) indicates a significant difference ($p < 0.05$, t-test).

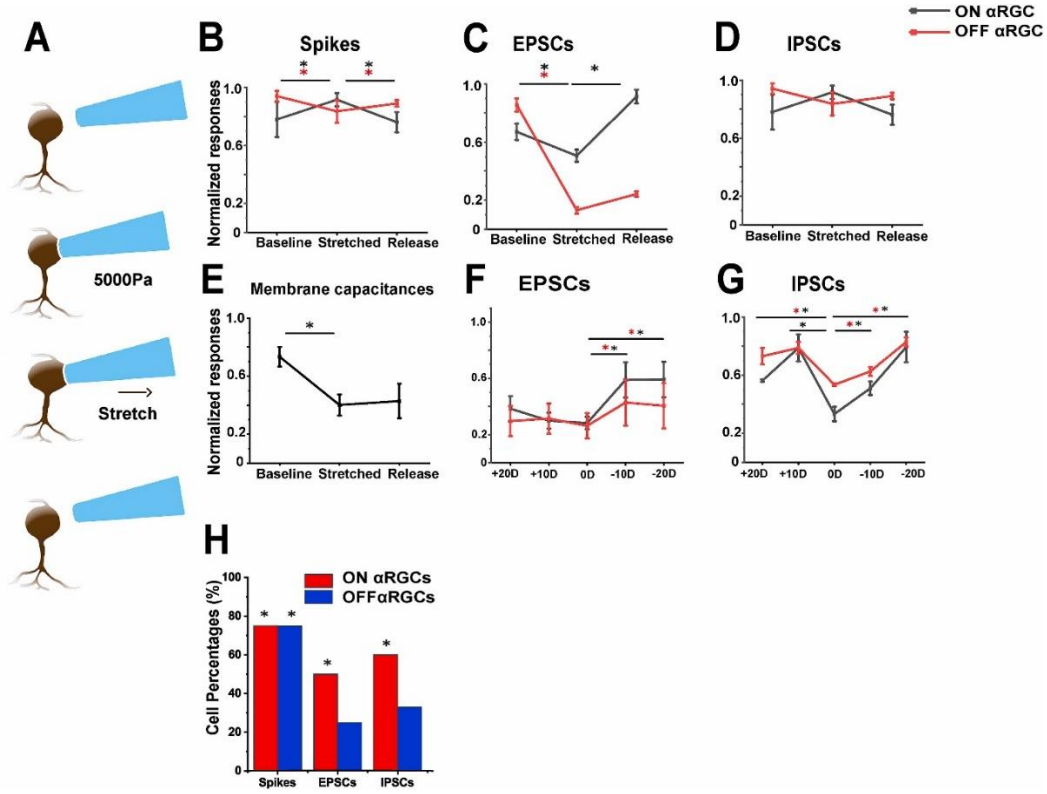

Figure 3. 2 Differential response of αRGC biophysical properties to soma stretching mimicking myopia

A: The schematic shows an αRGC soma stretching by 8 μm using a pipette with approximately 5000 Pascal (Pa) of negative pressure. The stretching occurred in the direction of the optic nerve and amounted to 5% of the soma's size. Spike rates (B), EPSCs (C), and membrane capacitances

(E) exhibited significant differences due to the stretching in the illustrated αRGC, while there was no significant difference observed in IPSCs (D). F and G: EPSCs and IPSCs of αRGCs responded differently to defocused images in comparison to focused images. H: Statistical results of spikes, EPSCs and IPSCs of ON and OFF αRGCs before and after soma stretching. An asterisk (*) indicates a significant difference ($p < 0.05$, t-test in B to G). (*) indicates significance based on the Wilcoxon signed ranks test in H.

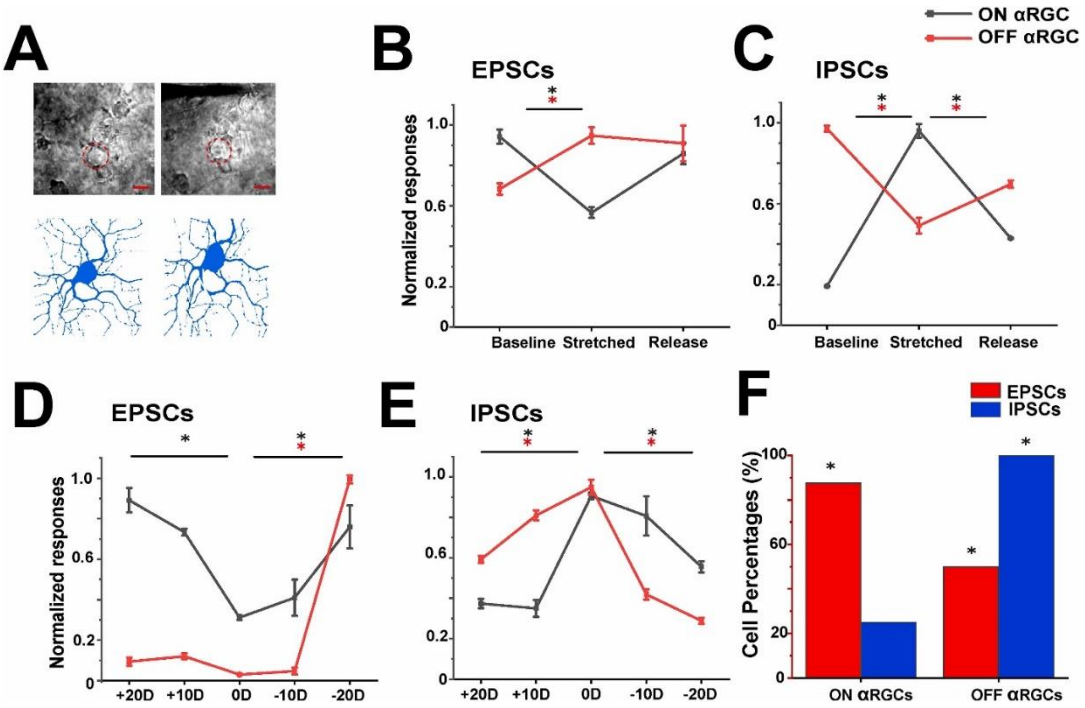

Figure 3. 3 Alterations in Biophysical properties of αRGCs following retinal stretching to mimic myopia

A: A sharp electrode was inserted into the retina and stretched away toward the direction of the optic nerve. The red dashed circle indicates the recorded RGC. The lower blue schematic diagram shows RGC soma and dendritic field shape changes after retinal stretching. B and C: αRGCs exhibited significantly different responses in EPSCs (B) and IPSCs (C) following cell stretching.

D and E: Compared to a focused image (0 D), ON and OFF αRGCs responded differently in EPSCs and IPSCs under defocused images. F: 87.5% of ON αRGCs and 50% of OFF αRGCs showed significant differences in EPSCs between focused and defocused images. 25% of ON αRGCs and all OFF αRGCs exhibited a significant difference in IPSCs responses. There was a significant difference ($p < 0.05$) between EPSCs of ON and OFF αRGCs and IPSCs of OFF αRGCs before and after soma stretching (Wilcoxon signed ranks test). An asterisk (*) indicated a significant difference ($p < 0.05$, t-test in B to E and Wilcoxon signed ranks test in H).

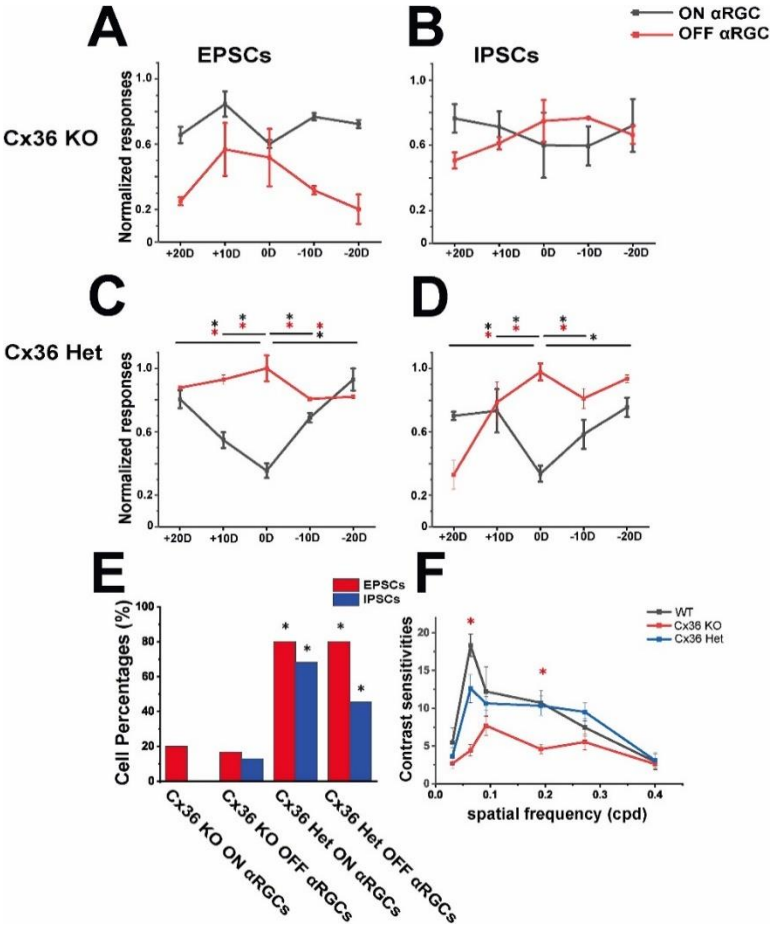

Figure 3. 4 The biophysical properties of RGCs in Cx36 KO mice

A and **B:** More than 80% of ON and OFF αRGCs in Cx36 KO mice showed no difference in responses for EPSCs and IPSCs between focused (0 D) and defocused images (equal to ±10 and ± 20 D). **C and D:** ON and OFF αRGCs in Cx36 Het mice exhibited significant differences in EPSCs and IPSCs between focused and defocused images. **E**: Summary of αRGCs percentage demonstrated differences in EPSCs and IPSCs between focused and defocused images in Cx36 KO mice and Cx36 Het mice. There was a significant difference ($p < 0.05$) in EPSCs/IPSCs of ON and OFF αRGCs between Cx36 KO and Cx36 Het mice (Wilcoxon signed ranks test). **F**: Cx36 KO mice exhibit significantly decreased contrast sensitivity based on optokinetic reflex (OKR) testing. An asterisk (*) indicates a significant difference ($p < 0.05$, *t*-test in A to D and F; Wilcoxon signed ranks test in E)

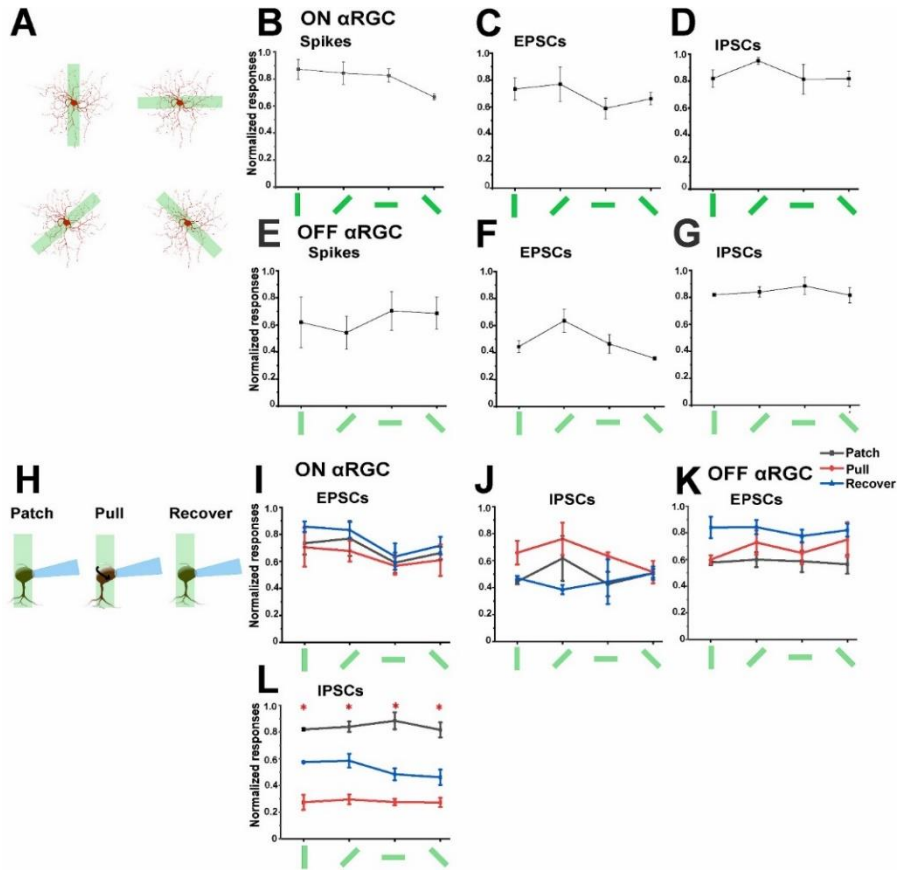

Figure 3. 5 Biophysical properties of αRGCs under different image projection directions

A: The schematic illustration shows how different light bar directions are projected onto the receptive fields of αRGC. **B to G:** Normalized spikes, EPSCs, and IPSCs of ON and OFF αRGCs showed no differences in response to different image projection directions. **H**: The schematic indicated that an αRGC soma was pulled using a suction pipette to change the light projection angle, mimicking an astigmatic defocus. **I to K:** Under twisted soma conditions, ON and OFF αRGCs showed no differences in EPSCs and IPSCs across four light bar directions, respectively. **L:** 80% OFF αRGCs (4 of 5) exhibited significant differences in IPSCs in the four directions. An asterisk (*) indicates a significant difference ($p < 0.05$, *t*-test).

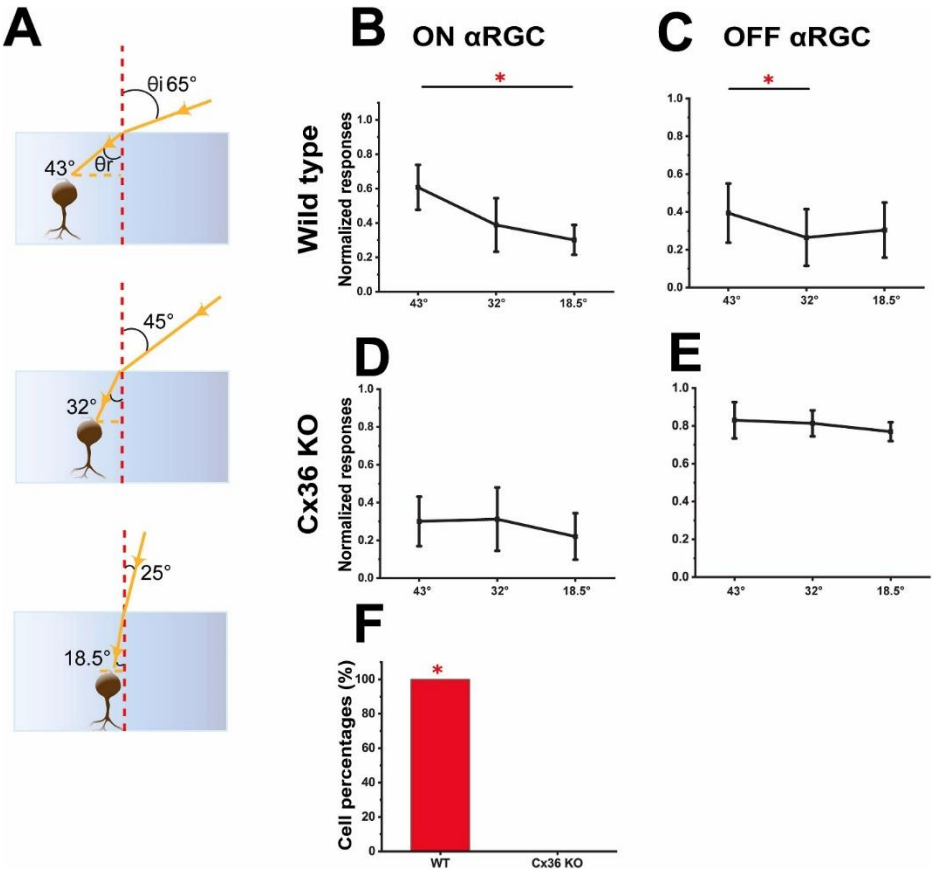

Figure 3. 6 Biophysical properties of αRGCs respond differently to light passing through a solution to simulate astigmatism

A: The schematic shows the deviation of the laser beam entering the immersing solution to simulate astigmatism. **B and C**: The normalized EPSCs from ON and OFF αRGCs showed significant differences in response to different refractive angles of light projections in WT mice. **D and E**: EPSCs of ON and OFF αRGCs did not differ in response to different angles of light refraction in Cx36 KO mice. **F**: All αRGCs in WT mice responded differently to the various angles of light refraction, but this response pattern was absent in Cx36 KO mice. There were significant differences ($p < 0.05$) in EPSCs of αRGCs between Cx36 KO and WT mice (Wilcoxon signed ranks test). An asterisk (*) indicates a significant difference ($p < 0.05$, *t*-test in B to E; Wilcoxon signed ranks test in F).

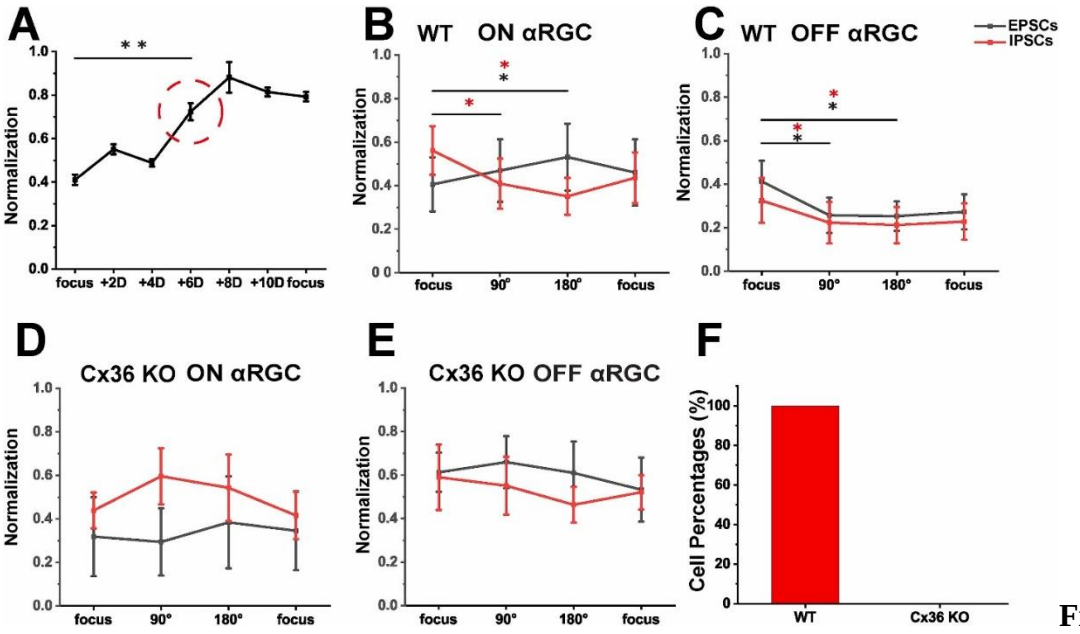

Figure 3.7

Figure 3. 7 Biophysical properties of αRGCs respond differently to astigmatic defocused images

A: The astigmatic defocused images were generated using a custom-made device, and the cell responses were measured in spikes by adding plano-cylindrical lenses ranging from +2D to +10D. In the experiments, a +6.00D astigmatic lens was applied with an axis at 90° and 180°. **B and C:** ON and OFF αRGCs showed significantly different responses in EPSCs and IPSCs to the astigmatic blur as compared to the focused image in the WT retinas. **D and E:** ON and OFF αRGCs showed no significant different response in EPSCs and IPSCs to the astigmatic blur in the Cx36 KO retinas**. F:** αRGC showed significantly different responses to astigmatically defocused images in the WT mice but not in Cx36 KO mice. An asterisk (*) indicates a significant difference ($p < 0.05$, *t*-test).

The methodology used to generate defocused images on the retina in vitro has been described previously[64]. A customized light projection system with an adaptable astigmatic lens was developed to project optically simulated astigmatic images onto photoreceptor cells using a physically moveable lens rather than digitally simulated astigmatic images. Based on the previous report showing that an axial elongation of 5 μm would induce a 1 Diopter (D) refractive error in the mouse retina[93], a 100 μm defocus would be expected to generate plus or minus 20 D of refractive error in the mouse retina under microscopy depending on the direction of defocus. The system also produces 525 nm of different sizes of light using the Mightex Polygon1000 (labeled in green in Fig 3.5).

The defocused images are generated using a microdisplay that projects a grating image, oriented vertically or horizontally, onto the photoreceptors via an infinity-corrected microscope. The details of the device were previously applied and published[64]. Light from the microdisplay is collimated via a collimating lens. The collimated light then passes through an astigmatic (plano-cylindrical)

trial lens (Cylinder: +6/0 D, Axis meridian: 180°). The astigmatic lens splits the light into two principal foci onto the retina (Fig 3.8):

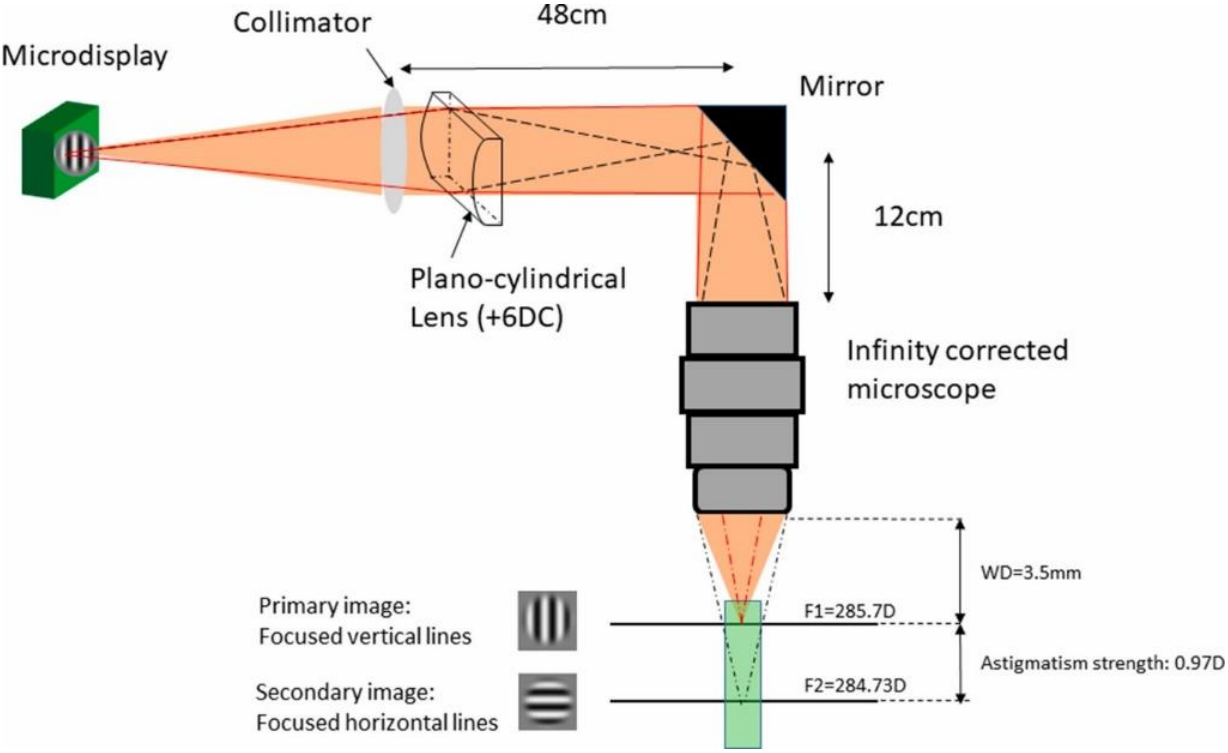

Figure 3. 8 Detailed schematics of generating astigmatically blurred images

AS = F2-F1 F: Focus AS: Astigmatism Strength. WD = 3.5mm, dx = 12um.

The axial position for which the vertical grating is sharply imaged (red dotted rays) corresponds to the first focus (vertical focal line), and the position where the horizontal grating is sharply imaged (black dotted rays) corresponds to the second focus (horizontal focal line). For a +6 D astigmatic lens, the separation between the two focal lines represents an astigmatic blur magnitude of approximately 0.97 D. The light intensity for the two focal lines does differ depending on the size of the microscope aperture, as it can block certain rays.

2.4 Stretch the RGCs in vitro

The αRGC soma was fully exposed. Then, negative pressure was provided using an open-tip (diameter around 7–8 μm) patch pipette attached to a vacuum source (LEM512-OEC, Lefoo industrial components, Hangzhou, Zhejiang, China). The RGC was gently elongated in the axial direction. (Fig 3.9). Another approach was to pull on the retina directly with a patch pipette to stretch the RGCs. RGCs with a diameter increase of >5% were included in the analysis. The direction of the retina was carefully aligned with the axial.

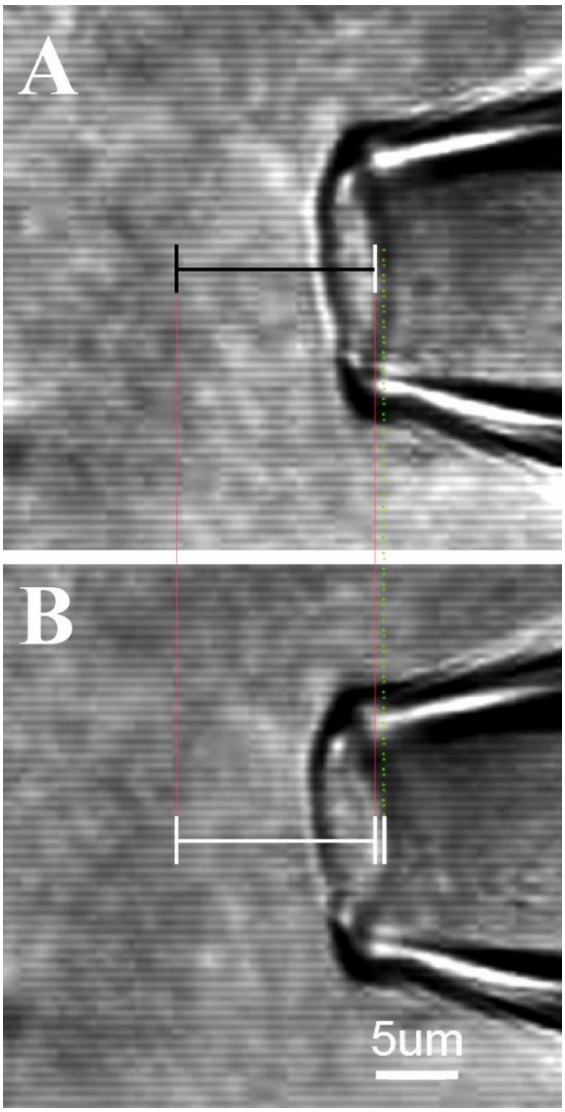

Figure 3. 9 Schematic of RGC soma stretching to simulate myopic status

A: Negative pressure was applied using an open tip with a diameter of approximately 7–8 μm, exerting around 5000Pa suction on the soma of the RGC. **B:** The RGC soma was pulled by a pipette to cause a 5% increase in diameter**.**

2.5 Electrophysiology

Extracellular and whole-cell recordings were obtained from single αRGCs of the mid-peripheral retina in the nasotemporal plane. Recordings were performed using an Axopatch 700 B amplifier connected to a Digidata 1550 B interface and pCLAMP 10 software (Molecular Devices, San Jose, CA). To improve the space clamp and to block spiking, the whole-cell excitatory postsynaptic potentials were recorded with an internal solution containing caesium methanosulfonate instead of potassium gluconate. The chloride equilibrium potential (ECl) with these internal solutions was approximately −63 mV. The excitatory and inhibitory current responses were isolated by holding the membrane potential approximately at the chloride or cation equilibrium/reversal potentials, −63 and −10 mV, respectively.

Spike trains were recorded digitally at a sampling rate of 10 kHz with Axoscope software (Molecular Devices), sorted by an Offline Sorter (Plexon, Dallas, TX) and NeuroExplorer (Nex Technologies, Littleton, MA, USA) software. In the whole-cell recording, the kinetics (amplitudes) of excitatory postsynaptic currents (EPSCs) and inhibitory postsynaptic currents (IPSCs) and membrane capacitances were measured and compared. For comparison purposes, the spike responses were normalized among the stimuli of focused and defocused images. The recorded cells were dye-injected using pipette tips filled with 4% Neurobiotin (Vector Laboratories, Burlingame, CA, USA) and 0.5% Lucifer Yellow-CH (Molecular Probes, Eugene)[7].

2.6 Optokinetic reflexes

The optomotor responses of mice were measured using the OptoMotry System (CerebralMechanics, Lethbridge, Alberta, Canada). The photopic vision was tested with a background light of ∼70 cd*s/m^2. OptoMotry software was used with the screens of contrasting bars of light not visible to the investigator, and the investigator was blinded to the groups to minimize bias. Visual acuity testing was performed at 100% contrast with varying spatial frequency thresholds, while contrast-sensitivity testing was performed at a fixed spatial frequency threshold (0.092 cpd). The temporal frequency was set at 1.5 Hz for both tests. After a series of test episodes, the same computer program was applied to both eyes to determine the acuity or contrast sensitivity.

2.7 Data acquisition and analysis

For comparison purposes, the maximal responses normalized all the spike, EPSCs and IPSCs data of αRGCs. Statistical analyses were performed using Origin software (OriginLab, Northampton, MA). Statistically, significant differences ($p < 0.05$) were determined by the Student t-test and Wilcoxon signed ranks test.

3. Results

3.1 Biophysical properties of RGCs in response to focused/defocused image projection

One second of custom images with a diameter of 125 μm and spatial frequency 0.0067 cpd (525 nm, light intensities ranged from 3.74 × 104 Rh*/rod/s) were projected onto the receptive field of αRGCs and precisely focused on the outer segment of photoreceptor cells. Myopic or hyperopic defocused images were generated by adjusting the focus plane of the projected images on the retina (i.e., in front of or behind the photoreceptor). As shown previously[93], a shift in the focus plane of 5 μm corresponds to approximately 1 D of defocus in the mouse retina. A diopter of 0 defines an image that is precisely focused on the outer segment of the photoreceptor layer. Thus, by shifting 100 μm in different directions, the projected images were blurred by about ±20 D of defocus (Fig 3.1A).

EPSCs and IPSCs in ON and OFF αRGCs were recorded and analyzed from WT retinas (Fig 3.1A). The recorded ON or OFF αRGCs were confirmed by Neurobiotin injection after patch recording, as in previous experiments[131] (Fig 3.10).

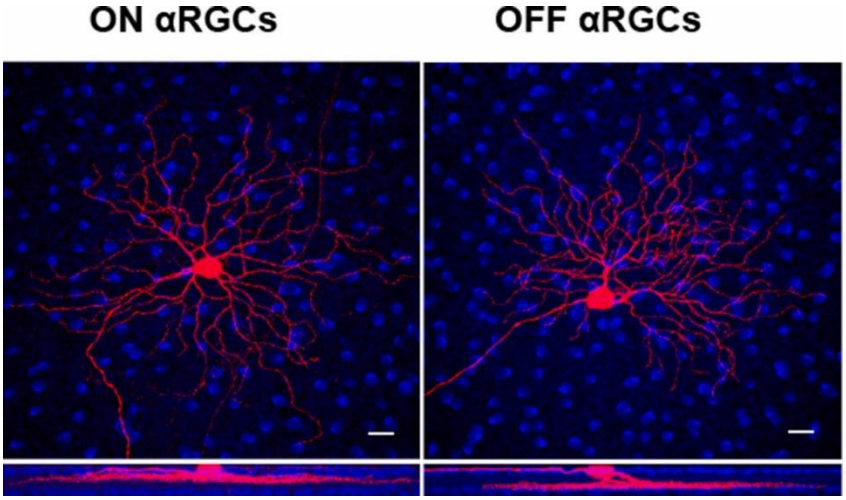

Figure 3. 10 ON and OFF αRGCs in the wild-type mouse retinas

Representative images show ON (left) and OFF (right) αRGCs in the WT mouse retina labeled and visualized with Cy3 (red) after patch recording. The stratification of ON and OFF αRGCs was double-labeled with anti-ChAT antibody (blue) in the WT mouse retina. Scale bar: 20 μm.

For example, (Fig 3.1B), the amplitude of EPSCs in ON and OFF αRGCs ranged from a few picoamps up to >500 pA. The maximal amplitude was applied to normalize the amplitude of EPSCs and facilitate the comparison. The normalized EPSCs showed significant differences between an optically focused image (0 D) and equal to ±10D or ±20D defocused image projection ($p < 0.05$, t-test for comparisons between focused and defocused images). However, there was no significant difference in normalized IPSCs in the illustrated ON αRGC between optically focused and defocused images. In contrast, the normalized IPSCs of OFF αRGC showed a significant difference between optically focused images and equal to −20D defocused images (Fig 3.1B).

There are four subtypes of αRGCs: ON-transient, ON-sustained, OFF-transient, and OFF-sustained. Although these subtypes were consistently recorded, the results indicate that EPSCs and IPSCs of all ON-sustained (n = 3) and OFF-transient (n = 3) αRGCs showed significant differences between focused (0 D) and defocused images (±10 and ± 20 D). Among ON-transient αRGCs (n = 13), 85% (11 of 13) of cells responded differently in EPSCs between optically focused and at least one of the defocused images, in contrast to 62% (8 of 13) showed different responses in IPSCs. Of the recorded OFF-sustained αRGCs (n = 10), 100% exhibited significantly different responses in EPSCs between optically focused and defocused images. Only 60% 6 of 10) of these cells responded differently in IPSCs. In the subsequent experiments, only ON and OFF αRGCs will be categorized due to the small quantities of ON-sustained and OFF-transient αRGCs.

3.2 Biophysical effects of soma stretching on αRGCs

The mouse eye axial length averages 3 mm, measured from the cornea to the nerve fiber layer. If the axial length is extended to 3.1 mm, the refractive error will become −20 D myopic. Considering only the retina, which is extended from a 1.5 mm radius to 1.55 mm, RGCs would stretch by 6.7% along the axial. In the study, αRGCs were stretched by 5% to simulate the myopic status for the convenience of measurement and calculation (Fig 3.9).

Negative pressure (approximately 5000 Pa) was applied with an 8 μm tip glass microelectrode to mimic myopia, which may vary depending on the tip size. This pressure is applied opposite a 3–5% radius increase, which stretches RGC somata. Then, a 1-s, 125 μm, 0.0067 cpd diameter (light intensities:3.74 × 104 Rh*/rod/s) sinusoidal grating image was projected onto different photoreceptors layers to mimic various powers of defocused images. The responses of ON and

OFF αRGCs, such as spikes, EPSCs, IPSCs, and capacitances, were tested in WT mouse retinas. To determine whether stretching RGC soma to simulate myopic status could affect postsynaptic current, EPSCs/IPSCs were recorded before stretching as the baseline and recovery after stretching removal (Fig 3.2A).

The spike rates of exampled ON and OFF αRGC in response to light stimuli increased during stretching. Compared to un-stretched status, the illustrated spike of ON and OFF αRGCs had significant differences under cell stretching ($p < 0.05$, t-test). The same significant changes can also be observed in EPSCs and membrane capacitances in the illustrated ON αRGCs ($p < 0.05$, t-test) but not in IPSCs of ON and OFF αRGCs; membrane capacitances of OFF αRGCs ($p < 0.05$, t-test). Interestingly, the membrane capacitances in the illustrated αRGCs decreased after stretching ($p < 0.05$, t-test) (Fig 3.2B–E).

75% of ON αRGCs (n = 8) and OFF αRGCs (n = 8) demonstrated significant differences in spike activities between stretched and un-stretched cells. Similarly, 50% of ON (n = 6) αRGCs and 25% of OFF αRGCs (n = 6) showed a significant difference in EPSCs after stretching, while 67% of ON αRGCs (n = 6) and 33% of OFF αRGCs (n = 6) exhibited significant differences in IPSCs. Consequently, all αRGCs displayed decreased capacitances after stretching (n = 7).

There was a difference ($p < 0.05$) in spike activities, EPSCs/IPSCs of ON αRGCs before and after stretching were analyzed and compared by the Wilcoxon signed ranks test (Fig 3.2H).

With stretching RGC soma to simulate myopic status, EPSCs of both illustrated ON and OFF αRGCs showed significant differences between focused images (0 D), and yielded either maximal or minimal responses under focused stimuli) and optically defocused images equal to −10 and −20D ($p < 0.05$, t-test for comparisons between focused and defocused images). 80% ON αRGCs

(n = 5) and OFF αRGCs (n = 5) exhibited significant differences in EPSC responses between optically focused and defocused images. IPSCs in ON αRGC also demonstrated significant differences between focused and defocused images (Fig 3.2F and G). In addition, all recorded ON αRGCs (n = 5) and OFF αRGCs (n = 5) showed significant differences in cell responses between optically focused (0 D) and at least one of the defocused images (±10 or ±20D). The results indicated the αRGCs responded significantly differently between optically focused and defocused images under stretching status to mimic myopia.

3.3 The biophysical properties of RGCs following retinal stretching to mimic myopia

To accurately mimic myopic conditions, the entire retina was stretched instead of only RGC somas, and the responses of αRGC were observed. This retinal stretching method, which differs from solely stretching the somas, allows for extending RGC dendrites and better approximates pathophysiological changes during myopia development.

A sharp pipette was applied to pull and stretch the retina along with the direction of the axial as a whole. Due to difficulty in controlling the applied power, the soma of recorded RGCs was observed after exposure for patch recording (Fig 3.3A). The stretched RGCs somas increased by 50 μm and were then recorded. Subsequently, a 1-s, 125 μm in diameter with a 0.0067 cpd, was projected at different photoreceptor layers to mimic different powers of optically defocus.

First, EPSCs, IPSCs of ON αRGCs (n = 12), and OFF αRGCs (n = 11) were tested in the retinas of WT mice. The postsynaptic currents (EPSCs and IPSCs) in both ON and OFF αRGCs showed significant differences following retina stretching (Fig 3.3B and C).

The illustrated ON αRGC showed significant differences in EPSC responses between focused (0 D) and equal to ±20D defocused image projections ($p < 0.05$, t-test for comparisons between focused and defocused images), whereas the illustrated OFF αRGCs showed significant differences only with −20D defocused image. IPSCs of the ON and OFF αRGCs differed significantly between focused images and ±20D defocused images (Fig 3.3D and E).

86% of ON αRGCs (n = 14) and 50% of OFF αRGCs (n = 12) demonstrated significant differences in EPSCs between focused and defocused images under stretching conditions. Additionally, 25% of ON αRGCs and all OFF αRGCs showed significant differences in IPSCs between focused (0D) and defocused images (±10 or ±20D) after stretching. There was a significant difference ($p < 0.05$) in EPSCs of ON and OFF αRGCs and IPSCs of OFF αRGCs before and after stretching (Wilcoxon signed ranks test) (Fig 3.3F).

3.4 The biophysical properties of RGCs in Cx36 knockout mice

The postsynaptic currents of RGCs were recorded in Cx36 KO (Cx36−/−) mice under focused and defocused image projections to evaluate the role of the Cx36-involved neural circuitry in decoding refractive error images. This aimed to assess whether abnormal circuits impacted RGC biophysical properties. Additionally, visual performance differences were compared among C57BL6 wild type(Cx36+/+), Cx36 KO, and Cx36 Het (Cx36+/−) mice through behavior testing.

In the case of both illustrated ON and OFF αRGCs, there were no significant differences ($p > 0.05$, t-test for comparisons between focused and defocused images) in EPSCs between focused (0D) and defocused images stimuli (equal to ±10 and 20 D) (Fig 3.4A). However, 20% (1 of 5) of ON

αRGCs (n = 5) displayed notable differences in EPSCs between focused and defocused images, while none of the OFF αRGCs (n = 5) in Cx36 KO mice exhibited such differences (Fig 3.4E).

The IPSCs of both illustrated ON and OFF αRGC showed no difference ($p > 0.05$, t-test for comparisons between focused and defocused images) between focused (0D) and defocused images stimuli (equal to ±10 and ± 20 D) (Fig 3.4B). Only 17% (1 of 6) of ON αRGCs (n = 6) and 14% (1 of 7) of OFF αRGCs (n = 7) exhibited significant differences in IPSCs between focused and defocused images in Cx36 KO mice (Fig 3.4E).

Cx36 Het mice were tested as the control. Example ON and OFF αRGC showed significant differences in EPSCs and IPSCs between focused and defocused images (equal to ±10 and ± 20 D) (Fig 3.4C and D). In Cx36 Het mice, 80% (8 of 10) of ON αRGCs (n = 10) and 80% (8 of 10) of OFF αRGCs (n = 10) exhibited significant differences in EPSCs between focused and defocused images. Additionally, 70% of ON αRGCs (n = 10) and 50% of OFF αRGCs (n = 10) showed significant differences in IPSCs, similar to the results observed in WT mice retinas (Fig 3.4E). Statistically, there was a significant difference ($p < 0.05$) in EPSCs/IPSCs of ON and OFF αRGCs between Cx36 KO and Cx36 Het mice (Wilcoxon signed ranks test).

Additionally, Cx36 KO mice show significantly decreased contrast sensitivity of 0.064 cpd and 0.192 cpd compared to wild type and Cx36 Het mice in the behavior test (n = 8) (Fig 3.4F). Axial length (3.42 ± 0.02 mm; mean ± SEM, n = 10) of Cx36 KO was elongated ($p < 0.05$, t-test) compared with WT mice eyes (3.31 ± 0.01 mm, n = 10) (Fig 3.11).

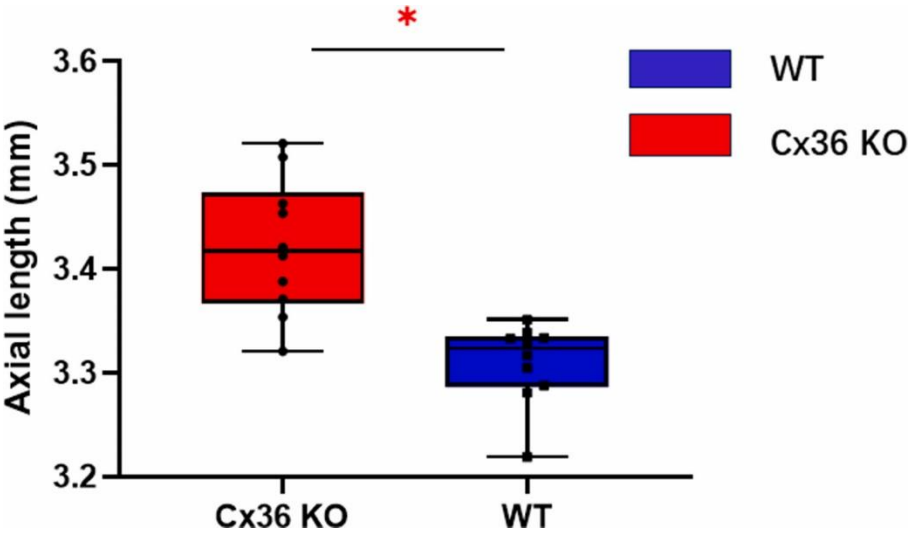

Figure 3. 11 Axial Length of Cx36 KO mice by Optical Coherence Tomography (OCT) measurement

Optical Coherence Tomography (OCT) was used to measure the axial length of the Cx36 KO (3.42 ± 0.02 mm; mean ± SEM, n = 10) and WT mice eyes (3.31 ± 0.01 mm, n = 10) from the corneal surface to the retinal pigment epithelium layer. An asterisk (*) indicated a significant difference ($p < 0.05$, *t*-test).

3.5 Biophysical properties of αRGCs with/without retinal twisting under the projection of astigmatically defocused images

Experiments were conducted to test the biophysical properties of αRGCs under retinal image projections simulating astigmatic defocus. First, a 20 μm × 200 μm 525 nm light bar (5.23×10^8 photons/um/s[110]) generated by the Mightex Polygon1000 system was projected onto the receptive fields of αRGCs in four different directions (90°, 180°, 45° and 135°) (Fig 3.5A).

Both ON (n = 6) and OFF (n = 7) αRGCs were recorded for spikes and postsynaptic currents (EPSCs and IPSCs).

There were no differences ($p > 0.05$, *t*-test) in responses to image projections in the receptive fields at the four angles in illustrated ON and OFF αRGCs (Fig 3.5B–G).

Secondly, the somas of ON and OFF αRGCs were pulled using a suction pipette to generate a 30-degree angled light projection (Fig 3.5H). Baseline, pulled, and recovery conditions were recorded, and then the same light bar was projected onto the receptive fields in four directions.

Recorded ON αRGCs (n = 5) and OFF αRGCs (n = 5) showed no difference ($p > 0.05$, *t*-test) in the EPSC's responses to the different light directions following twisting. However, 80% of OFF αRGCs (4 of 5) with pulled somas exhibited significant differences in IPSC compared to the patched status when exposed to the four different light bars (Fig 3.5I–L).

3.6 The biophysical properties of αRGCs respond to light passing through the solution

When light passes through a solution, it undergoes refraction. The angle of incidence of a laser beam (200 μm in diameter) passing through Ringer's solution was changed to test whether this refraction affected the biophysical properties of αRGCs.

According to Snell's law of refraction, $n1 \sin i1 = n2 \sin \theta$. Incident angles of 65°, 45° and 25° of light are equivalent to refractive angles of 43°, 32 and 18.5° of light, respectively (Fig 3.6A). Only EPSCs of αRGCs from both WT and Cx36 KO mice were recorded and normalized. αRGCs from Cx36 KO mice were recorded as a control to test the importance of intact retina circuits.

The illustrated ON and OFF αRGC showed significant changes in EPSCs when subjected to different angles of light projections (Fig 3.6B and C). All ON and OFF αRGC (total n = 12) responded differently in EPSCs to the different angles of projections (Fig 3.6F).

However, the ON and OFF αRGC did not exhibit any differences in EPSCs when exposed to different angles of light projections (Fig 3.6 D to F). Statistically, there was a significant difference ($p < 0.05$) in EPSCs of αRGCs between Cx36 KO and WT mice (Wilcoxon signed ranks test).

3.7 Biophysical properties of αRGCs' responses to astigmatically defocused images

The biophysical properties of αRGCs responses to astigmatically defocused images were tested by projecting computer-controlled grating images that were optically blurred using a custom device (Fig 3.8). Initially, αRGC spike responses were evaluated using astigmatic lenses with various powers (cylinder range: +2.00 D to +10.00 D) (Fig 3.7A). Even with a +8.00 D astigmatic lens, maximal spike responses were observed. Subsequent experiments utilized a +6.00 D astigmatic lens at 90°/180° as they produced images with less distortion compared to the +8.00 D astigmatic lens.

Significant differences ($p < 0.05$, *t*-test) were observed in EPSCs and IPSCs of both illustrated ON and OFF αRGCs in response to astigmatically defocused images compared to focused images in WT retinas (Fig 3.7B and C). However, illustrated ON and OFF αRGC showed no different ($p > 0.05$, *t*-test) responses in Cx36 KO retinas (Fig 3.7D and E). All types of αRGC showed significantly different responses to astigmatically defocused images in the WT mice (n = 7) but not in Cx36 KO mice (n = 5) (Fig 3.7F).

4. Discussion

Despite the significant burden of myopia and astigmatism[80], treatment options for preventing and slowing their progression remain limited. This is partly because the specific cellular mechanisms that account for normal refraction or refractive errors are not fully understood.

Evidence suggests that the retina can sense the focus of images and then generate signals to regulate eye growth during development. Transcriptomics studies have also provided substantial evidence supporting the involvement of the retina in the development of myopia[57, 99, 117-119]; Recent research, including the current study, has demonstrated that defocused images can change the signal responses of RGCs in the mouse retina[64]. This suggests that the responses of RGC subtypes to focused and defocused images may play a pivotal role(s) in modulating eye growth and, hence, the development of refractive errors. Therefore, understanding the biophysical properties of RGCs under the conditions of refractive errors may provide a framework for understanding the mechanism underlying refractive development. The study revealed that when αRGC soma was stretched to simulate myopia, it impacted αRGC spike activity. The responses of αRGCs exhibited significant differences between focused and astigmatically defocused images. However, this distinction was not observed in αRGCs of Cx36 KO mice.

4.1 Biophysical properties of RGCs under myopic blur

While heredity has been identified as a significant factor in myopia development, the visually-guided theory suggests that visual signal inputs to the retina play a crucial role in this process and during emmetropization. RGCs, which may act as neurons in the retina-to-scleral signaling

pathway, summarize image information and may communicate with other RGCs and amacrine cells through gap junctions[49]. This mechanism suggests that both input and output from RGCs are essential in modulating ocular growth.

Myopic eyes have the potential to stretch the peripheral retinas, leading to the elongation of RGC soma and retina[132]. To analyze the responses of RGCs, the study elongated the soma of RGCs and the retina. The area of the RGC neurons somata (S) can be calculated using the formula $S = 4\pi r^2$. The radius (r) of RGCs increases by roughly half the sum of the lens thickness (LT) and vitreous chamber depth (VCD) when negative pressure is applied to elongate RGCs in the peripheral retinas. In a study by Zhou[133], the LT, VCD, and retinal thickness (RT) of mice at 29 days of age were 1558.7 ± 18.0 μm, 707.4 ± 21.4 μm, and 186.9 ± 15.1 μm respectively. Based on these measurements, a 5% elongation of the radius of RGC somata would be expected to induce a refractive error of plus 42.57 ± 2.72 D.

The current study found that stretching of RGC soma and retina to mimic myopia affected αRGC spike rates, EPSCs/IPSCs, and membrane capacitances. Like non-stretched RGCs, stretched RGCs responded differently to focused and defocused images. Stretching the soma of RGCs to simulate myopia differs from the stretching and expansion changes observed in actual myopic conditions due to the involvement of the dendritic tree of RGCs. To better mimic the myopia status, the retina was stretched toward the optic nerve, and αRGCs were recorded. The αRGCs in the stretched retina responded differently to optically focused and defocused images. These results suggest that myopic conditions can affect various αRGCs' biophysical properties, including spikes, EPSCs/IPSCs, and membrane capacitances. Cell stretching is a form of stimulation that could elicit a reaction from neurons, for example, in RGCs. It is important to note that chronic retinal elongation and cell stretching occur in myopia, whereas the experiment performed here involved

acute cell stretching. In a clinical setting, various retinal pathological changes caused by myopia can be observed, including retinal tears and myopic maculopathy. These observations suggest that the stretching associated with myopia can impact the retinal structure, and synaptic connections may be involved. In addition, it was found that mechanical stretch injury can induce acute calcium influx in neurons and tenocytes, leading to cellular dysfunction and degeneration[35, 134]. The process of myopia development is a chronic mechanical stretching that could potentially affect the influx of calcium and have implications for neurons, including EPSCs/IPSCs. The definitive answer needs further experimental observation. Although there may be some minor modifications in the functioning of neurotransmitter receptor channels (no significant difference in the amplitude of EPSCs/IPSCs before and after stretching), αRGCs could still distinguish between focused and defocused images and reflected their differences in their responses at the single-cell level.

It is important to note that not all αRGCs exhibit significant differences in spike and EPSCs/IPSCs responses under stretching conditions. Some αRGCs did not exhibit distinct responses to focused and defocused images (Fig 3.2, Fig 3.3F). This phenomenon may arise from distinct subtypes of RGCs exhibiting reduced sensitivity to cellular stretching.

4.2 Biophysical properties of αRGCs under astigmatic blur

Astigmatism, a common vision disorder causing 13% of refractive errors globally[135], can lead to amblyopia and other visual problems if left untreated in preschool children. Animal experiments have suggested that the retina might contribute an ocular compensatory response to astigmatic defocus in chicks[121]. However, it is unclear whether RGCs can detect the specific patterns of defocus and to what extent are affected by modifying their biophysical properties under stretching

of the retina in myopic eyes. This study also investigated whether RGCs in the retina can sense the characteristic pattern of retinal astigmatic defocus, which involves a differential blur along the ocular meridian. The responses of αRGCs to changes in the angle of projected light and astigmatic blur study were examined. Initially, projecting light at different angles into αRGCs' receptive fields did not produce different spikes and EPSCs/IPSCs responses. However, twisting the soma of RGCs to generate a certain light projection angle resulted in significant IPSC response differences in 80% of αRGCs. This could be attributed to coupled amacrine cells sensing differences in light intensity and area and subsequently providing inhibition. Further investigation is needed to understand this process thoroughly.

Light refraction through a solution was used to change the pathway of light projection, which resulted in changes in EPSCs/IPSCs in αRGCs in wild-type retinas. However, these changes were not observed in Cx36 KO retinas. It should be noted that the light projection from different angles did not correspond to astigmatic defocus, and the variations in responses may be due to differences in light intensities and receptive field projections. This suggests that coupled amacrine cells may be responsive to these differences[64].

Thus, to generate astigmatic blur, a visual stimulator with an adaptable astigmatic lens was used to project an astigmatically defocused image onto the receptive field of the target αRGCs. The αRGCs in WT retinas responded significantly differently in EPSCs/IPSCs to astigmatically defocused images compared to focused images, whereas this difference was not observed in Cx36 KO mice. This indicates that the αRGCs can differentiate between astigmatic and focused images but cannot distinguish between perpendicular meridian blur. This could be attributed to the activation of different coupled amacrine cells, as the astigmatic beam projected on the amacrine cells varied. These results suggest that a single αRGC in mouse retinas can detect the difference

between spherical defocus along ocular meridian astigmatic defocus blur, although species differences in the induction of astigmatism have been observed in other studies[119].

4.3 An intact retinal circuit involving Cx36 is necessary for the αRGCs to sense the defocused images

When the retinal circuit is intact, visual information can be effectively and rapidly encoded in RGCs. However, in the case of myopic retinas, the signaling cascades and the transmission of visual signals from RGCs to the optic nerve may be altered[122]. Gap junctions play critical roles in the integration and propagation of visual signals in the retina, and Cx36 has been identified as a risk factor for refractive errors in humans through a genome-wide meta-analysis. Preliminary experiments showed increased phosphorylation of Cx36, indicating increased functional gap junctions in the coupling of AII ACs, which can be observed in mouse retinas with form-deprivation myopia. Cx36 modulates retinal signals in the mouse retina by adjusting fast visual signaling, signal-to-noise ratio, scotopic pathways, and synchronization of neuron activities[136].

As the predominant subunit of gap junctions in the proximal mouse retina, Cx36 is expressed by most ganglion cell subtypes; ON and OFF αRGCs lose their coupling in Cx36 KO mice[128]. Given that Cx36 is present in the outer retina and various cell types[137], utilizing conditional Cx36 knockout mice, specifically in the RGC layer, would be an excellent choice for a control group. At present, generating RGC conditional Cx36 KO mice is a challenging task. Therefore, Cx36 KO mice were used as a control of intact retinal circuits[122]. Results from optokinetic reflexes (OKR) showed that the contrast sensitivity at 0.064 and 0.192 cpd was significantly lower in $Cx36^{-/-}$ mice compared to C57BL6 mice. These results suggest that Cx36 is involved in the

retinal circuit that delivers accurate visual sensation and perception. The loss of coupled amacrine cells may explain the reduced contrast sensitivity in $Cx36^{-/-}$ mice, as defocused images and astigmatic blur may require feedback information from these cells.

The study indicated that certain types of RGCs or other neurons might be associated with myopia or astigmatism development. Further research is required to investigate this, as it has the potential to provide valuable insights into the targeted treatment of refractive errors in its early stages. Consequently, such research has the potential to effectively control the progression of refractive errors in clinical settings.

5. Conclusion

When the soma was stretched to simulate myopia, αRGCs exhibited significant differences in their responses. The majority of αRGCs' biophysical responses could accurately reflect the image projection of optical stimuli associated with myopic and astigmatic defocus. It is suggested that Cx36-mediated gap junctions may play a significant role in transmitting visual signals related to the development and perception of refractive errors.

6. Limitations

The stretching technique utilized to simulate myopic conditions at an individual RGC level, involving acute cell elongation, may differ from the RGCs found in naturally occurring myopic eyes, which undergo a chronic process. In vitro, stretching can mimic certain characteristics of the condition. However, it is important to note that the biochemical reactions induced by in vitro stretching may not fully mirror those in the myopic retina. Moreover, RGCs in the central region of the retina may undergo greater elongation than those in the peripheral region. These factors should be taken into consideration when employing the stretching method.

Furthermore, the data on the axial length of Cx36 KO mice only involved testing approximately 10 mice, and refractive errors could not be assessed due to the affected rod pathways. The role of Cx36 is not limited to any particular cell type by testing Cx36 KO mice. Further experiments are required to investigate the role of Cx36 in myopia development.

CHAPTER 4 Biophysical effects of focused and defocused image stimuli on dopaminergic amacrine cells and AII amacrine cells in the mouse retina

1. Introduction

The spatial contrast coding of RGCs is a result of their centre-surround receptive field (RF). This RF is formed by excitatory center neurons and inhibitory surround neurons, which are activated by feedforward and lateral interneurons, respectively. According to previous studies, the lateral inhibitory mechanism plays a crucial role in enhancing local contrast and improving edge detection[138, 139]. In the mouse retina, two inhibitory networks are triggered, consisting of a single type of horizontal cell that generates the initial RF and various types of amacrine cells (ACs) that process more complex visual signals[140]. A previous study has shown that a single RGC could reflect both focused and defocused images[141], indicating a signal alteration in the inner retinas. It is worth noting that defocused images differ significantly from focused images in terms of brightness, contrast, edge, and shape, which rule out horizontal cells as the sole interneurons responsible for such complicated spatial tuning[49].

Amacrine cells form the most diverse subset of retinal cells in mice, with over 60 subtypes identified on a molecular level[1]. Despite this abundance of information, much of their function remains unclear. Research suggests that dopaminergic DACs and AII ACs may be myopia-relevant

subtypes, supported by studies on dopamine[75, 142] and Connexin36 gap junctions[14, 143], respectively.

DACs are wide-field amacrine cells that stratify in the IPL. They possess 2-3 long primary dendrites, with a dendritic field that extends to 495um in diameter[18]. These cells uniquely control dopamine release in response to different light conditions and are the only source of retinal dopamine[66]. Since dopamine is considered the pivotal neurotransmitter in myopia development, DACs are of significant interest[59, 75, 144]. Importantly, DACs carry D2-autoreceptors that control dopamine synthesis, release, and uptake, and DA receptors are distributed throughout the retina[16, 145]. While high levels of dopamine are used to tune visual processing in photopic conditions, how DACs respond to myopic signals and impact emmetropization remains unclear.

In contrast, AII ACs are narrow-field amacrine cells that form lobular appendages, radiating in sublamina a and arboreal dendrites in sublamina b. These interneurons are a potential subtype of ACs linked to myopia development due to their impact on the visual pathway. Unlike other amacrine cells, which contribute mainly to vertical signal flow, AII ACs connect to most subtypes of cone bipolar cells, half of which form Cx36 gap junctions. Thus, the change in AII receptive field properties may influence signaling in the retinal output[58]. This study aimed to analyze the cone-to-AII AC pathway under photopic stimuli conditions. In addition, AII ACs are a crucial interneurons for scotopic vision[17]. They connect with neighboring AII ACs via homotypic Connexin 36 gap junctions and form ring connections with the fiber plexus of DACs[146, 147]. These structural features indicate that AII ACs may play a role in dopamine secretions, given that visually-guided ocular growth relies on rod pathways[67, 148, 149], and Cx36 GJs are phosphorylated in myopia. Dopamine affects gap junction and AII ACs coupling, which may

influence refractive error[143], and therefore, the relationship between DACs and AII ACs is intricate, particularly with respect to their signaling of defocused images.

The RF properties of both ACs are not well understood, unlike those of RGCs, which have been more extensively studied. Visual information processing in the retina often involves the center-surround RF region as the fundamental element for most RGCs[150]. Spots can be used to examine the center RF with the strongest light response, while annulus stimuli can be employed to explore the phenomenon of lateral inhibition[78]. Neurons' surrounding RFs can modulate sensitivity to fine spatial structures by altering how the center integrates visual information across space[79]. Thus, this study included spots and annuli of various sizes to reveal the polarity and center RF size of DACs and AII ACs and to gain a deeper understanding of visual processing.

It has not yet been determined whether defocused images have an impact on the signaling of DACs and AII ACs. However, in terms of their functional characteristics, Dopaminergic ACs release depolarizes in response to synaptic inputs driven by light[151], potentially influencing dopamine release and contributing to the development of myopia, while AII ACs exhibit coupling patterns that vary with light intensity and contrast[60], which probably possess the capability to eliminate noise related to defocused images. These findings offer evidence for a potential pathway for sensing visual stimuli via photoreceptors and transmitting signals to them[66].

The GJD2 gene encodes a protein called Cx36 gap junction (Cx36 GJs). These Cx36 GJs form connections between AII ACs and AII ACs to CBCs in the inner nuclear layer, which means that the opening and closing of the GJs can impact the flow of signals to the RGC layer. Research has demonstrated that communication through gap junctions in retinas can influence visual signal processing, potentially by modulating the growth of the eyeball through the retina-scleral pathway[143]. Numerous animal studies have associated the link between GJ phosphorylation and

the progression of myopia, but the findings are inconsistent[14, 152]. Therefore, applying a gap junction blocker may provide insight into the role played by GJs in encoding the defocused signals.

2. Methodology

2.1 Animal preparation

In this study, both adult EGR-1 transgenic mice and Fam-81a mice within the postnatal day 16-56 range, regardless of sex, were studied. All mice were housed in a 12-hour light/12-hour dark cycle and underwent deep anesthesia via intraperitoneal injection of ketamine and xylazine at doses of 80 mg/kg and 10 mg/kg (body weight), respectively. Prior to enucleation, lidocaine hydrochloride (20 mg/ml) was applied locally to the eyelids and surrounding tissues to minimize discomfort. To ensure consistency, all mouse retinas were collected at approximately 10 a.m. following overnight dark adaptation.

2.2 Retina slice preparation and immunostaining

The separation of the retina from the EGR-1 mice took place in a specialized chamber filled with extracellular solution. This solution comprised 120 mM of NaCl, 2.5 mM of KCl, 25 mM of NaHCO3, 0.8 mM of Na2HPO4, 0.1 mM of NaH2PO4, 1 mM of MgCl2, 2 mM of CaCl2, and 5 mM of D-glucose. The bath solution was continuously bubbled with a mixture of 95% O2 and 5% CO2 at a temperature of 32°C. A piece of the central retina was then embedded in type VII agarose from Sigma and cut with a vibratome (Leica Camera, Wetzlar, Germany) to achieve a thickness of 50 μm.

The retinal pieces, attached to filter paper (RGCs side up), were submersion-fixed in 2% N-(3-dimethyl aminopropyl)-N′-ethyl carbodiimide hydrochloride (“carbodiimide” or “EDAC”; E7750 et al. in 0.1 M phosphate buffer (PB), pH 7.5 for 30 min at room temperature. After fixation, the

retinas were separated from the filter paper and washed with phosphate-buffered saline (PBS) before being washed extensively with a 0.1 M phosphate buffer (PB, pH 7.4) and blocked with 3% donkey serum in 0.1 M PB 0.5% Triton-X 100 and 0.1% NaN3 overnight. The antibodies were diluted in 0.1 M PB with 0.5% Triton-X 100 and 0.1% NaN3, containing 1% donkey serum. The tissues then were incubated in primary antibodies (Anti-Tryosine Hydroxylase antibody (Sigma-Aldrich: AB152) for 3–7 days at 4°C and, after extensive washing, incubated in secondary antibodies overnight at 4°C. The secondary antibodies used were donkey anti-mouse Cy-3 (1:200) and Alexa Fluor® 488 anti-GFP Antibody (1:200). After washing with 0.1 M PB, the tissues were mounted in Vectashield (Vector Laboratories, Burlingame, CA) for observation.

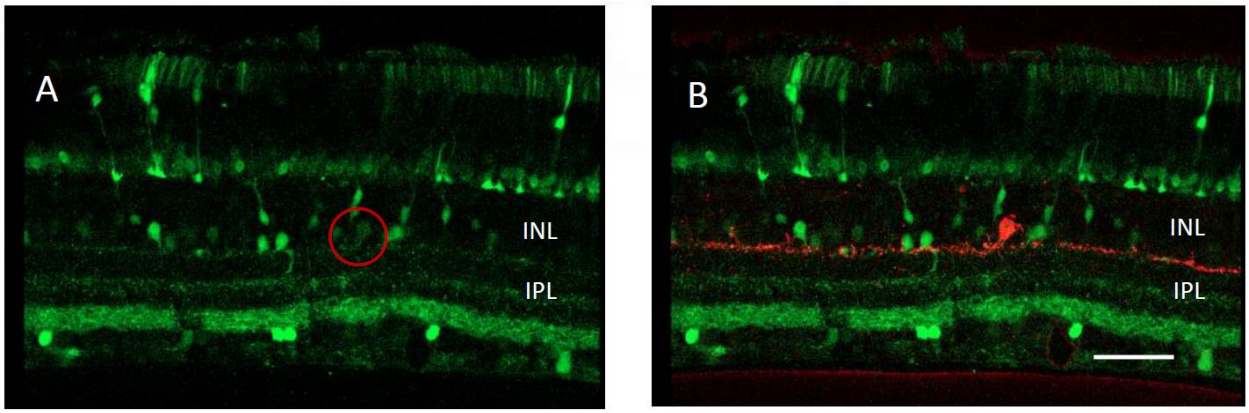

Figure 4. 1 Identification of dopaminergic amacrine cells in EGR-1 mice

[A] DACs can be located from the largest and weakest fluorescence signal (red circle) in the innermost inner nuclear layer (INL) of EGR-1 mouse retinas. **[B]** Tyrosine hydroxylase – positive. Bar: 50 μm

2.3 Retina preparation for recording

The mice were anesthetized, and their eyes were removed under dim red illumination. The retinas were dissected into four quadrants for patch-clamp recording and attached to a customized translucent Millicell filter ring. The flattened retinas were continuously supplied with oxygenated mammalian Ringer's solution at 37°C. The bath solution was infused with a mixture of 95% oxygen and 5% carbon dioxide and kept at around 32°C, as described in a previous study. The animals were euthanized by cervical dislocation immediately after eye removal.

2.4 Patterned light stimulation

An experiment was conducted using a green organic light-emitting display (OLED) (Olightek, Kunming, Yunnan, Chinaq) with a resolution of 800 × 600 pixels and a refresh rate of 85 Hz. The display was controlled by a Windows 7 computer with an Intel Core Duo processor. To observe the display, a Nikon 40x water-immersion objective was used, which produced a 250 μm diameter area that received light stimuli. The OLED had 15 μm diameter pixels, which appeared as 0.25 μm/pixels on the retina under the 40x objective. PsychoPy was used to create grating images with adjustable spatial frequency, which were then projected onto the photoreceptor layer. The background light intensity was around 700 isomerizations per rod per second, while the highest stimulus was approximately 1.816 × 105 isomerizations per rod per second. At this level of background illumination, the rod pathway was saturated, leaving the cone pathway to mediate the light response[92]. Each image was displayed for 1 second, followed by a 5-second break.

In this study, focused or defocused images with a 125 μm diameter and a spatial frequency of 0.0067 cycles/degree were applied. The process of creating defocused images on the retina in vitro

has been detailed in previous studies[64]. Previous research has suggested that an axial elongation of 5 µm would induce a 1 Diopter (D) refractive error in the mouse retina[93]. This means that 100 µm would result in plus or minus 20 diopters of refractive error in the mouse retina when viewed under microscopy.

The Mightex Polygon1000 system enables the production of annulus/spots at 525 nm wavelength. Polyscan3 software provided stimulation in the form of spot sizes ranging from 30 to 180um in diameter. Annulus is defined as the difference between the outer and inner diameters, as shown in Fig 4.2.

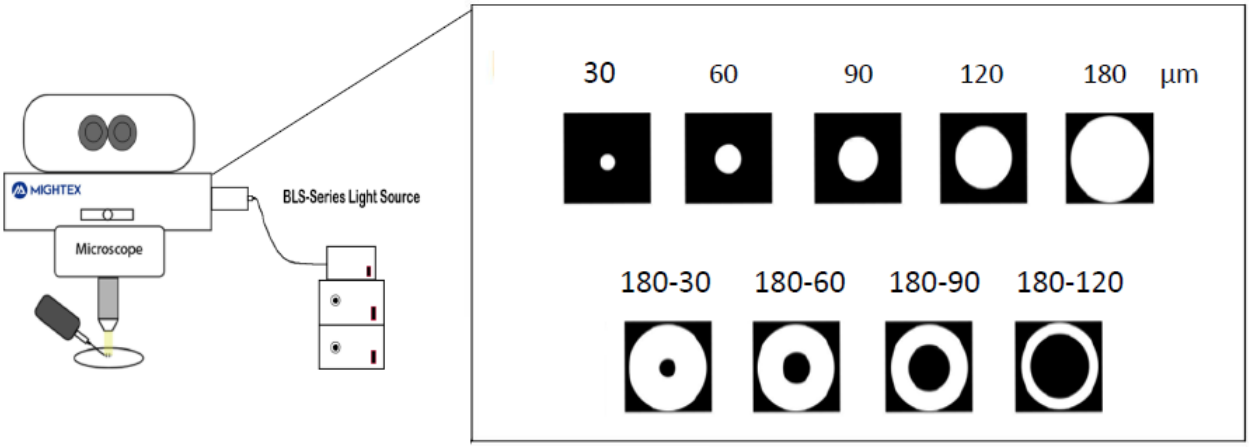

Figure 4. 2 The pattern of annulus and spot

Various spot sizes including 30 µm, 60 µm, 90 µm, 120 µm and 180 µm. Annulus is defined by the outer and inner diameters at 180 µm - 30 µm, 180 µm - 60 µm, 180 µm -90 µm, and 180 µm - 120 µm.

2.5 Electrophysiology

Whole-cell recordings on individual HCs in the mid-peripheral retina were conducted by using advanced equipment, including an Axopatch 700B amplifier, a Digidata 1550B interface, and pCLAMP 10 software (Molecular Devices, San Jose, CA, USA). To ensure optimal results, an internal solution containing caesium methanosulfonate was used instead of potassium gluconate to improve space clamp and block spiking. The study focused on comparing the kinetics (amplitudes) of excitatory postsynaptic currents (EPSCs) and inhibitory postsynaptic currents (IPSCs) in response to light stimuli using whole-cell recording. To facilitate comparison, the whole-cell response amplitude was normalized across the stimuli of focused/defocused images. Additionally, dye was injected into the recorded cells using pipette tips filled with 4% Neurobiotin (Vector Laboratories, Burlingame, CA, USA) and 0.5% Lucifer Yellow-CH (Molecular Probes, Eugene, Oregon, USA).

2.6 Intracellular labeling

Following the recording, the recorded neurons were visually impaled using pipette tips filled with a mixture of 4% Neurobiotin in distilled water and backfilled with 3 M KCl. The electrode resistance measured ∼100 MΩ. Subsequently, biphasic current (+1.0 nA, 3 Hz) was administered to the impaled cells, after which retinal pieces were fixed with 4% paraformaldehyde for 15-20 min. The tissues were incubated in primary antibodies (Anti-Prox1 antibody (catalog#PRB-238C) for identification of AII amacrine cells and Anti-Tryosine Hydroxylase antibody (Sigma-Aldrich: AB152) for dopaminergic amacrine cells for 3–7 days at 4°C. After extensive washing, the tissues were then incubated overnight at 4°C in a solution of 0.1 M phosphate buffer with 0.5% Triton-X

100 and 0.1% NaN3, containing 1% donkey serum. Following further washing, the tissues were incubated with secondary antibodies Cy5-conjugated streptavidin (Invitrogen) at a concentration of 1:200 overnight at 4°C. Finally, the tissues were mounted in Vectashield (Vector Laboratories) for microscopic observation.

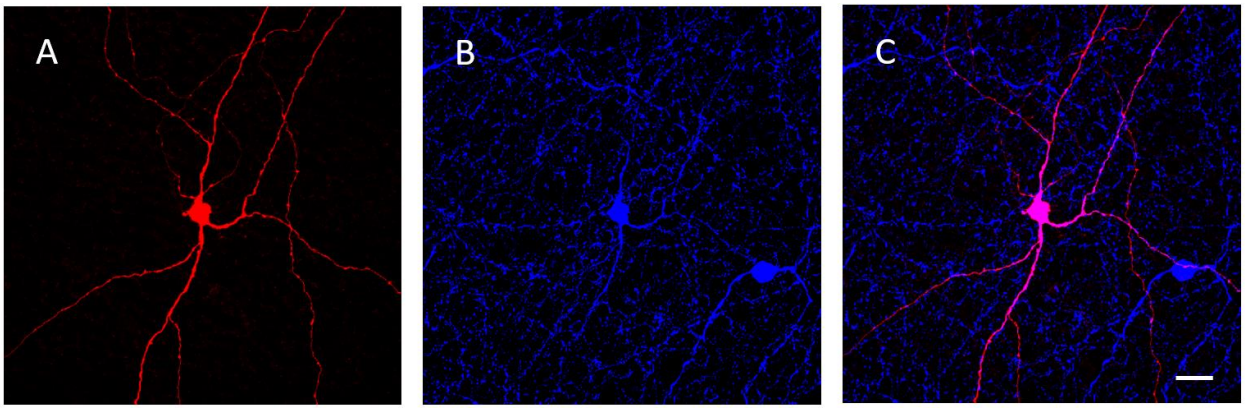

Figure 4. 3 Intracellular injection after DAC recording

The recorded cells were confirmed by intracellular injection and Cy-3 staining **[A]**, overlapped with TH-positive **[B]** as seen in the merged image C, bar: 20um.

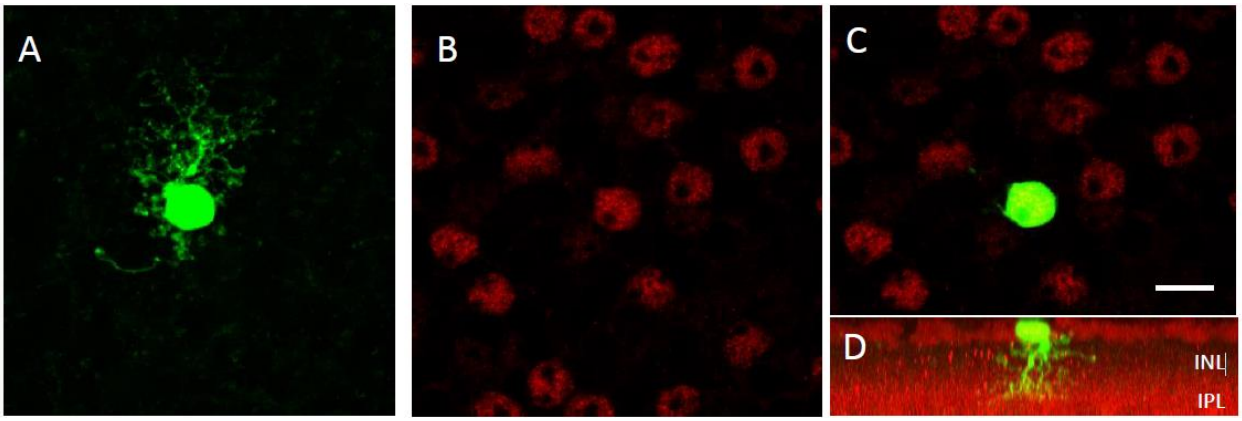

Figure 4. 4 Intracellular injection after AII AC recording

The recorded cells were confirmed as AII AC by neurobiotin-injection **[A]** and prox-1 –positive (B, C) in the innermost part of the inner nuclear layer **[D]**, bar: 10µm

2.7 Imaging and Analysis

Retinal whole mounts were captured using a Zeiss LSM 800 confocal microscope equipped with an Airyscan using a 40× objective lens (N.A. 1.3) and a 63× objective (NA 1.4). Imaging conditions were kept identical for all retinas, including the laser intensity, pinhole, photomultiplier amplification, and z-stack step size. The microscope's optical resolution was 120 nm in the x- and y-axes and 350 nm in the z-axis. The images were taken with two channels (Cy3 and 488) superimposed, and Z-axis steps of 0.35 µm. The data were analyzed as previously described and presented as mean ± S.E.M. Statistical significance was determined at $P < 0.05$ using a Wilcoxon Signed Rank test. Analysis was performed using Origin software and SPSS version 25.

3. Results

3.1 Dopaminergic ACs response to various sizes of spot and annulus

Dopaminergic amacrine cells were searched for the largest and weakest GFP-fluorescence signals in flat-mount retinas of EGR-1 mice. Various sizes of spots ranging from 30 to 180 um in diameter were projected to the target cells in order, followed by different annuli stimulation. Intracellular labeling was performed after whole-cell recording.

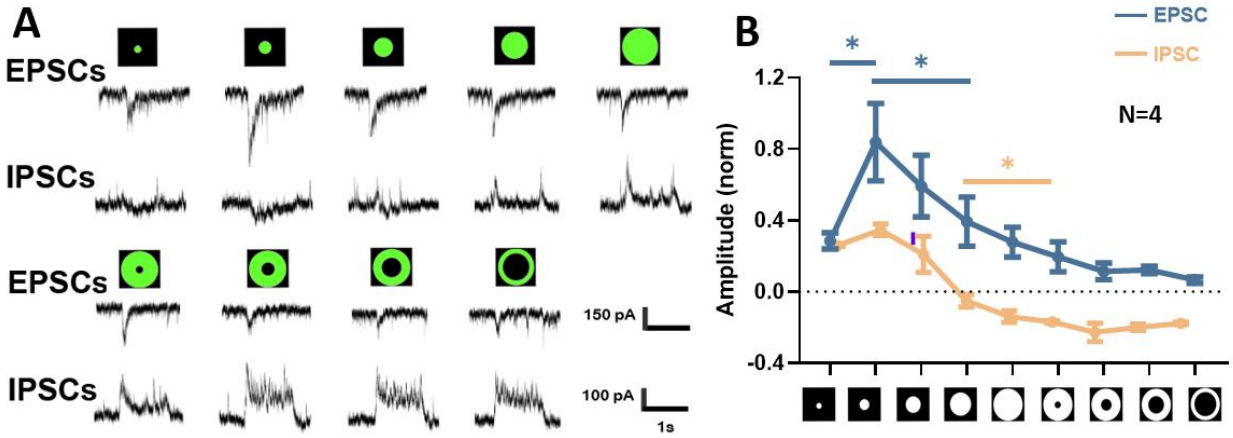

Figure 4. 5 The excitatory postsynaptic currents (EPSCs) and inhibitory postsynaptic currents (IPSCs) of DACs displayed significant variations when exposed to spot and annulus stimuli

[A] In the EPSC setting, DACs exhibited depolarization ranging from 30 μm to 180 μm in response to spot stimuli and from 180-30 μm to 180-120 μm in response to annulus stimuli. The maximum depolarization occurred with a 60 μm spot stimulus. In the IPSC setting, DACs remained depolarized at 30 μm and 60 μm spot stimulation, but hyperpolarization commenced at 90 μm spot stimulation. **[B]** There was a significant difference observed between the 30 μm to 60 μm and 60

μm to 120 μm EPSC responses to spot stimulus, as well as between the 120 μm spot and 180-30 μm annulus responses. These results have been presented in normalized amplitude.

The way that Dopaminergic ACs receive light input from different pathways, including rod and cone pathways, as well as intrinsically photosensitive retinal ganglion cells (ipRGCs), has been studied[66]. However, the specific circuits that connect and affect DACs are not yet fully understood. The center size of an RF can be determined by identifying the minimum stimulus spot required to elicit maximum neuron depolarization. This research indicates that DACs exhibit a maximum response to spot stimuli measuring approximately 60 μm, and can even be activated with IPSC clamping. Furthermore, larger spots (> 60 μm) and annulus (<60 μm) stimuli have been shown to elicit the DAC response, likely due to the robust and irregular RF center, which extends throughout the retina via the dendritic processes. Nevertheless, the limited range of spot and annulus stimuli available for experimentation makes it challenging to fully explore the receptive field of DACs.

3.2 Dopaminergic ACs response to focused/defocused images

According to a 2208 study[93], a clear image projection on the outer segment of the retina was defined as 0 Diopters. Moving 5 μm away from the photoreceptor induced a ±1 Diopter refractive error in mouse retinas, depending on the direction. Therefore, 50 μm induced ±10D, and 100 μm induced ±20D. EPSC and IPSC were recorded by projecting ±10D ±20D and 0D to DACs.

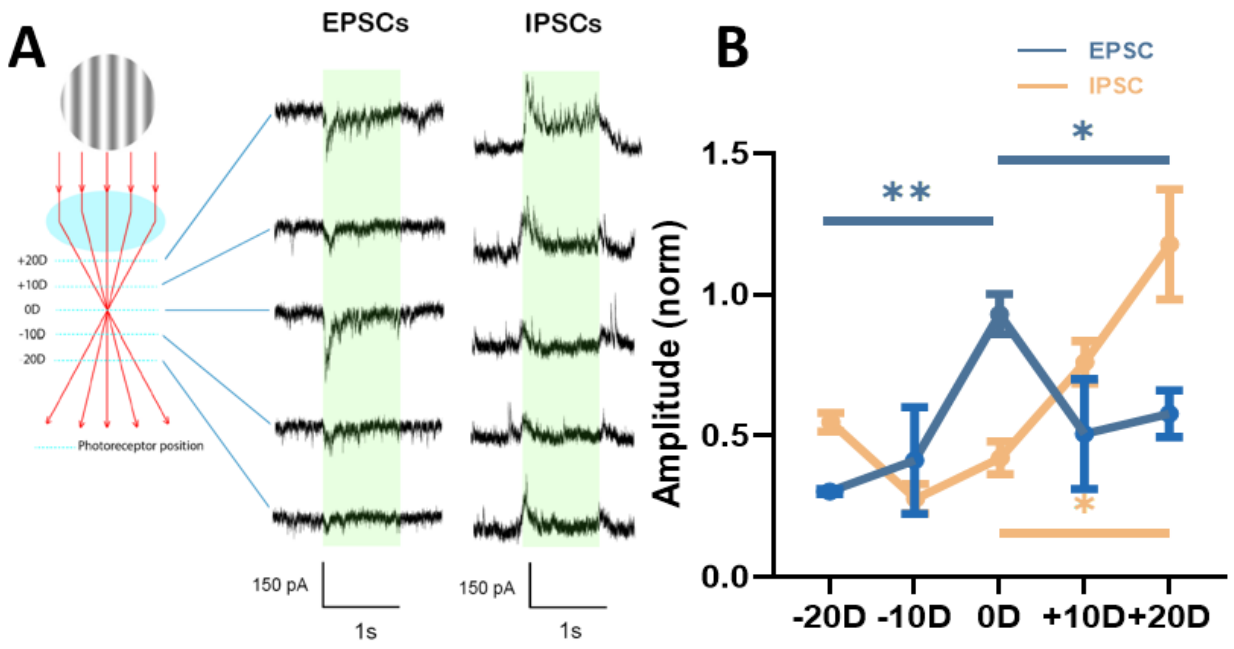

Figure 4. 6 Dopaminergic ACs response to focused and defocused images

[A] A 0.0067 cycle per degree (cpd) sinusoidal grating was achieved via the microscopy lens to the retinas. Depolarization at EPSCs and IPSCs was presented to focused and defocused image projection. **[B]** There were significant differences between the -20D versus 0D and +20D versus 0D in the EPSC setting as well as +20D versus 0D in the IPSC setting of dopaminergic ACs.

Animal studies have revealed a connection between induced myopia and lower levels of dopamine in the eye[153, 154]. Dopamine plays a crucial role in controlling axial elongation via a signaling pathway. According to visually-guided ocular growth theory, dopaminergic ACs help regulate eye growth by receiving defocused signals and utilizing dopamine neurotransmitters. For this to happen, DACs must be able to react differently to focused and defocused signals. This study's findings reveal that EPSCs of DACs experience maximum depolarization when dealing with focused images, while IPSCs experience the minimum. These varying responses between focus and defocus suggest that defocused images impact the signaling of DACs and influence dopamine

secretion. However, the receptive field of dopaminergic ACs has yet to be defined. Importantly, the sinusoidal grating area projected in this study was 150 μm, which may be smaller than the RF center of DACs. This is because the average diameter of a dendritic arbor was 495 μm[18].

3.3 AII ACs response to various sizes of spot and annulus

Under scotopic light conditions, AII ACs receive input from RBC, while under bright light conditions, they receive major input from cone bipolar cells via Cx36 GJs. Together, these sign-conserving inputs form the AII AC's receptive field (RF) center, which can vary in size based on the coupling status of the AII ACs and CBCs. Accordingly, overnight dark adaptation preceded cell recording. Since more coupling leads to a larger RF center for each AII AC[58], it allowed the use of a gap junction blocker to attempts to explore the receptive field of a single AII AC. The study also examined the effects of Meclofenamic acid (MFA) on uncoupled AII ACs in response to spots and annulus of varying sizes (Fig 4.7). MFA with 100 μm could effectively block gap junctions for up to 20-40 minutes[155].

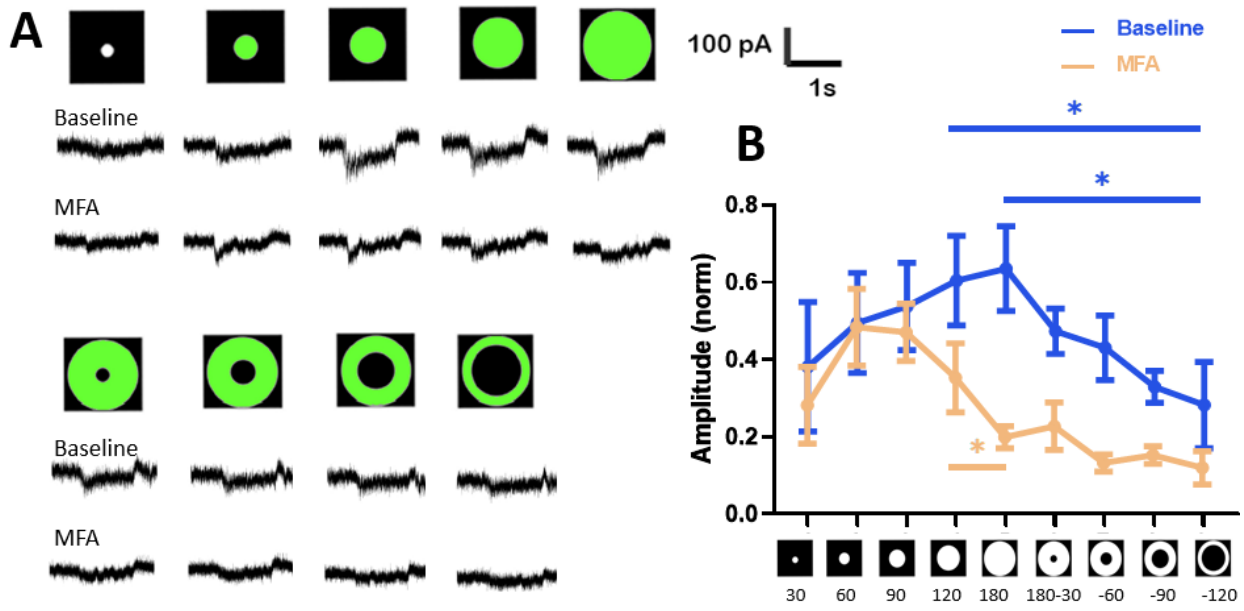

Figure 4. 7 Coupled AII ACs and uncoupled AII ACs respond to various sizes of spot and annuli

[A] AII ACs exhibited depolarization ranging from 30 µm to 180 µm in response to spot stimuli and from 180-30 µm to 180-120 µm in response to annulus stimuli. Maximum depolarization was not obviously observed. After MFA (50 µm, 10 minutes) perfusion, AII ACs reduced depolarization. **[B]** There was a significant difference observed between the 120 µm spot versus 180-120 µm annulus stimulus and the 180 µm spot versus 180-120 µm annulus stimulus. After MFA application, there was only a significant difference between 120 µm versus 180 µm spot stimulus. These results have been presented in normalized amplitude.

According to Masland RH et al. (2008), the RF ON centre for uncoupled AII ACs is typically 60-80 µm, while the OFF surround is around 100-130 µm. As a result, spot stimuli greater than 90 µm

tend to elicit less of a response in terms of EPSCs. Conversely, coupled AII ACs experience an increase in RF and allow for EPSC summation in response to larger stimuli[13]. When annulus stimuli are used, the response of coupled AII ACs decreased in a linear fashion as the center-area stimuli decreased. In contrast, uncoupled AII ACs experienced a significant reduction, while when larger OFF-surround was stimulated or did not respond at all when the annulus stimuli fell outside of the receptive field (annulus with outer diameter in 180 μm and inner diameter in 120 μm).

3.4 AII ACs response to focused/defocused images

Comparison of focused and defocused images revealed noticeable differences in size, light intensity, and edge. In the retinas of dark-adapted rabbits and mice, a small number of AII amacrine cells are linked together, which probably affects the way signals related to focused and defocused images are interpreted[13, 156]. Under photopic conditions, AII ACs receive signals from ON CBC and transmit them to RGCs. By using MFA to block gap junctions in vitro, the study aimed to provide insight into how AII amacrine cells that are not linked together process these signals compared to those that are linked.

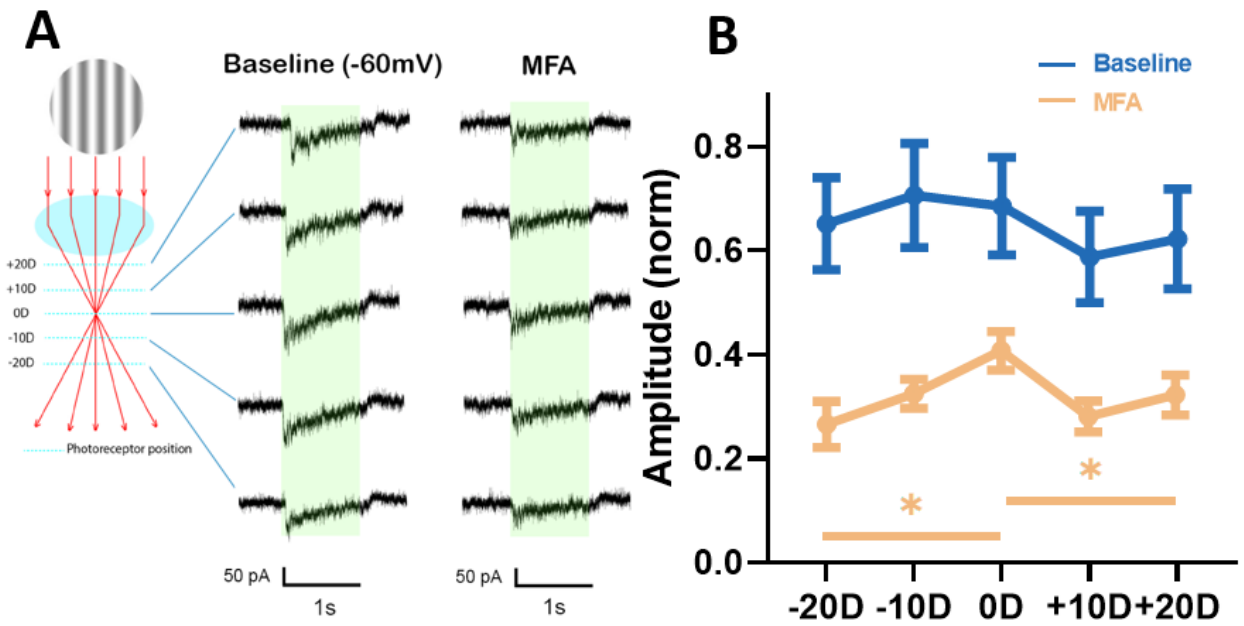

Figure 4. 8 Coupled AII ACs and uncoupled AII ACs response to focused/defocused images

[A] A 0.0067 cycle per degree (cpd) sinusoidal grating was produced through the microscopy lens to the retinas. Depolarization at EPSCs with and without MFA application was presented to focused and defocused image projection. **[B]** There were non-significant differences between the focused image (0D) compared to any defocused images (± 10D and ± 20D). However, there were significant differences between +20D versus 0D and -20D versus 0D after MFA perfusion.

Coupled AII ACs did not exhibit significant differences in EPSCs when exposed to focused or defocused image stimuli. However, the application of a gap junction blocker (MFA, 50 µM) revealed significant divergence in EPSCs of uncoupled AIIACs between focused and defocused image stimuli.

MFA was used to uncouple AII ACs and ON-CBCs. The coupling of amacrine cells with ON CBCs enlarges the receptive field center and synchronizes signals through gap junctions,

indicating that noisy signals or oscillations may be dispersed to each coupled cell and neutralized in the receptive field. This potentially allows for greater tolerance to noisy information. The current study findings supported this hypothesis, as defocused signals were either filtered out or presented as trade-offs with focused signals without any significant differences. The coupling of gap junctions was found to filter out defocused images, which typically present noisier signals to the retina[49]. However, the coupling of AII ACs was robust. This electrical coupling makes it challenging to study a single AII AC in the mouse retina.

4. Discussion

The process of visual computing is incredibly complex, requiring the retina's circuits to be intact to accurately compute images. Abnormalities in the images cause a chain reaction in chemical and electrical pathways, ultimately leading to eye compensation. A previous study from this group revealed that retinal signal changes are reflected by a population of αRGCs or single αRGCs. However, in Cx36 KO mice, this reflection was lost, highlighting the crucial role of gap junctions in processing specific image stimuli[14, 64].

Two inhibitory networks are involved in modulating the visual signal. The first network comprises the same type of horizontal cells found in mouse retinas, while the secondary networks consist of at least 63 types of amacrine cells[157]. Both networks are thought to contribute to modulations in focused and defocused signals. In particular, the secondary inhibitory networks process more complex visual information, likely involving the modulation of defocused signals. Although the specific types of amacrine cells that are strongly associated with myopia have not yet been identified, the study initially focused on two types of amacrine cells that are likely to be involved in emmetropization: dopaminergic amacrine cells and AII amacrine cells.

4.1 The biophysical properties of dopaminergic ACs can respond distinctively to focused and defocused images

Dopaminergic amacrine cells play a crucial role in dopamine release, which in turn modulates signaling at the cellular, synaptic, and gap junction levels across retinal layers. This has a significant impact on the signals processed by retinal circuits and output. Some studies have

suggested that dopamine could be the stop signal to excessive ocular growth, offering potential benefits for myopia intervention[75]. In particular, light is a key factor in dopamine secretion, with bright conditions triggering the release of more dopamine to optimize visual processing, while scotopic conditions require less dopamine[16]. Further exploration into how different visual stimuli affect dopamine secretion could lead to a better understanding of the dopaminergic ACs involved in myopia progression. Unfortunately, measuring the active amount of dopamine is impractical. To address this, the EPSCs and IPSCs of dopaminergic ACs were recorded to reflect the likelihood of dopamine release by projecting various sizes of spot and annulus, followed by focused/defocused images.

The EPSCs and IPSCs of DACs showed significant variability when exposed to spot and annulus stimuli. It is noteworthy that the highest EPSC response was observed when a 60μm spot stimulus was projected (Fig 4.5), indicating exploration of a center-respective field. However, the inhibitory surround was not detectable within a 180 μm x 180μm area. Within this region, a focused 125 μm diameter image with a spatial frequency of 0.0067 cycles/degree was projected to the RF of DACs. There were noticeable differences in the responses of dopaminergic ACs to focused and defocused images. EPSC exhibited the maximum response when a clear image was projected, potentially exerting the greatest influence on dopamine release in the retina while receiving excitatory input from intrinsically photosensitive ganglion cells (ipRGCs) and ON CBC. In the IPSC setting, the input comes from glycine and Gamma-aminobutyric acid (GABA). With blurry images, DACs experienced significant suppression. Both EPSC and IPSC depolarized DACs, potentially influencing dopamine release and contributing to the development of myopia[158].

4.2 Uncoupled AII ACs exhibit the capacity to detect both focused and defocused images, whereas coupled AII ACs do not

AII ACs are vital neurons in rod pathways that have been shown to be significant contributors to myopia development[67]. They establish connections with other AII ACs and most of the cone bipolar cells through Cx36 gap junctions, which ultimately influence the outflow signals to RGCs. This underscores the importance of studying AII ACs in the context of myopia progression. As in photopic conditions, cone bipolar cells input AIIs with little contribution from rod bipolar cells[58, 159]. To investigate the impact of Cx36 GJs in interpreting defocused images, meclofenamic acid (MFA) was used to block gap junctions between cone bipolar cells and AII ACs, as well as between AII ACs themselves.

With the projection of various spot and annulus stimuli, the coupled AII amacrine cells were unable to evoke the maximum EPSC response within a 180μm spot stimulus, while uncoupled AII ACs (with the application of MFA) demonstrated that their centre RF is less than 120 μm. However, achieving complete isolation of the AII amacrine cells from electrical synapses with 50μM and 10 min of perfusion appears to be unattainable. Instead, it has been suggested that a higher concentration of 100μM with 20-40 minutes of perfusion is necessary to achieve this outcome, although concerns about toxicity have been raised[155]. Furthermore, the EPSCs of coupled AII amacrine cells exhibited significant variations when exposed to spot and annulus stimuli, and these variations increased after the application of MFA. Overall, this highlights that AII amacrine cells' smaller center receptive field, which tends to uncouple or become less coupled, indicates a higher discernible ability.

AII ACs with coupled connections showed no significant differences in EPSCs when presented with focused or defocused image stimuli. However, the introduction of a gap junction blocker revealed significant variations in the EPSC responses of uncoupled AII ACs when exposed to focused and defocused images. This suggests that uncoupled AII ACs can detect both focused and defocused images, while AII ACs with strong coupling can effectively filter out noise associated with defocused images.

The connection between DACs and AII ACs is intricate. Dopamine is released by DACs when exposed to bright light, which results in disconnection of AII ACs[29]. This disconnection could reduce the sensitivity to AC ACs, as synchronous activity was no longer or less able to be summed up[13]. Both DACs and AII ACs could influence the integrated signals of retinal ganglion cells through the retinal-to-sclera pathway or directly affect the sclera formation, leading to axial elongation.

5. Conclusion

The biophysical properties of dopaminergic ACs allow these cells to respond distinctively to focused and defocused images, thereby potentially influencing dopamine release in the retina and contributing to the development of myopia. Uncoupled AII ACs exhibit the capacity to detect both focused and defocused images, whereas AII ACs with robust coupling possess the capability to eliminate noise related to defocused images.

6. Limitation

A larger spot stimulus size was required to fully investigate the central receptive field of coupled AII amacrine cells, as their maximum EPSC response was not observed. The IPSC response of AII amacrine cells was not analyzed or presented in this study due to the insignificant and unstable response amplitude, possibly influenced by photopic stimulation or fluorescence GFP visualization in the dark-adapted mouse retinas.

CHAPTER 5 Horizontal cells

1. Introduction

The terminal neurons in the retina, known as retinal ganglion cells (RGCs), summate visual information from the retina and transmit it to the visual cortex. In murine retinas, defocused stimuli have been found to alter the firing pattern of RGCs[49]. Alpha retinal ganglion cells, which act as fundamental ON/OFF channels, have been investigated for contrast stimulation[23]. Research on αRGCs has shown different spiking activities under focused and defocused image stimuli[64, 129]. However, the method by which the retinal pathway encodes and modulates different optical powers remains unknown.

The retina's visual pathways exhibit a columnar unit structure consisting of photoreceptors, BCs, and RGCs[160]. This glutamatergic pathway starts by producing visual signals and culminates in transmitting these to the brain. Two lateral inhibitory networks are involved in shaping the signal transmission within the vertical pathway, with the first category of inhibitory neurons made up of horizontal cells (HCs) and the secondary inhibitory networks comprising amacrine cells (ACs)[140].

HCs play an important role in modulating the flow of information from rod and cone photoreceptors. In mice and rats, only one axon-bearing type of Horizontal cell has been identified within the outermost inner nuclear layer[161, 162]. In the course of light response, the HCs receive input from photoreceptors, which respond to light. HCs then release inhibitory neurotransmitters to suppress the activity of neighboring photoreceptor cells. This mechanism of lateral inhibition serves to enhance the contrast between areas of light and darkness in the visual field[43]. In

addition, HC cells contribute to the antagonistic centre-surround receptive fields of RGCs via a feedback pathway to photoreceptors. This, in turn, modulates the receptive field and ultimately affects the discharge rate of RGCs[161]. In visual processing, the signal from photoreceptors is transformed into an electrical form. The crucial step that follows refines this signal for the next-order neurons. The interaction between photoreceptor and horizontal cells plays a significant role in maintaining an optimal balance while adjusting to varying light contrasts and intensities. This provides a potential mechanism for distinguishing and processing focused/defocused signals to RGCs. When an image is defocused, it exhibits unique characteristics, including varying contrast and edges that differ from those of a focused image[49]. To determine whether HCs contribute to modulating focused/defocused signals, it is first necessary to determine whether they can reflect the difference in response to focus and defocus, which was the aim of this study.

2. Methodology

2.1 Animal preparation

Adult wild-type (WT) C57BL/6J (RRID: IMSR_JAX:000664) of either sex (postnatal day 16-56) were used in this study. All mice were housed in a 12-hour light/12-hour dark cycle. The mice were deeply anesthetized with an intraperitoneal injection of ketamine and xylazine [80 mg/kg and 10 mg/kg (body weight), respectively], and lidocaine hydrochloride (20 mg/ml) was applied locally to the eyelids and surrounding tissues before enucleation. For consistency, all mouse retinas were collected around 10 a.m. after overnight dark adaptation.

2.2 Retina preparation

The eyes of the mice were removed under dim red illumination and the retinas were dissected into four quadrants for the patch-clamp recording. The prepared retinas were attached to customized translucent Millicell filter rings (Millipore, Bedford, MA). The flattened retinas were continuously supplied with oxygenated mammalian Ringer's solution at a temperature of 37 °C[90]. The bath solution was constantly infused with a mixture of 95% oxygen and 5% carbon dioxide and kept at around 32°C, as previously reported[7]. The anesthetized animals were euthanized by cervical dislocation immediately after removal of their eyes

2.3 Patterned light stimulation

A green organic light-emitting display (OLED) (Olightek, Kunming, Yunnan, China) with a resolution of 800 × 600 pixels and a refresh rate of 85 Hz was applied., The display was controlled by a Windows 7 computer with an Intel Core Duo processor. To observe the display, a Nikon 40x water-immersion objective, which allowed a 250 μm diameter area of the retina to receive light stimuli, was used. The OLED had 15 μm diameter pixels, which appeared as 0.25 μm/pixels on the retina under the 40x objective. PsychoPy was used to create grating images with adjustable spatial frequency, which were then projected onto the photoreceptor layer. The background light intensity was around 700 isomerizations per rod per second, while the highest stimulus was approximately 1.816 × 105 isomerizations per rod per second. At this level of background illumination, the rod pathway was saturated, leaving the cone pathway to mediate the light response[92]. Each image was displayed for 1 second, followed by a 5-second break. Focused or defocused images with a 125 μm diameter and a spatial frequency of 0.0067 cycles/degree were applied.

The process of creating defocused images on the retina in vitro has been described previously[64]. It has been reported that an axial elongation of 5 μm would induce a 1 Diopter (D) refractive error in the mouse retina[93], which means a 100 μm would result in plus or minus 20 diopters of refractive error in the mouse retina when viewed under microscopy. Additionally, the system allowed for the production of various sizes of annulus/spots at 525nm wavelength using the Mightex Polygon1000. By using polyscan3 software, annulus/spot sizes ranging from 30 to 180um in diameter were provided as stimulation.

2.4 Electrophysiology

Whole-cell recordings of individual HCs in the mid-peripheral retina were produced using an Axopatch 700B amplifier connected to a Digidata 1550B interface and pCLAMP 10 software (Molecular Devices, San Jose, CA, USA). To improve space clamp and block spiking, whole-cell recordings were performed with an internal solution containing caesium methanosulfonate instead of potassium gluconate.

During whole-cell recording, the kinetics (amplitudes) of inhibitory postsynaptic currents (IPSCs) were compared in response to light stimuli. Whole-cell response amplitudes among the stimuli of focused/defocused images and various light-intensity stimuli were normalized. Finally, the dye was injected into the recorded cells using pipette tips filled with 4% Neurobiotin (Vector Laboratories, Burlingame, CA, USA), and 0.5% Lucifer Yellow-CH (Molecular Probes, Eugene, Oregon, USA) as previously described[7].

2.5 Intracellular labeling

Following the recording, the recorded neurons were visually impaled using pipette tips filled with a mixture of 4% Neurobiotin and Alexa Fluor 594 (Thermo-Fisher, Waltham, MA, USA) in distilled water and backfilled with 3 M KCl. The electrode resistance measured ∼100 MΩ. Subsequently, biphasic current (+1.0 nA, 3 Hz) was administered to the impaled cells, after which retinal pieces were fixed with 4% paraformaldehyde for 15-20 minutes. The tissues were then incubated overnight at 4°C in a solution of 0.1 M phosphate buffer with 0.5% Triton-X 100 and 0.1% NaN3, containing 1% donkey serum. Following washing, tissues were incubated with Cy-conjugated streptavidin (Invitrogen, Waltham, MA, USA) at a concentration of 1:200 overnight at

4°C. Finally, the tissues were mounted in Vectashield (Vector Laboratories, Newark, CA, USA) for microscopic observation.

2.6 Imaging and Data Analysis

Retinal mounts were imaged using a ZEISS LSM 800 microscope with an Airyscan (Zeiss, Thornwood, NY, USA) confocal system and a 40x objective lens (N.A. 1.3) /20x objective lens (N.A. 0.8). The microscope had an optical resolution of 120 nm in the x- and y-axes, and 350 nm in the z-axis. The images were captured with two channels (594 and Cy3) superimposed, and Z-axis steps of 0.35 μm. The data were analyzed as described previously and presented as mean ± S.E.M. Statistical analysis was performed using Origin software (OriginLab, Northampton, MA, USA) and SPSS version 25 (IBM, Amonk, NY, USA), with a Wilcoxon Signed Rank test determining statistical significance at $P < 0.05$.

3. Results

The depolarization of horizontal cells, also known as dark responses, is a direct result of glutamate release from photoreceptors. As photoreceptors respond to light with hyperpolarization, there is a decrease in glutamate release, leading to hyperpolarization of the HCs[163]. Therefore, the amplitude of light responses in HCs can be traced back to the reduction of glutamate release from photoreceptors.

3.1 The identification of horizontal cells

In the murine retina, dendrites from horizontal cells extend into the outer plexiform layer and form an axon terminal. Vital retinas contain horizontal cells that can be distinguished by their relatively large soma (compared to bipolar cells and amacrine cells), located in the outermost part of the inner nuclear layer (INL). These cells are further identified by their response to light, which causes them to hyperpolarize, and by calbindin immunostaining. The somata located in the inner nuclear layer (INL) were labeled with 4% Neurobiotin. These cells were identified by the presence of Monoclonal anti-Calbindin-D-28K antibody (at a 1:200 concentration), which is specific to calcium-binding proteins involved in calcium transport, and is only present in horizontal cells when staining in the outermost layer of the INL[164] (see Fig. 1).

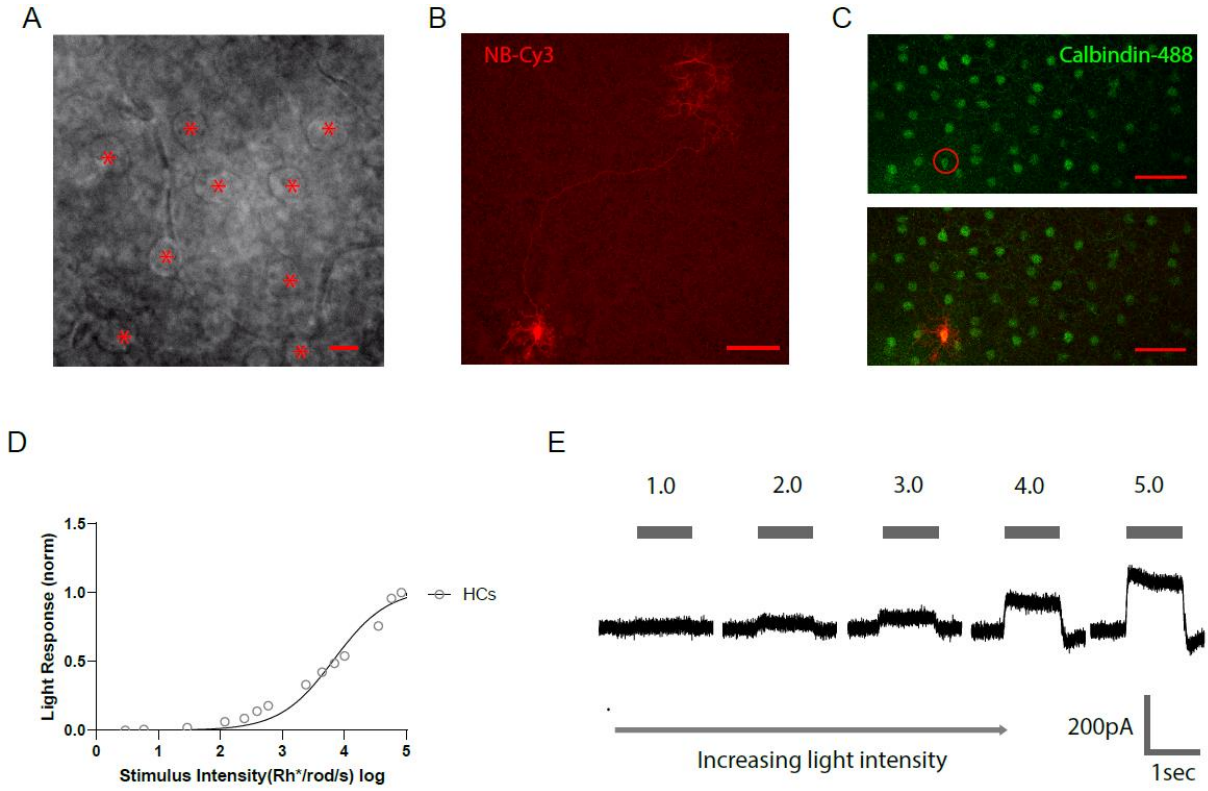

Figure 5. 1 The identification of horizontal cells in the mouse retina and their light sensitivity

[A] The relatively large soma of neurons (Asterisk) in the outermost area of the inner nuclear layer were targeted to record the light response and by intracellular labeling. Scale bar, 10 µm. [**B]** Horizontal cells were visualized by neurobiotin-Cy3, which extends their axons to axonal terminals and establishes a relatively small dendritic field. Scale bar, 50 µm. **[C]** The horizontal cells were identified by calbindin-positive staining. Scale bar, 50 µm. **[D, E]** Light intensity was increased (525nm in wavelength), and horizontal cell response in C57BL6 was noted. The light response of HCs (N = 9) was fitted to the Michaelis-Menten function (R^2 = 0.8940), and the response threshold (T = 2141.89 Rh*/rod/s) was accordingly calculated. Stimulus intensity is given in log units.

3.2 The morphology of Horizontal cells

HCs from wild-type mice were analyzed for their dendritic field diameter, soma size, and axon terminal area.

Horizontal cells were identified as located in the outermost layer of the inner nuclear layer and were found to exhibit a large hyperpolarizing response to light. The cells were then labeled by injecting a mixture of Alexa Fluor 594 and 4% Neurobiotin in a ratio of 1:3 (Fig 2A, B). Six primary dendrites extend from the soma, forming a dendritic field with an average area of 4619± 288 µm², soma diameter of 12.19± 0.42 µm, and an axonal terminal with an average area of 6583.37± 434 µm² in wild-type mice. Each cell contacts six neighboring other HCs, creating a mosaic distribution.

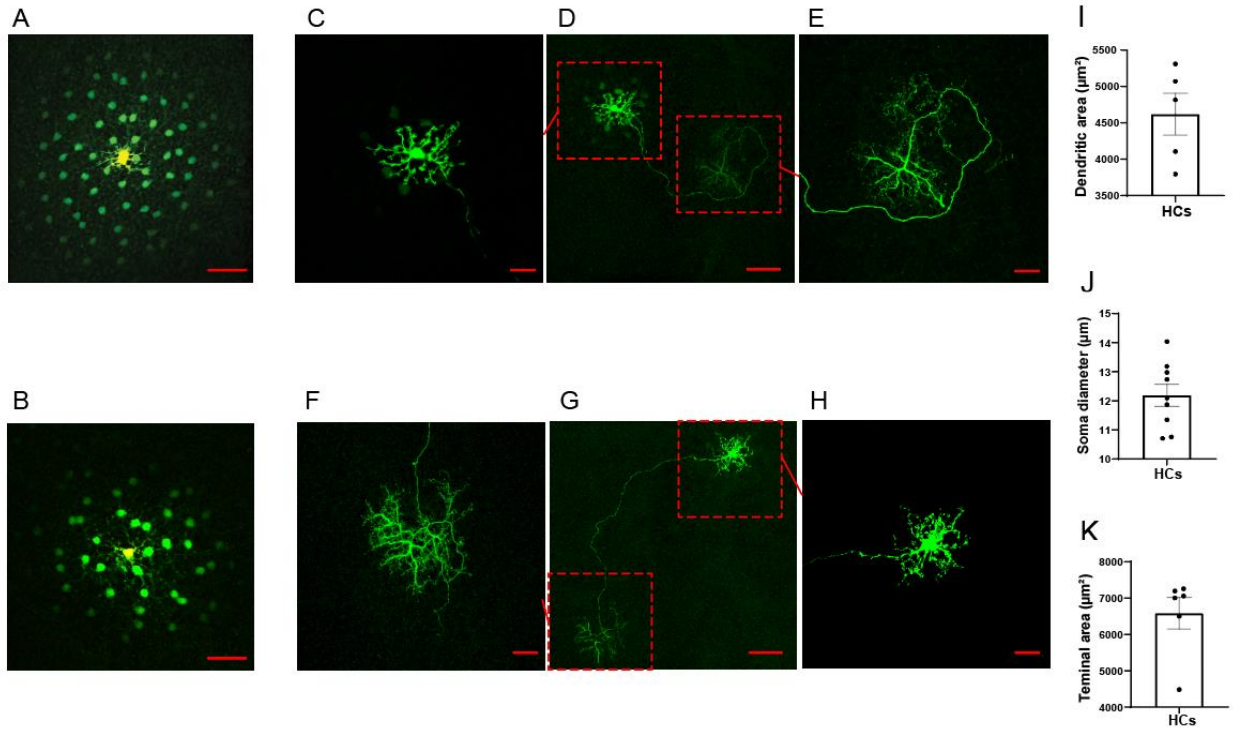

Figure 5. 2 The morphology of retinal horizontal cells was visualized in wild-type mice

[A to B] Horizontal cells displayed strong coupling. A horizontal cell can be visualized by mixed color (yellow) using Alexa Fluor 594 and Neurobiotin-488, which allows for the identification of injected cells, while the coupling cells were demonstrated by the presence of Neurobiotin-488 (green). Scale bar, 50 µm. **[C to H]** The soma and axon terminals of the horizontal cells are connected by a long axon, which is made visible via Neurobiotin injection. C, E, F and H scale bar, 20 µm. D and G scale bar,50 µm. **[I to K]** Horizontal cells have a dendritic field (N= 5) with an average area of 4619± 288 µm², soma diameter (N= 8) of 12.19± 0.42 µm, and an axonal terminal (N= 6) with an average area of 6583.37± 434 µm² in wild-type mice. Error bars represent SEM. WT, wild-type.

3.3 Horizontal cells in response to various sizes of annulus and spots

The horizontal cells play an important role in processing visual information by receiving signals from both rod and cone photoreceptors and providing inhibitory feedback that enhances contrast, edge perception, and the generation of center-surround receptive field in cones and bipolar cells[165]. However, limited studies have been performed on the response properties of Horizontal cells to specific pattern stimuli.

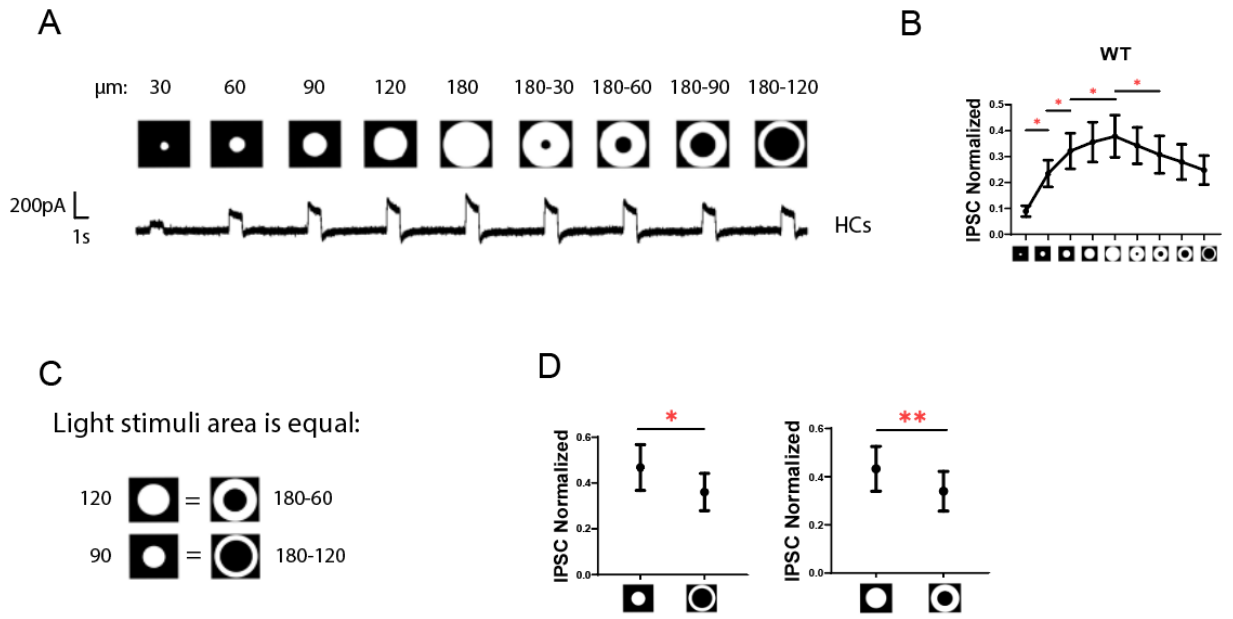

Figure 5. 3 The response of horizontal cells to stimuli of varying spot sizes and annulus

[A] The horizontal cells' response to spot sizes ranging from 30 to 180µm in diameter. The annulus size was calculated by subtracting the inner diameter from the outer diameter. **[B]** The inhibitory postsynaptic current (IPSCs) measurements of HCs displayed a significant variation in response to spot /spots and spot/annulus stimuli (*p<0.05). **[C]** The stimuli area of a 120µm diameter spot was equivalent to the area of an annulus with an outer diameter of 180µm and an inner diameter of 60µm. Similarly, a 90µm spot was equivalent to an annulus with an outer diameter of 180µm and an inner diameter of 120µm. **[D]** IPSCs of Horizontal cells respond differently to stimuli in the same area but in different shapes. Error bars represent SEM.

3.4 Horizontal cells in response to focused and defocused images

A major reason for recording horizontal cells in the soma was to investigate their response to defocused and unfocused images. Custom-made images of 125 µm and 0.0067 c/d spatial frequency were projected onto the receptive field of horizontal cells, with a focus on the photoreceptor cell layer at 0 diopters. In murine retinas, a focused image placed 50 µm in front of or behind the photoreceptor layer could result in an equivalent of ±10 diopters, while 100 µm could result in ±20 diopters, depending on the direction[93].

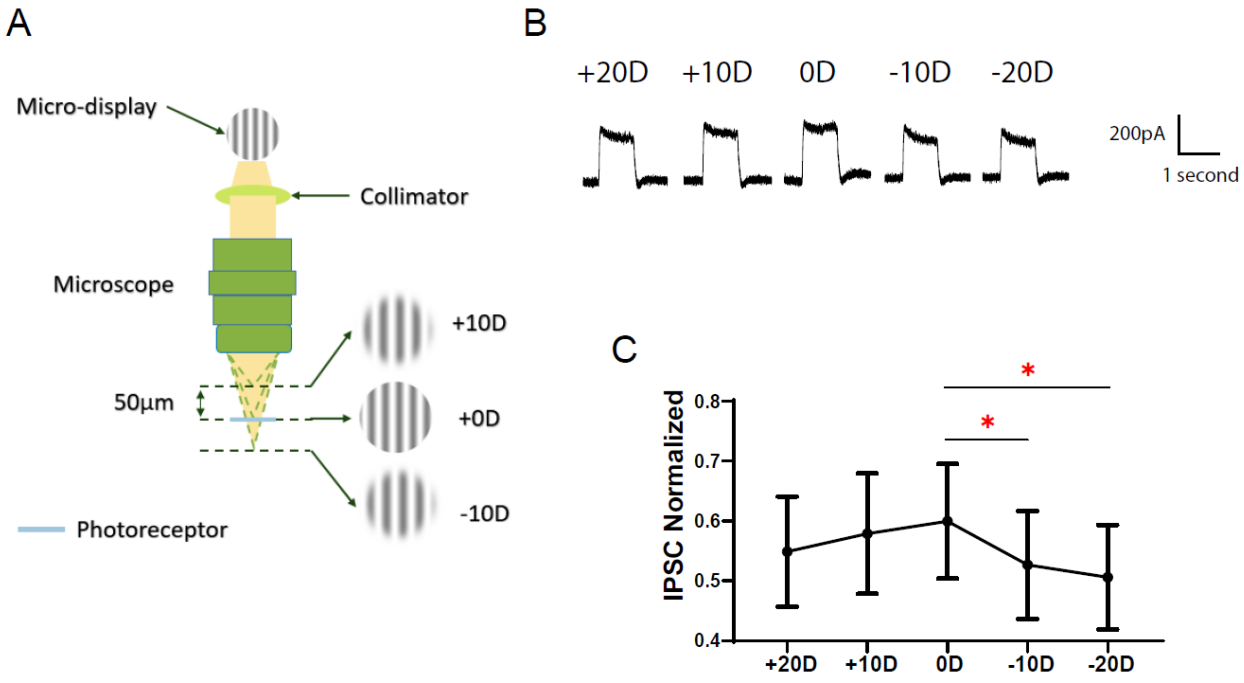

Figure 5. 4 The response of horizontal cells to focus and defocus in wild-type mice

[A] The diagram indicates the position of the photoreceptor in relation to the focused plane. **[B]** The ± 20D, ± 10D, and 0D were created and projected to the receptive field of horizontal cells,

and IPSCs of HCs were recorded accordingly. **[C]** Horizontal cells in wild-type exhibited a significant difference between 0D and -10D, 0D and -20D, *$p < 0.05$. Error bars represent SEM.

4. Discussion

There are two inhibitory networks that modulate the visual signal. The lateral network in the OPL consists of single type of horizontal cells in mouse retinas, while the lateral networks in IPL are consisted of at least 63 types of amacrine cells[157]. Both networks might potentially contribute to focused and defocused signal modulations. To determine how the horizontal cell responds to focused or defocused image stimuli, this study investigated the biophysical properties of the retinal horizontal cells.

Previous research has shown that retinal ganglion cells in the vertical pathway could respond and reflect focus and defocused image stimuli[122]. In this study, when focused and unfocused images were projected onto the receptive fields of horizontal cells, HC in the lateral pathway in OPL could also respond to focused and defocused image stimuli. The results showed significant differences in response properties of HCs between focus and +10 D defocus and focus versus +20 D defocus. This indicates that HCs encode the focused and defocused image from photoreceptors, encode the focused and defocused image from the photoreceptor to the bipolar cell in the first layer of the vertical path. Previous research by the team has shown that the defocused image induced a blurred edge, change of the light ring, contrast, and light intensity[49]. HCs provide negative feedback to the photoreceptor cells, possibly meaning that the retina begins to adjust and correct the signaling under defocused images from the very first step when the image is projected on the retina.

5. Conclusion

The biophysical properties of HCs have the ability to reflect spot/annulus pattern stimuli and focused/defocused images. This indicates that HCs represent the primary class of inhibitory neurons involved in regulating focus/defocus and play a role in the output of retinal ganglion cells (RGCs) in response to defocused signals.

CHAPTER 6 Conclusion and Future Studies

It is projected that by 2050, half of the global population will suffer from myopia. It is believed that visually guided ocular growth may be the cause of myopia. However, questions about the exact pathways and the specific neurons involved still remain. The studies described in this thesis aimed to clarify the role of the retinal neurons in myopia development at single-cell levels, with a particular focus on electrophysiology.

Focused and defocused image stimuli may influence ocular development and axial elongation. The study first explored the role of a single αRGC in decoding focused and defocused visual signals. As the main output neurons in the retina, RGCs convert all the visual information from photoreceptors into action potentials that travel to the brain via axons in the optic nerve. Second, horizontal cells and AII ACs in the lateral inhibitory pathway were investigated to understand how they shaped the focused/defocused signals transmitted in the vertical pathway. In addition, the potential effect of defocused images on the responses of dopaminergic ACs and their dopamine release was studied. Finally, the role of Cx36 GJs in influencing the focused and defocused signals was investigated.

Focused/defocused images were projected into the receptive fields of single αRGC. Generalized linear models (GLMs), which can capture stimulus-dependent changes in real neurons with spike timing precision and reliability, were used to predict the responses of αRGCs in both myopic and normal retinas. There are differences in encoding performance between myopic and normal retinas, which indicate the possible amendment and plasticity of the retinal circuit in myopic retinas. Additionally, under conditions of stretched soma and retina to mimic the myopic status,

αRGCs have the ability to detect focused, spherically, and astigmatically defocused images and exhibit differential responses ex vivo.

HCs and AII ACs both make up the inhibitory network in the retina. They have the ability to detect both focused and defocused stimuli. However, couplings between AII ACs minimize the ability to discern the focus/defocused images.

Interestingly, dopaminergic ACs, the only source of dopamine, responded differently when exposed to focused/defocused stimuli. The result indicates that defocused images may influence dopamine release in the retina and contribute to myopia development.

Cx36 exists between cones, AII ACs and CBCs, and ACs and RGCs. As a control, Cx36 GJs knockout mice or GJs blockers were used to investigate the role of Cx36 in decoding focused/defocused signals to αRGCs and AII ACs. αRGCs ability to distinguish focus/defocus was lost in the absence of Cx36 GJs. This suggests that Cx36 plays a key role in the transmission of focus/defocused image signals within the retinal circuit.

In summary, the retinal neurons, including αRGCs, HC, AII ACs and dopaminergic ACs, have the ability to respond differently to the focused/defocused images. Gap junctions in retinal circuits may play a key role in visually-guided myopia development.

Further research is required to investigate which subtypes of RGCs may be associated with myopia or astigmatism development, as this may have the potential to provide valuable insights into the targeted treatment of refractive errors in their early stages.

References

1. Yan, W., et al., Mouse Retinal Cell Atlas: Molecular Identification of over Sixty Amacrine Cell Types. J Neurosci, 2020. 40(27): p. 5177-5195.

2. Mustafi, D., A.H. Engel, and K. Palczewski, Structure of cone photoreceptors. Prog Retin Eye Res, 2009. 28(4): p. 289-302.

3. Fu, Y. and K.W. Yau, Phototransduction in mouse rods and cones. Pflugers Arch, 2007. 454(5): p. 805-19.

4. Ofri, D.J.M.a.P.E.M.a.R., Chapter 1 - Structure and Function of the Eye. Slatter's Fundamentals of Veterinary Ophthalmology. 2008.

5. Tsukamoto, Y. and N. Omi, Classification of Mouse Retinal Bipolar Cells: Type-Specific Connectivity with Special Reference to Rod-Driven AII Amacrine Pathways. Front Neuroanat, 2017. 11: p. 92.

6. Nelson R, C.V., Bipolar Cell Pathways in the Vertebrate Retina. Webvision, 2007.

7. Pan, F., et al., Inhibitory masking controls the threshold sensitivity of retinal ganglion cells. J Physiol, 2016. 594(22): p. 6679-6699.

8. Boije, H., et al., Horizontal Cells, the Odd Ones Out in the Retina, Give Insights into Development and Disease. Front Neuroanat, 2016. 10: p. 77.

9. Chapot, C.A., T. Euler, and T. Schubert, How do horizontal cells 'talk' to cone photoreceptors? Different levels of complexity at the cone-horizontal cell synapse. J Physiol, 2017. 595(16): p. 5495-5506.

10. Elgueta, C., et al., Electrical coupling between A17 cells enhances reciprocal inhibitory feedback to rod bipolar cells. Sci Rep, 2018. 8(1): p. 3123.

11. Pérez de Sevilla Müller, L., et al., Prox1 Is a Marker for AII Amacrine Cells in the Mouse Retina. Front Neuroanat, 2017. 11: p. 39.

12. Meadows, M.A., et al., Regulation of neurotransmitter release during crossover inhibition. Investigative Ophthalmology & Visual Science, 2019. 60(9): p. 547-547.

13. Bloomfield, S.A. and B. Völgyi, Function and plasticity of homologous coupling between AII amacrine cells. Vision Res, 2004. 44(28): p. 3297-306.

14. Banerjee, S., et al., Increased Connexin36 Phosphorylation in AII Amacrine Cell Coupling of the Mouse Myopic Retina. Front Cell Neurosci, 2020. 14: p. 124.

15. Bloomfield, S.A. and D. Xin, Surround inhibition of mammalian AII amacrine cells is generated in the proximal retina. J Physiol, 2000. 523 Pt 3(Pt 3): p. 771-83.

16. Roy, S. and G.D. Field, Dopaminergic modulation of retinal processing from starlight to sunlight. J Pharmacol Sci, 2019. 140(1): p. 86-93.

17. Farsaii M, C.V., AII Amacrine Cells. 2005.

18. Keeley, P.W. and B.E. Reese, Morphology of dopaminergic amacrine cells in the mouse retina: independence from homotypic interactions. J Comp Neurol, 2010. 518(8): p. 1220-31.

19. Contini, M. and E. Raviola, GABAergic synapses made by a retinal dopaminergic neuron. Proc Natl Acad Sci U S A, 2003. 100(3): p. 1358-63.

20. Pérez-Fernández, V., et al., Rod Photoreceptor Activation Alone Defines the Release of Dopamine in the Retina. Curr Biol, 2019. 29(5): p. 763-774.e5.

21. Newkirk, G.S., et al., Inhibitory inputs tune the light response properties of dopaminergic amacrine cells in mouse retina. J Neurophysiol, 2013. 110(2): p. 536-52.

22. Laboissonniere, L.A., et al., Molecular signatures of retinal ganglion cells revealed through single cell profiling. Sci Rep, 2019. 9(1): p. 15778.

23. Krieger, B., et al., Four alpha ganglion cell types in mouse retina: Function, structure, and molecular signatures. PLoS One, 2017. 12(7): p. e0180091.

24. Wang, F., et al., OFF-transient alpha RGCs mediate looming triggered innate defensive response. Curr Biol, 2021. 31(11): p. 2263-2273.e3.

25. Tapia, M.L., G. Nascimento-Dos-Santos, and K.K. Park, Subtype-specific survival and regeneration of retinal ganglion cells in response to injury. Front Cell Dev Biol, 2022. 10: p. 956279.

26. Völgyi, B., et al., Morphology and tracer coupling pattern of alpha ganglion cells in the mouse retina. J Comp Neurol, 2005. 492(1): p. 66-77.

27. Heflin, S.J. and P.B. Cook, Narrow and wide field amacrine cells fire action potentials in response to depolarization and light stimulation. Vis Neurosci, 2007. 24(2): p. 197-206.

28. Bjelke, B., et al., Dopaminergic transmission in the rat retina: evidence for volume transmission. J Chem Neuroanat, 1996. 12(1): p. 37-50.

29. Popova, E., Role of Dopamine in Retinal Function, in Webvision: The Organization of the Retina and Visual System, H. Kolb, E. Fernandez, and R. Nelson, Editors. 1995, University of Utah Health Sciences Center Copyright: © 2024 Webvision . Salt Lake City (UT).

30. Flood, M.D. and E.D. Eggers, Dopamine D1 and D4 receptors contribute to light adaptation in ON-sustained retinal ganglion cells. J Neurophysiol, 2021. 126(6): p. 2039-2052.

31. Mills, S.L. and S.C. Massey, Differential properties of two gap junctional pathways made by AII amacrine cells. Nature, 1995. 377(6551): p. 734-7.

32. Traynelis, S.F., et al., Glutamate receptor ion channels: structure, regulation, and function. Pharmacol Rev, 2010. 62(3): p. 405-96.

33. Hansen, K.B., et al., Structure, function, and allosteric modulation of NMDA receptors. J Gen Physiol, 2018. 150(8): p. 1081-1105.

34. Niswender, C.M. and P.J. Conn, Metabotropic glutamate receptors: physiology, pharmacology, and disease. Annu Rev Pharmacol Toxicol, 2010. 50: p. 295-322.

35. Flores-Herr, N., D.A. Protti, and H. Wässle, Synaptic currents generating the inhibitory surround of ganglion cells in the mammalian retina. J Neurosci, 2001. 21(13): p. 4852-63.

36. Popova, E., Ionotropic GABA Receptors and Distal Retinal ON and OFF Responses. Scientifica (Cairo), 2014. 2014: p. 149187.

37. Popova, E., GABAergic neurotransmission and retinal ganglion cell function. J Comp Physiol A Neuroethol Sens Neural Behav Physiol, 2015. 201(3): p. 261-83.

38. Yang, X.L., Characterization of receptors for glutamate and GABA in retinal neurons. Prog Neurobiol, 2004. 73(2): p. 127-50.

39. Elgueta, C., et al., Acetylcholine induces GABA release onto rod bipolar cells through heteromeric nicotinic receptors expressed in A17 amacrine cells. Front Cell Neurosci, 2015. 9: p. 6.

40. Sethuramanujam, S., et al., A Central Role for Mixed Acetylcholine/GABA Transmission in Direction Coding in the Retina. Neuron, 2016. 90(6): p. 1243-1256.

41. Hutchins, J.B., Acetylcholine as a neurotransmitter in the vertebrate retina. Exp Eye Res, 1987. 45(1): p. 1-38.

42. Fadjukov, J., et al., Gap junctions and connexin hemichannels both contribute to the electrical properties of retinal pigment epithelium. J Gen Physiol, 2022. 154(4).

43. Mangel, S.C., Analysis of the horizontal cell contribution to the receptive field surround of ganglion cells in the rabbit retina. J Physiol, 1991. 442: p. 211-34.

44. Haarman, A.E.G., et al., Phenotypic Consequences of the GJD2 Risk Genotype in Myopia Development. Invest Ophthalmol Vis Sci, 2021. 62(10): p. 16.

45. Chen, C.X., et al., Connexins and cAMP Cross-Talk in Cancer Progression and Metastasis. Cancers (Basel), 2020. 13(1).

46. Telkes, I., et al., Connexin-36 distribution and layer-specific topography in the cat retina. Brain Struct Funct, 2019. 224(6): p. 2183-2197.

47. Bloomfield, S.A. and B. Völgyi, The diverse functional roles and regulation of neuronal gap junctions in the retina. Nat Rev Neurosci, 2009. 10(7): p. 495-506.

48. Teves, M., et al., The role of cell-cell coupling in myopia development and light adaptation. Investigative Ophthalmology & Visual Science, 2014. 55(13): p. 3036-3036.

49. Banerjee, S., et al., Defocused Images Change Multineuronal Firing Patterns in the Mouse Retina. Cells, 2020. 9(3).

50. Grzybowski, A., et al., A review on the epidemiology of myopia in school children worldwide. BMC Ophthalmol, 2020. 20(1): p. 27.

51. Morgan, I.G., K. Ohno-Matsui, and S.M. Saw, Myopia. Lancet, 2012. 379(9827): p. 1739-48.

52. Nouraeinejad, A., More Than Fifty Percent of the World Population Will Be Myopic by 2050. Beyoglu Eye J, 2021. 6(4): p. 255-256.

53. Foulds, W.S., V.A. Barathi, and C.D. Luu, Progressive myopia or hyperopia can be induced in chicks and reversed by manipulation of the chromaticity of ambient light. Invest Ophthalmol Vis Sci, 2013. 54(13): p. 8004-12.

54. Tejedor, J. and P. de la Villa, Refractive changes induced by form deprivation in the mouse eye. Invest Ophthalmol Vis Sci, 2003. 44(1): p. 32-6.

55. Howlett, M.H. and S.A. McFadden, Form-deprivation myopia in the guinea pig (Cavia porcellus). Vision Res, 2006. 46(1-2): p. 267-83.

56. Norton, T.T., J.A. Essinger, and N.A. McBrien, Lid-suture myopia in tree shrews with retinal ganglion cell blockade. Vis Neurosci, 1994. 11(1): p. 143-53.

57. Troilo, D., M.D. Gottlieb, and J. Wallman, Visual deprivation causes myopia in chicks with optic nerve section. Curr Eye Res, 1987. 6(8): p. 993-9.

58. Nath, A., W.N. Grimes, and J.S. Diamond, Layers of inhibitory networks shape receptive field properties of AII amacrine cells. Cell Rep, 2023. 42(11): p. 113390.

59. Shu, Z., et al., The Role of Retinal Dopamine D1 Receptors in Ocular Growth and Myopia Development in Mice. J Neurosci, 2023. 43(48): p. 8231-8242.

60. Kothmann, W.W., S.C. Massey, and J. O'Brien, Dopamine-stimulated dephosphorylation of connexin 36 mediates AII amacrine cell uncoupling. J Neurosci, 2009. 29(47): p. 14903-11.

61. Schmidt, T.M., et al., A role for melanopsin in alpha retinal ganglion cells and contrast detection. Neuron, 2014. 82(4): p. 781-8.

62. Stoimenova, B.D., The effect of myopia on contrast thresholds. Invest Ophthalmol Vis Sci, 2007. 48(5): p. 2371-4.

63. Liu, X., et al., Contrast Sensitivity Is Associated With Chorioretinal Thickness and Vascular Density of Eyes in Simple Early-Stage High Myopia. Front Med (Lausanne), 2022. 9: p. 847817.

64. Pan, F., Defocused Image Changes Signaling of Ganglion Cells in the Mouse Retina. Cells, 2019. 8(7).

65. Asari, H. and M. Meister, Divergence of visual channels in the inner retina. Nat Neurosci, 2012. 15(11): p. 1581-9.

66. Munteanu, T., et al., Light-dependent pathways for dopaminergic amacrine cell development and function. Elife, 2018. 7.

67. Park, H., et al., Visually-driven ocular growth in mice requires functional rod photoreceptors. Invest Ophthalmol Vis Sci, 2014. 55(10): p. 6272-9.

68. Brown, D.M., et al., Exogenous All-Trans Retinoic Acid Induces Myopia and Alters Scleral Biomechanics in Mice. Invest Ophthalmol Vis Sci, 2023. 64(5): p. 22.

69. Ishibashi, M., et al., Analysis of rod/cone gap junctions from the reconstruction of mouse photoreceptor terminals. Elife, 2022. 11.

70. Smith, E.L., 3rd, et al., Peripheral vision can influence eye growth and refractive development in infant monkeys. Invest Ophthalmol Vis Sci, 2005. 46(11): p. 3965-72.

71. Banerjee, S., et al., Functional connexin35 increased in the myopic chicken retina. Vis Neurosci, 2021. 38: p. E008.

72. Demb, J.B. and J.H. Singer, Intrinsic properties and functional circuitry of the AII amacrine cell. Vis Neurosci, 2012. 29(1): p. 51-60.

73. Liu, A.L., et al., The role of ipRGCs in ocular growth and myopia development. Sci Adv, 2022. 8(23): p. eabm9027.

74. Huang, F., et al., Retinal Dopamine D2 Receptors Participate in the Development of Myopia in Mice. Invest Ophthalmol Vis Sci, 2022. 63(1): p. 24.

75. Zhou, X., et al., Dopamine signaling and myopia development: What are the key challenges. Prog Retin Eye Res, 2017. 61: p. 60-71.

76. Yin, J., et al., Structure of a D2 dopamine receptor-G-protein complex in a lipid membrane. Nature, 2020. 584(7819): p. 125-129.

77. Takeshita, D. and T. Gollisch, Nonlinear spatial integration in the receptive field surround of retinal ganglion cells. J Neurosci, 2014. 34(22): p. 7548-61.

78. Wienbar, S. and G.W. Schwartz, The dynamic receptive fields of retinal ganglion cells. Prog Retin Eye Res, 2018. 67: p. 102-117.

79. Turner, M.H., G.W. Schwartz, and F. Rieke, Receptive field center-surround interactions mediate context-dependent spatial contrast encoding in the retina. Elife, 2018. 7.

80. Zhang, J., et al., Epidemiology and Burden of Astigmatism: A Systematic Literature Review. Optom Vis Sci, 2023. 100(3): p. 218-231.

81. Fricke, T.R., et al., Global prevalence of visual impairment associated with myopic macular degeneration and temporal trends from 2000 through 2050: systematic review, meta-analysis and modelling. Br J Ophthalmol, 2018. 102(7): p. 855-862.

82. Holden, B.A., et al., Global Prevalence of Myopia and High Myopia and Temporal Trends from 2000 through 2050. Ophthalmology, 2016. 123(5): p. 1036-42.

83. Weber, A.I. and J.W. Pillow, Capturing the Dynamical Repertoire of Single Neurons with Generalized Linear Models. Neural Comput, 2017. 29(12): p. 3260-3289.

84. Pillow, J.W., et al., Prediction and decoding of retinal ganglion cell responses with a probabilistic spiking model. J Neurosci, 2005. 25(47): p. 11003-13.

85. Pillow, J.W., et al., Spatio-temporal correlations and visual signalling in a complete neuronal population. Nature, 2008. 454(7207): p. 995-9.

86. Crapper, D.R. and W.K. Noell, RETINAL EXCITATION AND INHIBITION FROM DIRECT ELECTRICAL STIMULATION. J Neurophysiol, 1963. 26: p. 924-47.

87. Granit, R., The distribution of excitation and inhibition in single-fibre responses from a polarized retina. J Physiol, 1946. 105: p. 45-53.

88. Tkatchenko, T.V., Y. Shen, and A.V. Tkatchenko, Mouse experimental myopia has features of primate myopia. Invest Ophthalmol Vis Sci, 2010. 51(3): p. 1297-303.

89. Duan, X., et al., Subtype-specific regeneration of retinal ganglion cells following axotomy: effects of osteopontin and mTOR signaling. Neuron, 2015. 85(6): p. 1244-56.

90. Bloomfield, S.A. and R.F. Miller, A physiological and morphological study of the horizontal cell types of the rabbit retina. J Comp Neurol, 1982. 208(3): p. 288-303.

91. Völgyi, B., et al., Gap junctions are essential for generating the correlated spike activity of neighboring retinal ganglion cells. PLoS One, 2013. 8(7): p. e69426.

92. Borghuis, B.G., et al., Two-photon imaging of nonlinear glutamate release dynamics at bipolar cell synapses in the mouse retina. J Neurosci, 2013. 33(27): p. 10972-85.

93. Schaeffel, F., Test systems for measuring ocular parameters and visual function in mice. Front Biosci, 2008. 13: p. 4904-11.

94. Pan, F., S.L. Mills, and S.C. Massey, Screening of gap junction antagonists on dye coupling in the rabbit retina. Vis Neurosci, 2007. 24(4): p. 609-18.

95. Truccolo, W., et al., A point process framework for relating neural spiking activity to spiking history, neural ensemble, and extrinsic covariate effects. J Neurophysiol, 2005. 93(2): p. 1074-89.

96. Potter, S.M., A. El Hady, and E.E. Fetz, Closed-loop neuroscience and neuroengineering. Front Neural Circuits, 2014. 8: p. 115.

97. Paninski, L., Maximum likelihood estimation of cascade point-process neural encoding models. Network, 2004. 15(4): p. 243-62.

98. Benjamin, A.S., et al., Modern Machine Learning as a Benchmark for Fitting Neural Responses. Front Comput Neurosci, 2018. 12: p. 56.

99. Jiang, X., et al., A highly efficient murine model of experimental myopia. Sci Rep, 2018. 8(1): p. 2026.

100. Farajian, R., et al., Masked excitatory crosstalk between the ON and OFF visual pathways in the mammalian retina. J Physiol, 2011. 589(Pt 18): p. 4473-89.

101. Field, G.D. and E.J. Chichilnisky, Information processing in the primate retina: circuitry and coding. Annu Rev Neurosci, 2007. 30: p. 1-30.

102. Gollisch, T. and M. Meister, Eye smarter than scientists believed: neural computations in circuits of the retina. Neuron, 2010. 65(2): p. 150-64.

103. Kaplan, E. and R.M. Shapley, The primate retina contains two types of ganglion cells, with high and low contrast sensitivity. Proc Natl Acad Sci U S A, 1986. 83(8): p. 2755-7.

104. Völgyi, B., S. Chheda, and S.A. Bloomfield, Tracer coupling patterns of the ganglion cell subtypes in the mouse retina. J Comp Neurol, 2009. 512(5): p. 664-87.

105. Chichilnisky, E.J., A simple white noise analysis of neuronal light responses. Network, 2001. 12(2): p. 199-213.

106. Shapley, R., Linear and nonlinear systems analysis of the visual system: why does it seem so linear? A review dedicated to the memory of Henk Spekreijse. Vision Res, 2009. 49(9): p. 907-21.

107. Olveczky, B.P., S.A. Baccus, and M. Meister, Segregation of object and background motion in the retina. Nature, 2003. 423(6938): p. 401-8.

108. Quint, W.H., et al., Loss of Gap Junction Delta-2 (GJD2) gene orthologs leads to refractive error in zebrafish. Commun Biol, 2021. 4(1): p. 676.

109. Verhoeven, V.J., et al., Genome-wide meta-analyses of multiancestry cohorts identify multiple new susceptibility loci for refractive error and myopia. Nat Genet, 2013. 45(3): p. 314-8.

110. Barathi, V.A., et al., Two models of experimental myopia in the mouse. Vision Res, 2008. 48(7): p. 904-16.

111. Graham, B. and S.J. Judge, The effects of spectacle wear in infancy on eye growth and refractive error in the marmoset (Callithrix jacchus). Vision Res, 1999. 39(2): p. 189-206.

112. Hung, L.F., M.L. Crawford, and E.L. Smith, Spectacle lenses alter eye growth and the refractive status of young monkeys. Nat Med, 1995. 1(8): p. 761-5.

113. Irving, E.L., J.G. Sivak, and M.G. Callender, Refractive plasticity of the developing chick eye. Ophthalmic Physiol Opt, 1992. 12(4): p. 448-56.

114. Norton, T.T., Animal Models of Myopia: Learning How Vision Controls the Size of the Eye. Ilar j, 1999. 40(2): p. 59-77.

115. Schaeffel, F., A. Glasser, and H.C. Howland, Accommodation, refractive error and eye growth in chickens. Vision Res, 1988. 28(5): p. 639-57.

116. Shaikh, A.W., J.T. Siegwart, Jr., and T.T. Norton, Effect of interrupted lens wear on compensation for a minus lens in tree shrews. Optom Vis Sci, 1999. 76(5): p. 308-15.

117. Huang, J., L.F. Hung, and E.L. Smith, 3rd, Effects of foveal ablation on the pattern of peripheral refractive errors in normal and form-deprived infant rhesus monkeys (Macaca mulatta). Invest Ophthalmol Vis Sci, 2011. 52(9): p. 6428-34.

118. Raviola, E. and T.N. Wiesel, Neural control of eye growth and experimental myopia in primates. Ciba Found Symp, 1990. 155: p. 22-38; discussion 39-44.

119. Thomas, S. and F. Schaeffel, Developmental compensation of imposed astigmatism is not initiated by astigmatic accommodation in chickens. Vision Res, 2000. 40(26): p. 3553-8.

120. Flüeler, U.R. and D.L. Guyton, Does a tilted retina cause astigmatism? The ocular imagery and the retinoscopic reflex resulting from a tilted retina. Surv Ophthalmol, 1995. 40(1): p. 45-50.

121. Popa, A.V., C.S. Kee, and W.K. Stell, Retinal control of lens-induced astigmatism in chicks. Exp Eye Res, 2020. 194: p. 108000.

122. Wang, Q., et al., Retinal ganglion cells encode differently in the myopic mouse retina? Exp Eye Res, 2023. 234: p. 109616.

123. Baden, T., et al., The functional diversity of retinal ganglion cells in the mouse. Nature, 2016. 529(7586): p. 345-50.

124. Miura, T., et al., Mechanism of skull suture maintenance and interdigitation. J Anat, 2009. 215(6): p. 642-55.

125. Nath, A. and G.W. Schwartz, Electrical synapses convey orientation selectivity in the mouse retina. Nat Commun, 2017. 8(1): p. 2025.

126. Peichl, L., Alpha ganglion cells in mammalian retinae: common properties, species differences, and some comments on other ganglion cells. Vis Neurosci, 1991. 7(1-2): p. 155-69.

127. Söhl, G., S. Maxeiner, and K. Willecke, Expression and functions of neuronal gap junctions. Nat Rev Neurosci, 2005. 6(3): p. 191-200.

128. Pan, F., et al., Connexin36 is required for gap junctional coupling of most ganglion cell subtypes in the mouse retina. J Comp Neurol, 2010. 518(6): p. 911-27.

129. Wang, Q., et al., Unmasking inhibition prolongs neuronal function in retinal degeneration mouse model. Faseb j, 2020. 34(11): p. 15282-15299.

130. Jeon, C.J., E. Strettoi, and R.H. Masland, The major cell populations of the mouse retina. J Neurosci, 1998. 18(21): p. 8936-46.

131. Wang, Q., et al., The Effect of Low-Dose Atropine on Alpha Ganglion Cell Signaling in the Mouse Retina. Front Cell Neurosci, 2021. 15: p. 664491.

132. Chui, T.Y., et al., Retinal stretching limits peripheral visual acuity in myopia. Vision Res, 2005. 45(5): p. 593-605.

133. Zhou, X., et al., Biometric measurement of the mouse eye using optical coherence tomography with focal plane advancement. Vision Res, 2008. 48(9): p. 1137-43.

134. Marrese, M., et al., Investigating the Effects of Mechanical Stimulation on Retinal Ganglion Cell Spontaneous Spiking Activity. Front Neurosci, 2019. 13: p. 1023.

135. Yang, Z., et al., Prevalence of and factors associated with astigmatism in preschool children in Wuxi City, China. BMC Ophthalmol, 2022. 22(1): p. 146.

136. O'Brien, J. and S.A. Bloomfield, Plasticity of Retinal Gap Junctions: Roles in Synaptic Physiology and Disease. Annu Rev Vis Sci, 2018. 4: p. 79-100.

137. Asteriti, S., C. Gargini, and L. Cangiano, Connexin 36 expression is required for electrical coupling between mouse rods and cones. Vis Neurosci, 2017. 34: p. E006.

138. Yeonan-Kim, J. and M. Bertalmío, Retinal Lateral Inhibition Provides the Biological Basis of Long-Range Spatial Induction. PLoS One, 2016. 11(12): p. e0168963.

139. Huang, J.Y. and D.A. Protti, The impact of inhibitory mechanisms in the inner retina on spatial tuning of RGCs. Sci Rep, 2016. 6: p. 21966.

140. Diamond, J.S., Inhibitory Interneurons in the Retina: Types, Circuitry, and Function. Annu Rev Vis Sci, 2017. 3: p. 1-24.

141. So, C., et al., The response of retinal ganglion cells to optical defocused visual stimuli in mouse retinas. Exp Eye Res, 2024. 241: p. 109834.

142. Feldkaemper, M. and F. Schaeffel, An updated view on the role of dopamine in myopia. Exp Eye Res, 2013. 114: p. 106-19.

143. van der Sande, E., et al., The Role of GJD2(Cx36) in Refractive Error Development. Invest Ophthalmol Vis Sci, 2022. 63(3): p. 5.

144. Zhang, J. and G. Deng, Protective effects of increased outdoor time against myopia: a review. J Int Med Res, 2020. 48(3): p. 300060519893866.

145. Ford, C.P., The role of D2-autoreceptors in regulating dopamine neuron activity and transmission. Neuroscience, 2014. 282: p. 13-22.

146. Meyer, A., et al., AII amacrine cells discriminate between heterocellular and homocellular locations when assembling connexin36-containing gap junctions. J Cell Sci, 2014. 127(Pt 6): p. 1190-202.

147. Voigt, T. and H. Wässle, Dopaminergic innervation of A II amacrine cells in mammalian retina. J Neurosci, 1987. 7(12): p. 4115-28.

148. Mazade, R. and M.T. Pardue, Rod pathway electrical activity is modulated in the myopic mouse. Investigative Ophthalmology & Visual Science, 2023. 64(8): p. 843-843.

149. Mohanty, P., et al., Rod pathway signaling has protective effects on myopia susceptibility in dim, but not bright light. Investigative Ophthalmology & Visual Science, 2021. 62(8): p. 1395-1395.

150. Ahn, J., et al., Synchrony of Spontaneous Burst Firing between Retinal Ganglion Cells Across Species. Exp Neurobiol, 2020. 29(4): p. 285-299.

151. Ivanova, E., C.W. Yee, and B.T. Sagdullaev, Disruption in dopaminergic innervation during photoreceptor degeneration. J Comp Neurol, 2016. 524(6): p. 1208-21.

152. Zhi, Z., et al., The Role of Retinal Connexins Cx36 and Horizontal Cell Coupling in Emmetropization in Guinea Pigs. Invest Ophthalmol Vis Sci, 2021. 62(9): p. 27.

153. Bergen, M.A., et al., Altered Refractive Development in Mice With Reduced Levels of Retinal Dopamine. Invest Ophthalmol Vis Sci, 2016. 57(10): p. 4412-4419.

154. Bartmann, M., et al., Constant light affects retinal dopamine levels and blocks deprivation myopia but not lens-induced refractive errors in chickens. Vis Neurosci, 1994. 11(2): p. 199-208.

155. Veruki, M.L. and E. Hartveit, Meclofenamic acid blocks electrical synapses of retinal AII amacrine and on-cone bipolar cells. J Neurophysiol, 2009. 101(5): p. 2339-47.

156. Bloomfield, S.A. and R.F. Dacheux, Rod vision: pathways and processing in the mammalian retina. Prog Retin Eye Res, 2001. 20(3): p. 351-84.

157. Peng, Y.R., Cell-type specification in the retina: Recent discoveries from transcriptomic approaches. Curr Opin Neurobiol, 2023. 81: p. 102752.

158. Jain, V.a.L., Phillip J. M. and Raja, Sushmitha and Mikhael, Meena and Cameron, Morven A, Light activation of the dopaminergic system occurs after eye-opening in the mouse retina. Frontiers in Ophthalmology, 2023.

159. McLaughlin, A.J., et al., Glycinergic Inhibition Targets Specific Off Cone Bipolar Cells in Primate Retina. eNeuro, 2021. 8(1).

160. Boccuni, I. and R. Fairless, Retinal Glutamate Neurotransmission: From Physiology to Pathophysiological Mechanisms of Retinal Ganglion Cell Degeneration. Life (Basel), 2022. 12(5).

161. Chapot, C.A., et al., Local Signals in Mouse Horizontal Cell Dendrites. Curr Biol, 2017. 27(23): p. 3603-3615.e5.

162. Peichl, L. and J. González-Soriano, Morphological types of horizontal cell in rodent retinae: a comparison of rat, mouse, gerbil, and guinea pig. Vis Neurosci, 1994. 11(3): p. 501-17.

163. Kamermans, M. and H. Spekreijse, The feedback pathway from horizontal cells to cones. A mini review with a look ahead. Vision Res, 1999. 39(15): p. 2449-68.

164. Ströh, S., et al., Cell-specific cre recombinase expression allows selective ablation of glutamate receptors from mouse horizontal cells. PLoS One, 2013. 8(12): p. e83076.

165. Jackman, S.L., et al., A positive feedback synapse from retinal horizontal cells to cone photoreceptors. PLoS Biol, 2011. 9(5): p. e1001057.